NTNU

Norwegian University of
Science and Technology

Bifacial Solar Cells in Nordic Climate

Siw Anita Hansen

Materials Science and Engineering (MTMT)
Submission date: June 2018
Supervisor: Eivind Øvrelid, IMA
Co-supervisor: Birgit Ryningen, SINTEF

Norwegian University of Science and Technology
Department of Materials Science and Engineering

Acknowledgement

This Master‘s Thesis is the evaluation basis for the course TMT4900 Materials Chemistry and Energy Technology at the Norwegian University of Science and Technology (NTNU), and has been performed at the Department of Materials Science and Engineering. The work is in a collaboration with the FME SuSolTech (Research Center for Sustainable Solar Cell Technology).

I would like to show my gratitude to my supervisor Eivind J. Øvrelid and co-supervisor Birgit Ryningen (SINTEF) for their guidance and feedback throughout the whole master work. I am very grateful for the inspiring and motivating conversations throughout the semester. I would also like to thank Pål Tetlie (SINTEF) for help with the set-up, Bendik Sægrov-Sorte (SINTEF) for help with the data logger and sensors, Martin Bellmann (SINTEF) for good advices, Gaute Stokkan and Magnus Bentzen Følstad for letting me borrow Pyranometer and potentiostat, respectively.

Your help has been much appreciated!

Siw Anita Hansen
Trondheim, June 2018

Abstract

Bifacial solar cells can be the new trend within photovoltaic (PV) technology. They have the ability to take advantage of not only the direct irradiance from the sunlight, but also the indirect light which is reflected by the surroundings (albedo effect). This is due to the innovative design of a bifacial solar cell, by which can absorb light from both front and rear side of the cell, simultaneously, which again can increase the efficiency output of the cell. By use of a material of highly reflective characteristic surrounding the cells, this efficiency output can be increased even more. Bifacial solar cells offer a promising possibility to reduce the levelized cost of energy (LCOE) for many PV applications, and have numerous of different installation options.

The concept of bifacial solar cells is not new, it has been described earlier in the scientific literature by Luque et al. (1980) [1] as a new concept for improving the energy output of photovoltaic (PV) systems, and it has been investigated since the 1960s [2]. A module of bifacial solar cells can achieve a higher efficiency output on a smaller space, than what a module of monofacial solar cells can do, and hence fewer bifacial cells are needed to achieve the same output as with monofacial cells. Thereby, bifacial solar cells can be seen as more environment-friendly then that of monofacial solar cells.

In this study the effect of the Nordic climate on a bifacial solar cell was studied. This climate is characterized by relatively low temperatures and cold weather. Snow, temperature and rime ice were parameters that were tested for on the solar cell. Different tilt angles on the bifacial solar cell were studied. In addition, it was investigated how the reflection material underneath the cell affected the efficiency output of the bifacial cell.

The bifacial solar cell that was used in this study is a Zebra cell and is made of a 156x156 mm^2 n-type Czochralski (Cz) silicon wafer. The solar cell was placed in a stand along with an ISET sensor connected to a data logger, which measured the irradiance and temperature on the cell. The experiment was performed inside a chamber with a LED lamp, as well as outside with the sun as the light source.

Based on the results, the Nordic climate seem to have the ability to increase the efficiency output of bifacial solar cells, due to the low temperatures that are present, and by which have a positive affect on the conversion of the incident radiation into electricity. Rime ice on the cell has also shown, interestingly enough, good results. The tilt angle on the bifacial solar cells, is to a large degree dependent on the position to where the cells are mounted according to the sunlight. Based on the reflection material that was tested for, paper with a scale of colours ranging from white to dark, white and black colour - the two extremes - were proven to give the highest and lowest output of the solar cell, respectively.

Sammendrag

Tosidige solceller kan bli den nye trenden innen fotovoltaisk (PV) teknologi. De kan utnytte den direkte strålingen fra sollyset, og i tillegg indirekte lys som blir reflektert av omgivelsene (albedo effekten). Det er det innovative designet som gjør det mulig å absorbere lys fra både fram- og baksiden av cellen samtidig, noe som vil bidra til økt effekt av cellen. Ved bruk av et material med god refleksjons karakteristikk rundt cellene, kan effekten ytterligere forbedres. Tosidige solceller kan være en svært god mulighet til å redusere LCOE (levelized cost of energy) for mange PV applikasjoner, og samtid kunne utnyttes i flere konsepter.

Tosidige solceller er ikke et nytt konsept, men har vært beskrevet tidligere i vitenskapelig litteratur av Luque m.fl. (1980) [1], som et konsept for å forbedre energiutbyttet av fotovoltaiske system. Det har pågått forskning på området siden 1960-tallet [2]. En modul av tosidige solceller kan oppnå et høyere effektivitetsutbytte på et mindre areal enn hva en modul av ensidige solceller kan oppnå. Tosidige solceller kan derfor også bli sett på som mer miljøvennlige i forhold til ensidige solceller.

I dette studiet ble det undersøkt hvilken betydning det nordiske klimaet har for tosidige solceller, hvor dette klimaet er karakterisert av relativt lav temperatur, rim og snø. Parametere som ble testet var snø, temperatur og rim på cellen. Forskjellige vinkler på den tosidige cellen i forhold til lyskilden ble studert, i tillegg til hvordan refleksjonsmaterialet under cellen har påvirket effektivitetsutbyttet på den tosidige solcellen.

Den tosidige solcellen som ble brukt i dette studiet er en Zebra celle. Den er laget av en 156x156 mm^2 n-type Czochralski (Cz) silisium wafer. Solcellen var plassert i et oppsett med en ISET sensor koblet til en data logger, som målte innstrålingen og temperaturen på cellen. Eksperimentet ble utført inne i et kammer med en LED lampe og utendørs med solen som lyskilde.

Basert på resultatene, indikeres det at det nordiske klimaet har evnen til å øke effektivitetsutbyttet til tosidig solceller. Lav temperatur gir en positiv påvirkning av omdannelsen av den innstrålte strålingen til elektrisitet. Rim på cellen gir noe overaskende gode resultater. Vinkelen på hvordan solcellene er montert, er avhengig av posisjonen til hvor cellene monteres i forhold til sollyset. Refleksjonsmaterial ble testet med ark med en skala av farger fra hvit til svart. De to mest ekstreme tilfellene, hvit og svart, gav henholdsvis det høyeste og laveste utbyttet fra solcellen.

Table of Contents

List of Abbreviations

Fundamental Constants

c	speed of light in vacuum
h	Plank‘s constant
k_B	Boltzmann‘s constant
q	charge on the electron

Acronyms

AM	Air Mass
AM1.5	Air Mass 1.5 spectrum - standard for solar cell calibration
APCVD	Atmospheric Pressure Chemical Vapor Deposition
AR	anti-reflection
ARC	anti-reflection coating
BRL	boron rich layer
BSF	back surface field
CDI	Carrier Density Imaging
CMMM	conventionally mounted monofacial modules
Cz	Czochralski
DC	direct current
EQE	External Quantum Efficiency
EVA	ethylene vinyl acetate
IBC	integrated back contact
IQE	Internal Quantum Efficiency
K	Kelvin
LCOE	levelized cost of energy
PECVD	Plasma Enhanced Chemical Vapor Deposition
PV	photovoltaics
QE	Quantum Efficiency
SR	spectral response
STC	Standard Test Conditions
UV	ultraviolet
VMBM	vertically mounted bifacial modules

Symbols Used in the Text

A	surface area of a semiconductor that is exposed to light
A_{abs}	absorbance
A_c	surface area of a solar cell
c	concentration of the absorbing medium
d	thickness of sample
D_n	diffusion constant of minority carriers in n region
D_p	diffusion constant of minority carriers in p region
$e_{bifacial}$	specific energy yield of PV system with bifacial module
$e_{monofacial}$	specific energy yield of PV system with monofacial module
E	light irradiation
E_g	bandgap energy
E_{ph}	photon energy
FF	fill factor
$g_{bifacial}$	bifacial gain
I_o	dark saturation current
I_D	diode current
I_l	light-generated current
I_{mp}	current at the maximum power point
I_{sc}	short-circuit current
J_o	dark saturation current density
J_l	light-generated current density
l	length of the light path
L_n	diffusion length of minority carriers in n region
L_p	diffusion length of minority carriers in p region
m	empirical nonideality factor
m_e	effective mass of a electron
m_h	effective mass of a hole
n	number of data points in a population
$n_{AirMass}$	air mass factor
n_i	intrinsic carrier density
n_j	refractive index in a specific medium

$\mathcal{N}$	number of photons in the highlighted area of the spectrum
N_A	density of acceptor atoms
N_c	effective density of states in conduction band
N_D	density of donor atoms
N_v	effective density of states in valence band
P	transmitted radiant power
P_o	incident radiant power
P_{in}	incident power of radiation
P_{max}	maximum power point
R	reflectance
R_s	series resistance
R_{sheet}	sheet resistance
S	solar constant
T	temperature in kelvin
v_i	speed of light in a specific medium
V_{mp}	voltage at the maximum power point
V_{oc}	open-circuit voltage
x_i	a value in a data set

α	absorption coefficient
γ_s	angle of elevation of the sun
ϵ	molar absorptivity (molar absorption coefficient)
η	solar cell‘s energy conversion efficiency
θ_i	angle of incidence in a specific medium
λ	wavelength of light
μ	the mean of a data set
ν	frequency of light
ρ	resistivity
σ	standard deviation
φ	tilt angle

1 Introduction

The world energy demand is increasing and the U.S Energy Information Administration has projected from their latest International Energy Outlook 2017 (IEO2017), that the world energy consumption will grow by 28 % between 2015 and 2040. The increased energy demand is especially expected to come from countries where demand is driven by strong economic growth, particularly in Asia [3]. Since the anthropogenic emissions of carbon dioxide are a result primarily from combustion of fossil fuels, renewable energy sources have to be implemented in a much larger scale then before, worldwide.

The effect of global warming on Earth is of huge concern and occurs due to an increase in the greenhouse effect resulting especially from pollution. Hence, the carbon emissions must be reduced considerably faster than today, to mitigate the effects of climate change. At the Paris climate conference in December 2015, 195 countries adopted the first-ever universal, legally binding global climate deal. The Paris Agreement sets out a global action to put the world on track to avoid dangerous climate change by limiting global warming to well below 2 °C [4].The European Union‘s goal for 2020: ”renewable energies should have a 20 % share of the total energy production and overall CO_2 emission should be reduced by 20 %” [5], is another step in the right direction.

Renewable energy sources like sunlight, wind, waves and water, have potential to lower the speed of global warming when used instead of fossil fuels (coal, petroleum, natural gas, etc.). Sunlight, which is the most abundant energy source on Earth, can be utilized by different types of solar cells. Among them are bifacial solar cells, which simultaneously collect photons from incident and albedo radiation reaching both front and rear side of a solar module. Traditional, monofacial solar cells only collect photons reaching the front side of the module. Bifacial solar cells were initially described in the scientific literature by Luque et al. (1980) [1] as a new concept for improving the energy output of photovoltaic (PV) systems, and it has been investigated since the 1960s [2].

Bifacial solar cells could be the new direction within solar cell technology; when converting energy from sunlight to electricity. An increase of 50 % in electric power generation was showed by Cuveas et al. [6], which was obtained by simultaneously collecting direct and albedo radiation from the rooftop and surroundings around a module, using a concentrating device that increases albedo radiation. Consequently, an increase of the power density of photovoltaic (PV) modules was established by bifacial solar cells, while reducing area-related costs for PV power systems compared to monofacial cells [7].

The Earth consists of different climatic zones, which have an impact on the efficiency output a solar cell can achieve. The climate where a module of solar cells is installed, will to a large extent be of importance whether to select bifacial or monofacial solar cells to be profitable. The sun’s position according to the Earth throughout a year, hence the sun’s intensity, is an important factor to which climate is present on that respective position. The Nordic climate is characterized by relatively low temperatures and cold weather. This is due to the angle of incidence by which rays of sunlight are hitting the Nordic countries, which can be seen as small in comparison to for instance more Southern lying countries.

It has been shown from Guo et al. [8], that bifacial solar cells have better performance in the Nordic climate unlike monofacial cells. Where, under this global comparison, the vertically mounted bifacial modules were facing east-west and the conventional mounted monofacial modules were tilted according to the latitude (on that respective position) facing towards the equator (south). In this study it has been performed an

investigation on how the Nordic climate affect the bifacial solar cells and the correlation with the efficiency output of the cells. Different reflection materials have been investigated, along with different tilt angles on the cell. A monocrystalline silicon bifacial solar cell was used under the study, and the performed measurements were accomplished inside a chamber with a LED lamp, as well as outside with the sun as the light source.

Different characterization techniques[9;10] have been used up until now in order to characterize bifacial solar cells, as a standard technique do not yet exists. Bifacial solar cells present difficulties when measured due to their bilateral properties and hence external contributions from the measured systems itself[11]. An important challenge is to measure the efficiency output of the solar cell, in order to take into account contribution from both sides of the cell.

Light can pass through a bifacial solar cell, unlike a monofacial cell. Hence, a small portion of light is not absorbed at the back surface field (BSF), which will be consistent with spectral response measurements. If all light could be absorbed at the rear side of the cell, the spectral response could be maximized. Questions then arise, to whether an increase in efficiency will occur if part of the light passing through the cell is reflected and re-entering the rear side of the cell? If that is the case, what kind of reflection materials could be used beneath a bifacial solar cell? And what tilt angle is preferred under various conditions? The study's aim is to answer questions like these.

2 Theory

The essential theory for this project will be presented in this chapter. A description of how a bifacial solar cell is produced compared to a monofacial solar cell is given. Some theory about the solar energy is presented, along with an introduction to solar cell technology and solar cell performance. A description of the properties of light and its interaction with matter is given. Additionally, some important aspects on how the Nordic climate affect the bifacial solar cells are presented.

2.1 How a Bifacial Solar Cell is Produced

A bifacial solar cell can be produced using several different techniques and processing sequences, and here it will be explained one approach to create a bifacial solar cell. The cell described is developed on a p-substrate, but n-substrate is used as well in the bifacial solar cell production. A p-substrate and n-substrate are a positively and negatively doped silicon wafer, usually doped with boron and phosphorus, respectively. Figure 2.1 shows the cross-section view of standard p-substrate and n-substrate bifacial crystalline silicon solar cells [9]. The process of producing a bifacial solar cell is divided into nine steps, which will be explained in the following sections.

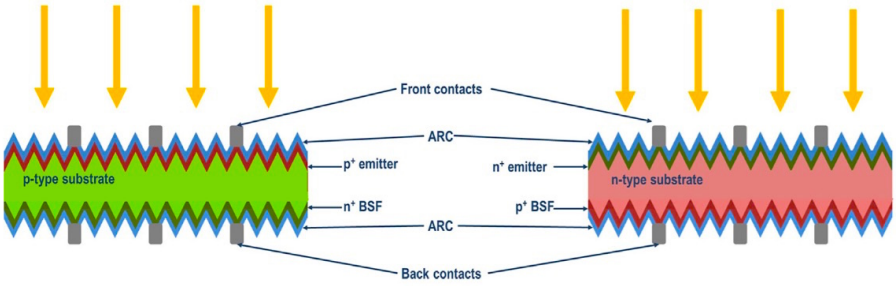

Figure 2.1: Cross-section view of standard p-type and n-type bifacial crystalline silicon solar cells [9].

2.1.1 Saw Damage Removal and Wafer Cleaning

Saw damage is created on the wafer during the wafer sawing step of the silicon bricks, which has to be removed before the wafer processing starts. A solution of sodium hydroxide (NaOH) is heated and the wafer is etched in the solution to remove about 4-6 μm of silicon from each side of the surface. The resulting surface on the Si-wafer has no saw damage and is polished.

Metallic impurities on the wafer are further removed in hydrogen chloride (HCl) bath, and then the wafer is dipped in concentrated hydrogen fluoride (HF) to make the wafer surface hydrophobic. The cleaning sequence up until this stage would be sufficient for phosphorous diffusion or other steps, but if the next step is boron diffusion, an extra cleaning step is needed to prevent the oven from contamination at high temperatures. A solution consisting of hydrogen peroxide (H_2O_2) and sulfuric acid (H_2SO_4) is then used, and is named IMEC bath or piranha bath. An oxide that removes the impurities from the surface is created in this bath, and the impurities are further removed in a second HF dip, which then completes the exhaustive cleaning process. The wafer is then dried in a nitrogen (N_2) air furnace [11].

2.1.2 BBr_3 Diffusion and In-Situ Oxidation

Boron diffusion to create the back surface field is the most decisive step in the solar cell process, when working with p-type substrates and to create the emitter when working with n-type substrates. Higher diffusion temperatures or longer processing times have to be applied for boron diffusion, due to the diffusivity of boron is much lower than that of phosphorous. Boron diffusion has to take place before the emitter diffusion, to avoid further diffusion of phosphorous atoms.

Diffusion is a controlled spread of particles from regions of higher concentration to regions of lower concentration, and it creates the p-n junction in the case of the semiconductor [12], when boron and phosphorous are diffused from either side, respectively. Diffusion can be achieved once the precursor is on the surface, by which there exist many modes to achieve: screen printing, roller printing, spin on or spray on coating, atmospheric pressure chemical vapor deposition (APCVD), among others, and high temperature is needed to step up the diffusion. This can be done in a special furnace, like an in-line (belt) furnace or a tube furnace.

The resulting sheet resistance (R_{sheet}), which is used to characterize the diffused layers, is affected by the carrier gas flow and the temperature. R_{sheet} is defined as the ratio of resistivity to sample thickness: $R_{sheet}=\rho/d$, where d is the thickness of the sample [11].

Boron can penetrate deep into the silicon to form thicker back surface fields, since the solubility limit of boron in silicon is 3.3x10^{20} cm^{-3} at 1100 °C and hence it can achieve an active surface concentration as high as 4x10^{20} cm^{-3} [13].

During the process of BBr_3 diffusion it is created a layer with a high concentration of boron silicon on the surface of the wafer which is named "boron rich layer" (BRL). It is important that this BRL is removed so the wafer can be hydrophobic, which is a necessary condition to continue the solar cell process. Also, in the boron rich layer the recombination of minority charge carriers is high. Recombination produces losses in the solar cell efficiency. An in-situ oxidation step is included during the diffusion process after the boron deposition, since the BRL layer is difficult to remove. The boron on the silicon diffuses into the silicon oxide, because the solubility of boron in silicon oxide is higher than in silicon. Thus, the concentration of boron will be reduced and therefore the carrier concentration of the direct surface is lowered. The direct surface is then oxidized. The boron rich layer is completely removed after a few minutes in hydrogen fluoride (HF), leading to a hydrophobic surface and allowing to continue with the processing steps [11].

A good diffused surface should be easy to be passivated and at the same time be deep enough to have a good contact formation in the region. These factors are a compromise and it is an important challenge to create a balance between all the elements, and to create a stable process in which the result is a homogeneous diffusion all over the wafer surface. The boron diffused layer has a surface concentration in the range of 1.5x10^{20} cm^{-3} and a good depth range would be between 0.2-0.4 μm.

The boron diffusion in a p-type solar substrate will create the back surface field (BSF) or rear side of the cell. The BSF of a solar cell is at the rear surface of the cell and consists of a higher doped region. An electric field forms at the interface between the high and low doped regions, due to these regions behave like a p-n junction. This again introduces a barrier to minority carrier flow to the rear surface. Thus, the minority carrier concentration is maintained at higher levels in the undoped region and the BSF has a net effect of passivating the rear surface.

In bifacial solar cells, long wavelengths have an indirect contribution when entering the device from the front side of the structure. Which contribute to the current generation at the rear side of the device, including the moving electrons into the bulk. The photons entering the device from the rear will directly contribute to this generation [11].

2.1.3 Silicon Oxide (SiO_2) / Silicon Nitride (SiN_x) Stack on the Rear Side

The quantum efficiency of the final solar cell can be improved, overall in the range of wavelengths below 700 nm. This can be achieved by passivate the boron diffused surfaces (p^+), by use of a double layer composed by silicon dioxide SiO_2 and silicon nitride SiN_x.

SiO_2 is a thin film (approx. 15 nm) of silica with high chemical stability, grown on the wafer surface through thermal oxidation. Then, a technique named Plasma Enhanced Chemical Vapor Deposition (PECVD) is used to create the SiN_x layer on top of the oxide, leading to the characteristic blue colour of the crystalline silicon solar cells.

The stack layer oxide-SiN_x serves as passivation and anti-reflection coating for the boron diffused surface. The produced layer also protects the rear side of the device against contamination when processing the front side of the device [11].

2.1.4 Front Side Etch Back and Texturization

On the top of the front side of the device, there exists a thin layer of silicon oxide covering a boron diffused layer, where both layers have come from previous steps as can be seen to the left in Figure 2.2 [11]. A front diffused-free surface is necessary, and hence these two layers must be removed before continuing to the next diffusion step. The phosphorus dopants coming in the next step, can otherwise not penetrate to diffuse into the silicon and form the emitter of the cell [11].

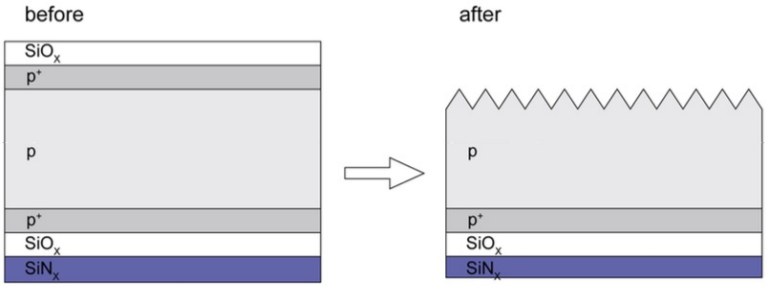

Figure 2.2: Cross section of the substrate before and after etch back and texturization [11].

Etch back of the front side of the substrate is done by first remove the silicon oxide layer in a HF solution during a few minutes, and then the boron diffusion is removed from the substrate by use of a NaOH solution. The resulting surface is polished silicon, and the substrates are ready to be textured [11].

To reduce the surface reflectance, texturization of the silicon surfaces is performed. An un-isotropic etch is used to form a pyramidal structure that can trap the light inside the cells by internal reflection. A heated solution mixture of potassium hydroxide (KOH) with water and isopropyl alcohol (IPA) is used as

the etchant. IPA helps to both remove hydrogen bubbles and to promote the formation of big pyramids. The wafers are completely submerged in the etch solution. The rear side of the device is protected by the SiO_2/SiN_x-layer, hence the texturization takes place only on the front side of the structure. The result of the texturization can be seen to the right in Figure 2.2 [11].

2.1.5 $POCl_3$ Emitter Diffusion

A cleaning step on the wafers are necessary after the texturization. This step includes HCl and HF dip to remove the metal contamination. Then, for p-type substrates, the n-type emitter is diffused using phosphoryl chloride ($POCl_3$). During the process of diffusion, phosphorous silicate glass is formed which must be removed before being passivated. This can be achieved by a HF dip for a few minutes [11].

2.1.6 Anti-Reflection Coating Silicon Nitride (SiN_x), Front Side

The anti-reflection coating (ARC) consists of a PECVD SiN_x:H layer, and its role is not limited to anti-reflection (AR) alone, it provides surface and bulk passivation as well. The standard SiN_x layer thickness can be between 70 to 75 nm with a refractive index of about $\sim$2, which lead to the characteristic blue colour of crystalline silicon solar cells [14] as mentioned in Section 2.1.3. In Section 2.1.3 a thicker layer of silicon nitride was needed. This was for processing further, some of the layer would be removed after cleaning the wafers in a solution of HF [11].

A minimum reflection at around 600-650 nm, is provided by the 70-75 nm thick SiN_x:H layer. This correspond to the maximum spectral emission of the sun between 400-700 nm, where most of this radiation is being absorbed by the solar cell surface.

Upon this stage the silicon substrates have a blue colour on both sides, but the front side looks a bit darker and is distinguishable to the rear side, due to the texturization which makes the surface less reflective. The rear side on the other hand is polished during the production, and it is very difficult to create a texturization on both sides. The front side is preferred to be textured, due to the fact that it will receive most of the solar radiation. Additionally, it is also instrumental for the conversion of light into electricity by the generation of charge carriers [11].

2.1.7 Screen Printing, Front Side

Silver paste is screen printed on the front side of the structure (with consecutive firing) to form the contacts, and it is the same material and grid pattern as the one used for standard (monofacial) solar cells. This is based on the approach to create a bifacial solar cell which uses the front side of a p-type solar cell, and hence it only changes the rear side to have more chances to capture reflected light coming from the bottom [11].

The design of the top contact is important, which involves the minimization of the finger[1] and busbar[2] resistance, but also includes the overall reduction of losses associated with the top contacts. These include the resistive losses in the emitter and in the metal top contact (thicker contact), and shading losses (thinner

[1] Fingers collect the generated direct current (DC) and deliver it to the busbar. The metallic and super-thin grid fingers are printed perpendicular to the busbars, and are connected by the busbar [15].

[2] Busbars conduct the electric DC power produced by the solar cell from the incoming photons [15].

contact). The critical features of the top contact design which determines these losses and need to be taken into consideration are: spacing of finger and busbar, metal height-to-width aspect ratio, minimum metal line width and resistivity of the metal[16]. Figure 2.3 shows how the busbars and fingers are printed according to each other on a solar cell[17].

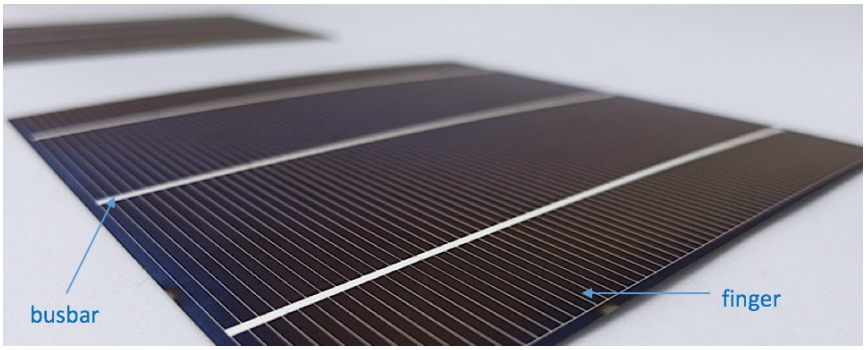

Figure 2.3: Polycrystalline silicon solar cell: busbars and fingers[17].

The measure of a standard screen printed finger is about 20 μm in height and 90-140 μm in width. In order to guarantee low series resistance and hence good fill factors, the amount of paste on 125x125 mm^2 substrates is about 110 mg. A cover of about 7-8 % of the active area is normal from the screen printed fingers and busbars, which cause shading losses[11].

2.1.8 Screen Printing, Open Rear Contact

The main aim of the bifacial solar cell is the collection of light from both the front and rear side of the solar cell, and for this reason aluminum paste (the back contact) cannot cover the rear side of the devise which is the case for a monofacial solar cell. The p$^+$-doped rear part of the device exhibits a blue silicon nitride-silicon oxide stack layer on the surface. It is then necessary to use another metal paste than aluminum to contact the rear side, since aluminum can not penetrate through the silicon nitride passivation.

A mixture of silver-aluminum (Ag/Al) paste is commonly used, which gives a sharp print and a good contact resistance to the p$^+$ back surface field. The rear side is printed in a similar mode to the front side, obtaining a finger of about 20 μm in height and 80-120 μm in width. The amount of paste on 125x125 mm^2 substrates is about 100 mg. A cover of about 7-8 % of the active area is normal from the screen printed fingers and busbars, and cause shading losses, which is the same value as for the front side of the device. Hence, the produced device is symmetric front and rear side in terms of the grid pattern, as can be seen from Figure 2.4[11].

When one side of the structure is printed, the cells go to a drier furnace to dry the metal paste for about 20 minutes at 200 °C. The normally used method to screen print the cells is to first print the front side, before drying the metal paste and then print the rear side. At this point in the process, the metal contacts have yet to be formed. To form the contacts, high temperature is needed in a process named co-firing, which will be explained in the next section, Section 2.1.9.

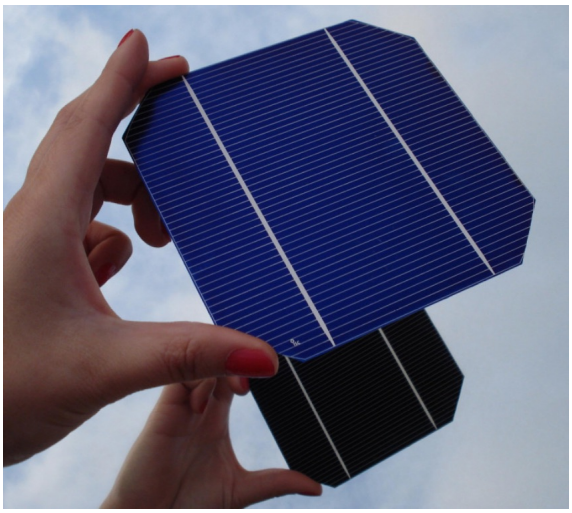

Figure 2.4: Picture of a finished bifacial solar cell with a mirror on the back to observe the grid pattern on both sides[11].

2.1.9 Co-Firing and Edge Isolation

The glass particles in the silver paste on the front side and those in the mixed silver-aluminum paste on the rear side, enable the penetration - throughout the firing process - of the paste through the silicon nitride layers to form contacts at the silicon surfaces.

The glass frits play a critical role on contact formation, where silver and silicon are dissolved in the glass frit upon firing. When the structure is cooled the Ag particles recrystallize, according to Schubert et al.[18]. Ballif et al. has further suggested that Ag crystallites serves as current pickup points, and that conduction from the Ag crystallites to the bulk of the Ag grid takes place via tunnelling[19].

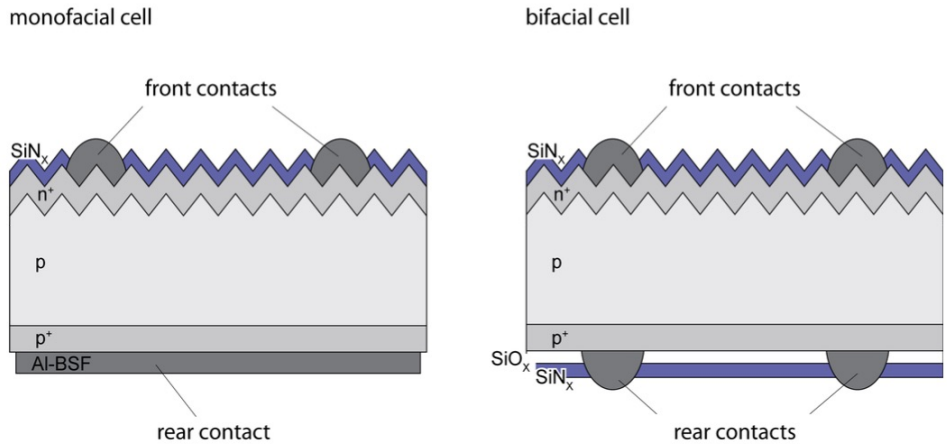

Figure 2.5: A schematic comparison for monofacial and bifacial solar cells[11].

Edge isolation is the last step to be performed, in order to avoid the short circuit between the emitter and the back contact of the cell, and then the solar cell process is complete. Laser scribing is one of the

most successful edge isolation processes, and is perfectly suitable for inline processing and the wafer remains untouched, which is an important requirement for the handling of thin wafers. Wet chemical etching, plasma etching, dicing saw or sand paper, are other possible techniques to perform edge isolation [20]. A schematic comparison for monofacial and bifacial solar cells can be seen in Figure 2.5 [11].

The sequence process can be maintained, when these cells (see Figure 2.5) are based on an n-type substrate instead of a p-type substrate. In that case the emitter (front side) would be the boron diffused surface (p^+) and the back surface field would be phosphorous (n^+).

2.2 Bifaciality

Bifacial solar cells can collect photons from incident and albedo radiation (Section 2.3.1.1) reaching both the front and rear side of a solar module, simultaneously. These cells offer a promising possibility to reduce the levelized cost of energy (LCOE) for many photovoltaic (PV) applications. There exists a huge application field for this new upcoming technology, such as sound blocking systems, floating systems and even in utility-scale systems using trackers. In addition to many potential application fields, there are different installation options: from standard slanted systems, to horizontal to even vertical bifacial installations with almost zero ground coverage [21]. Figure 2.6 depicts these different mounting geometries for bifacial solar cell modules: (a) slanted S/N (south/north) oriented mounting, (b) horizontal B/T (bottom/top) and (c) vertical E/W (east/west) oriented mounting [21]. Along with (d) the resulting daily power generation curves compared to monofacial ones in the same configuration. The best choice on how to mount the bifacial solar cell module, depends to a large extent on where in the world the system is positioned (latitude) and the application of the system itself.

Section 2.1 gives important information to how a bifacial solar cell is produced compared to a monofacial solar cell, which gives the background to why a bifacial cell operates as it does compared to a monofacial cell. The bifacial solar cell has a rear side that is slightly different from the front side, by which the front side of the cell has been textured to reduce the surface reflectance. Hence, a pyramidal structure has been formed that can trap the light inside the cell by internal reflection. The rear side of the bifacial solar cell has not been textured and hence will reflect away more of the light that strikes upon it than the front side does. In most cases, the front and rear side of a bifacial solar cell will not contribute equal to the efficiency output of the cell. This is because of that said above and because of the amount of radiation that reaches each side of the cell is different. The solar cell technology is explained in Section 2.4.

2.2.1 Definition of Bifacial Gain

Analyzing the bifacial gain - the difference in the energy yield if bifacial and monofacial devices with identical installation configurations are compared – is an obvious way to visualize the benefits of bifaciality. In a comparison like this, it is important that the devices are of similar type and with the same front side efficiency are compared. Hence, the best choice when you want to observe the bifacial gain only, is to use the same bifacial cell in a module with a black rear cover (or black back-sheet is required) as a reference [21]. The additional energy provided by the rear side only, will then be revealed when comparing this reference against the bifacial device. If e.g. a monofacial device is used as reference with a backsheet, the outcome of the bifacial gain will be different, due to differences in bifacial and monofacial solar cells, respectively.

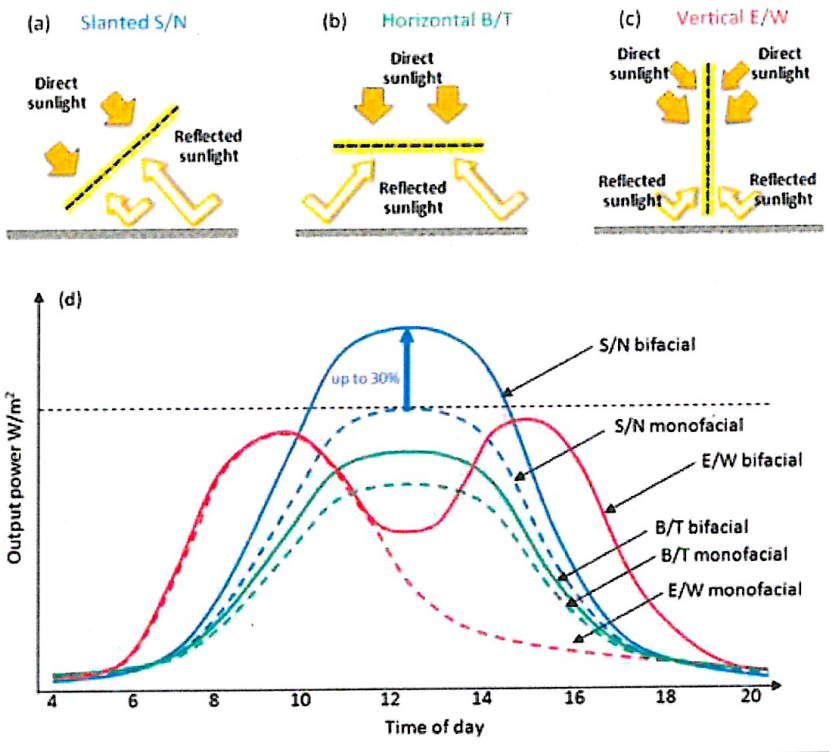

Figure 2.6: Possible mounting geometries for bifacial solar cell modules: (a) slanted S/N (south/north) oriented mounting, (b) horizontal B/T (bottom/top) and (c) vertical E/W (east/west) oriented mounting. And (d) resulting daily power generation curves compared to monofacial ones in the same configuration [21].

Bifacial gain can be defined as:

$$g_{bifacial}\,[\%] = \left(\frac{e_{bifacial} - e_{monofacial}}{e_{monofacial}}\right) \cdot 100 \tag{2.1}$$

where $e_{bifacial}$ is specific energy yield [kWh/kWp[3]] of the PV system with bifacial modules and $e_{monofacial}$ is the specific energy yield [kWh/kWp] of the PV system with monofacial modules on the same site, with the same configuration and during the same time period. The bifacial gain is a way to indicate the energy yield, and it is the metric that determines the LCOE [€/kWh], together with the total cost of installing and operating the bifacial PV system [21].

2.3 Solar Energy - Light Through the Atmosphere

Solar radiation is the electromagnetic radiation emitted by the sun, often referred to as the solar resource. Light with a range of wavelengths, spanning the ultraviolet, visible and infrared section of the electromagnetic spectrum is emitted by the sun. At the sun's surface the total emitted power density is 62 MWm^{-2}. As the distance to the sun increases, only a small portion of the solar power density reaches the Earth. Figure 2.7 shows the amount of radiant energy received at a point outside the Earth's atmosphere, from the sun

[3]kWp data usually reflects STC front side measurements of the bifacial module(s).

per unit area per unit time – the solar irradiance – as a function of wavelength [22]. This extraterrestrial spectrum resembles the spectrum of a *black body* and the Sun acts as a perfect emitter of radiation at 5760 kelvin (K) [23].

The mean solar radiation flux incident on a unit area perpendicular to the beam outside the Earth's atmosphere is known as the *solar constant* [24]:

$$S = 1367\, Wm^{-2} \tag{2.2}$$

2.3.1 Atmospheric Effects

When solar radiation passes through the Earth's atmosphere, some of the incident energy is removed by *scattering* and *absorption* by various atmospheric constituents, such as air molecules, clouds and particulate matter usually referred to as aerosols. Hence, the spectrum reaching the Earth's surface is both attenuated and changed in shape. Light of wavelengths less than 300 nm is filtered out by atomic and molecular oxygen, ozone and nitrogen. Water and CO_2 absorb mainly in the infrared part of the spectrum, which can be seen as dips in the absorption spectrum in Figure 2.7 [22].

Solar radiation that reaches the surface directly in line from the solar disc is known as *direct* or *beam radiation*, hence the radiation has not been scattered nor reflected [24]. *Diffuse radiation* means that a fraction of the light is scattered by the atmosphere, i.e. incident from all angles rather than direct from the sun. Fraction of diffuse radiation is on average approximately 15 %, but larger at higher latitudes and regions where it tend to be a significant amount of cloud cover [23].

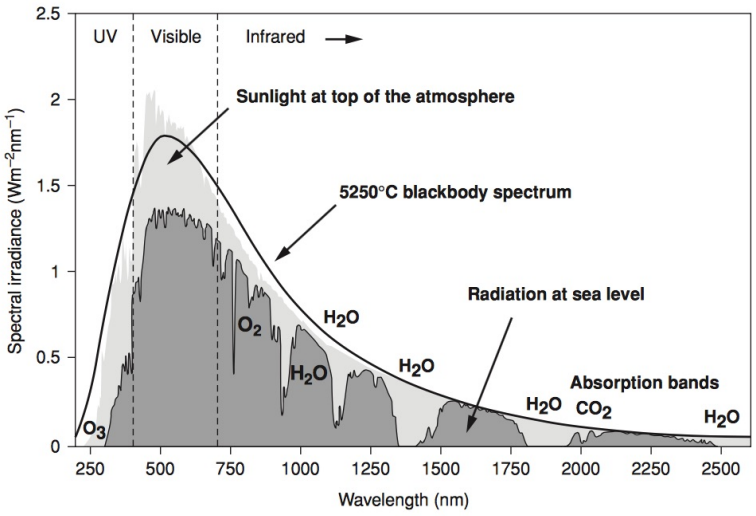

Figure 2.7: Extra-terrestrial (Air Mass 0) solar spectrum (shaded light grey), compared with the 5250 °C black body spectrum, which approximates the space spectrum of the sun (black line). As well as the standard terrestrial (Air Mass 1.5) spectrum, that survives the absorption of molecules such as H_2O and CO_2 in the Earth's atmosphere (shaded dark grey). Note also the substantial ozone (O_3) absorption in the UV part of the spectrum [22].

2.3.1.1 Albedo Effect

Albedo is radiation which reaches a specific site after being reflected from the ground. Bifacial solar cells can use this albedo effect as an advantage to increase it's effect, by using a material of highly reflective characteristic surrounding the cells. Total radiation consisting of direct- and diffuse radiation and albedo is named *global radiation* [24].

2.3.1.2 Air Mass

Attenuation of the Earth's atmosphere is quantified by the "Air Mass" factor, $n_{AirMass}$, defined as

$$\begin{aligned} n_{AirMass} &= \frac{optical\ path\ length\ to\ Sun}{optical\ path\ length\ if\ Sun\ directly\ overhead} \\ &= cosec\,\gamma_s \end{aligned} \tag{2.3}$$

where γ_s is the angle of elevation of the sun. The Air Mass $n_{AirMass}$ spectrum is an extraterrestrial solar spectrum attenuated by $n_{AirMass}$ thickness of an Earth atmosphere of standard thickness and composition. Hence, Air Mass is a concept which characterizes the effect of a clear atmosphere on sunlight.

Standard spectrum for temperature latitudes is *Air Mass 1.5* (abbreviated AM1.5), corresponding to the sun being at an angle of elevation of 42°. This atmospheric thickness should attenuate the solar spectrum to a mean irradiance of about 900 Wm^{-2}. Nevertheless, for convenience, the standard terrestrial solar spectrum is defined as the AM1.5 spectrum normalized, hence the integrated irradiance is 1000 Wm^{-2}. Actual irradiance will vary on account of both seasonal and daily variations in the position of the sun and orientation of the Earth and condition of the sky. Global annual average solar irradiance can vary from less than 100 Wm^{-2} at high latitudes to over 300 Wm^{-2} in the sunniest places, as can be seen in Figure 2.8 [23].

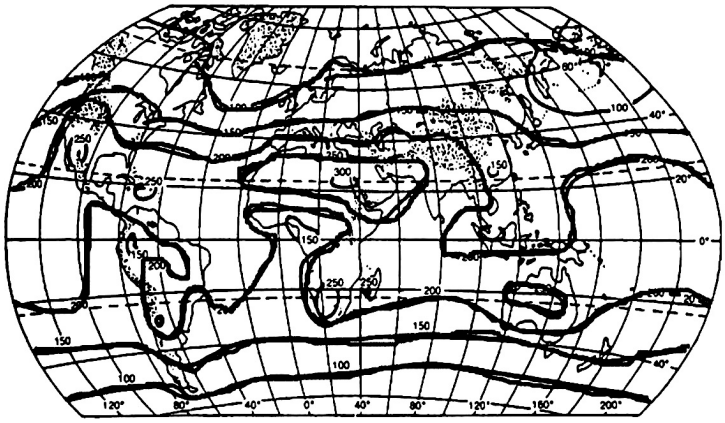

Figure 2.8: Global distribution of annual average solar irradiance. The values on the irradiance contours are given in Wm^{-2} [23].

2.3.2 Irradiation Variations on Earth

Global irradiance can be as high as 1 kWm^{-2}, due to rotation of the Earth and adverse weather conditions, although the available irradiance is usually considerably less than this maximum. For illustration, Figure

2.8 shows the mean annual irradiance in different parts of the world [23]. Near the latitudes of the tropics of Cancer and Capricorn the mean irradiance is highest, while it is lower in equatorial regions on account of the cloud cover. Solar radiation is weaker in higher latitudes, due to low solar elevation [24].

The output of light energy from the entire disk of the Sun, measured at the Earth, is known as the solar irradiance. The design of photovoltaic systems need to take into consideration the irradiance over one day, to be able to get the highest efficiency possible. Optimum panel angle for monofacial solar cells which tend to give a good efficiency, is usually close to the latitude angle of the site where it is going to be mounted. Whereby, bifacial solar cells can give a good efficiency by mounted vertically facing east-west [8].

2.4 Solar Cell Technology

2.4.1 Photovoltaic Effect

Solar cell technology is based on the ability of semiconductors to convert sunlight directly into electricity due to the *photovoltaic effect*. Through this process of converting the energy, the incident energy of light (sunlight) creates mobile charged particles in the semiconductor which are then separated by the device structure and produce electrical current [24].

Photovoltaic energy conversion relies on the quantum nature of light, by which light is perceived as a flux of particles - *photons* - which carry the energy

$$E_{ph}(\lambda) = h\nu = \frac{hc}{\lambda} \tag{2.4}$$

where h is the Planck constant, ν is the frequency of light, c is the speed of light, and λ is the wavelength of light. About 4.4x10^{17} photons strike a square centimetre of the Earth's surface every second on a clear day. Only those photons with energy in excess of the bandgap in the semiconductor material used (normally silicon (Si), energy gap 1.12 eV), can be converted into electricity by the solar cell [24]. When losses are neglected, each photon can contribute with one electron charge to the generation current. Hence, the light-generated current is than equal to

$$I_l = q\mathscr{N}A \tag{2.5}$$

where $\mathscr{N}$ is the number of photons in the highlighted area of the spectrum, and A is the surface area of the semiconductor that is exposed to light. Current density can be expressed as [24]

$$J_l = \frac{I_l}{A} \tag{2.6}$$

2.4.2 Conversion of Sunlight to Electrical Energy

Bifacial solar cells which absorb light coming from both sides of the cell, are not only dependent on sunlight, but also the albedo effect (Section 2.3.1.1) which is enhanced by use of good reflection material surrounding the cell.

A solar cell conducts like a diode in the dark and generates a photovoltage when charged by the sun. The I-V characteristic of a diode is given by the Shockley equation which relates the current and voltage under zero illumination:

$$I = I_o \left[exp\left(\frac{qV}{k_B T}\right) - 1 \right] \tag{2.7}$$

where I is the current, I_o is the *dark saturation current*, V is the voltage, k_B is the Boltzmann constant, q is the magnitude of the electron charge, and T is the absolute temperature in kelvin [24].

Incident photon flux generates *electron-hole pairs* on both sides of the p-n junction, by absorption of photons with energy in excess of the bandgap. Hence, each semiconductor is restricted to only converting a part of the solar spectrum. The generated minority carriers - electrons from the p-side and holes from the n-side (positively and negatively doped semiconductor, respectively) - then diffuse to the junction and are swept away by the electric field, thereby producing electric current across the cell. Due to the fact that electrons and holes carry opposite charges, the electric currents of these particles reinforce each other. The p-n junction therefore separates the carriers with opposite charge, and the generation current I_l between the bands get transformed into an electric current across the p-n junction [24].

I-V characteristic of a solar cell can be obtained by drawing an equivalent circuit of the devise, as can be seen in Figure 2.9(a) [25]. Generation of current I_l by light is represented by a current generator in parallel with a diode which represents the p-n junction. Output current I is equal to the difference between the light-generated current I_l and the diode current I_D. Equation (2.8) then gives

$$I = I_l - I_o \left[exp\left(\frac{qV}{k_B T}\right) - 1 \right] \tag{2.8}$$

Important to notice is that all light-generated current passes through the diode under open circuit when I=0. On the other hand, all this current passes through the external load under short circuit (V=0). Figure 2.9(b) shows the I-V characteristic Equation (2.8) and its relationship to the diode characteristic [26].

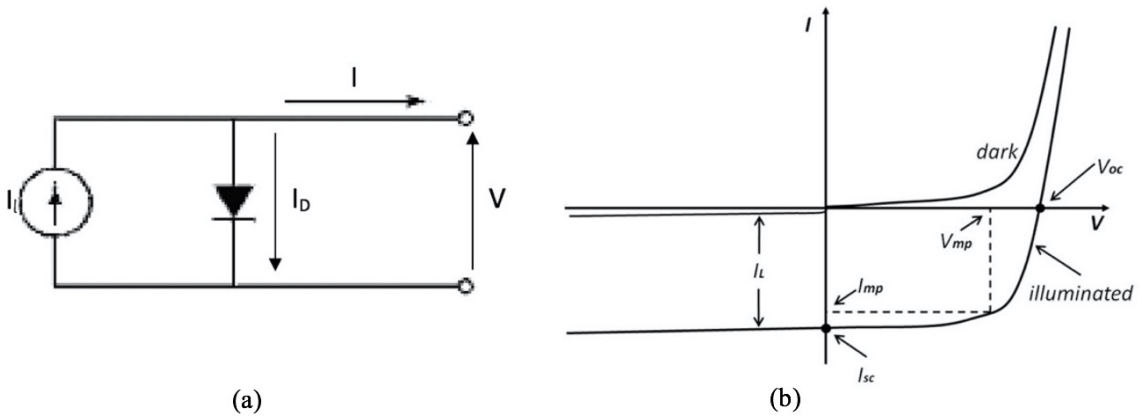

Figure 2.9: (a) Shows the equivalent circuit [25] and (b) the I-V characteristic [26] of a solar cell compared to a diode.

2.4.2.1 I-V Characteristics of a Solar Cell

The I-V characteristic of a solar cell contains some important points: (i) the short-circuit current I_{sc} which is simply the light-generated current I_l, and (ii) the open-circuit voltage V_{oc} is obtained by setting I=0:

$$V_{oc} = \left(\frac{k_B T}{q}\right) ln\left(\frac{I_l}{I_o} + 1\right) \tag{2.9}$$

Even though both I_l and I_o depend on the structure of the device, it is the value of I_o that determines the open-circuit voltage in practical devices. I_o can vary by many orders of magnitude, depending on the device geometry and processing[24].

2.4.2.2 Maximum Power Point and Efficiency

No power is generated under short or open circuit. On the other hand, the maximum power P_{max} is produced by the device on a point where the product IV reaches maximum. Figure 2.9(b) shows this graphically where the position of the *maximum power point* represents the largest area of the rectangle shown[26]. The fill factor FF is defined by

$$P_{max} = V_{mp} I_{mp} = FF V_{oc} I_{sc} \tag{2.10}$$

where V_{mp} and I_{mp} are the voltage and current at the maximum power point, respectively. A solar cell's energy conversion efficiency "η" can be seen as the percentage of incident light energy that actually ends up as electric power, and is defined as[11]

$$\eta = \frac{P_{max}}{P_{in}} = \frac{P_{max}}{E A_c} \tag{2.11}$$

where the power P_{max} is produced by the cell at maximum power point under standard test conditions, divided by the power of the radiation incident upon it P_{in}. P_{in} can be stated by the input light irradiation E [$\mathrm{Wm^{-2}}$] under standard test condition multiplied by the surface area of the solar cell A_c [$\mathrm{m^2}$]. Standard Test Condition (STC) for photovoltaic (PV) modules is specified by standard reference AM1.5 spectrum, an irradiance of 100 $\mathrm{mWcm^{-2}}$ (one-sun of illumination), and temperature 25 °C[24].

2.4.2.3 Power Losses in Solar Cells

Power losses decrease the efficiency output of a solar cell with a considerable amount. The I-V characteristic represented in Equation (2.8) is a sufficient description of a simplified solar cell, but due to losses and deviation from ideality, it might be necessary to include parameters which can compensate for this nonideality. The I-V characteristic of a practical device can be approximated by a modified expression:

$$I = I_l - I_o \left[exp\left(\frac{qV + IR_s}{mk_B T}\right) - 1\right] \tag{2.12}$$

which also includes the series resistance R_s, due to an impact of ohmic losses on the transmission of electric current by the solar cell. m is an empirical *nonideality factor* whose value is usually close to unity. The light-generated current in Equation (2.12) is a measured parameter which takes into account all the current losses in the cell.

Fundamental losses[4], recombination[5] and parasitic resistance[6], have a negatively effect on the theoretical maximum efficiency a solar cell can obtain, and need to be emphasized when the performance of a photovoltaic module is investigated [24].

2.4.3 Quantum Efficiency (QE)

Spectral response is another important method to characterize the performance of a solar cell, which is conceptually similar to the quantum efficiency (QE). This leads to

$$SR = \frac{q\lambda}{hc} \cdot QE \tag{2.13}$$

where QE can be seen as the ratio of the number of charge carriers collected by the solar cell to the number of photons of a given energy shining on the solar cell. Hence, the quantum efficiency can be related to the response of a solar cell to the various wavelengths in the spectrum of light shining on the cell, and is given as a function of either wavelength or energy.

Quantum efficiency of a solar cell is often divided into two types, namely External Quantum Efficiency (EQE) and Internal Quantum Efficiency (IQE). The EQE "is the ratio of the number of charge carriers collected by the solar cell to the number of photons of a given energy shining on the solar cell from outside (incident photons)" [11]. Whereby, the IQE "is the ratio of the number of charge carriers collected by the solar cell to the number of photons of a given energy that penetrate into the solar cell from outside and are absorbed by the cell" [11].

2.4.4 Temperature and Irradiance Effects

Solar cells do not operate under standard conditions in practical applications, mainly due to the variable temperature and irradiance. Temperature has an important effect on the power output from the solar cell, and the most significant is the temperature dependence of the voltage. The voltage decreases with increasing temperature, and the voltage decrease of a silicon cell is typically 2.3 mV per degree Celsius [24]. Equation (2.9) shows that V_{oc} is directly related to J_{sc} and J_o, where current density is related to current as shown in Equation (2.6), and $J_{sc} \approx J_l$ for a high-quality solar cell. A low J_o is necessary to achieve a high V_{oc}.

Since J_o is a measure of the leakage (or recombination) of minority carriers across the p-n junction in reverse bias, and the fact that the minority carriers are thermally generated, J_o is highly sensitive to temperature changes. Reverse saturation current density, J_o, for a p-n junction solar cell, can be estimated by

[4]Fundamental losses: Carrier generation in the semiconductor by light involves considerable dissipation of the generated carrier energy into heat. A considerable part of the solar spectrum is, in addition, not utilized because of the inability of a semiconductor to absorb the below-bandgap light [24].

[5]Recombination: An opposite process to carrier generation is recombination when an electron-hole pair is annihilated. Recombination usually occur at impurities or defects of the crystal structure, or at the surface of the semiconductor where energy levels may be introduced inside the energy gap. These levels act as stepping stones for the electrons to fall back into the valence band and recombine with holes [24].

[6]Parasitic resistance: The transmission of electric current by the solar cell involves ohmic losses. These can be grouped together and included as a resistance in the equivalent circuit (see Figure 2.9(a)). The series resistance mainly affect the cell operation by reducing the fill factor [24].

$$J_o = q\left(\frac{D_n}{L_n N_A} + \frac{D_p}{L_p N_D}\right) n_i^2 \tag{2.14}$$

where, n_i is the intrinsic carrier density, N_A and N_D are densities of acceptor and donor atoms, D_n and D_p are diffusion constants of minority carriers in p and n regions, and L_n and L_p are diffusion lengths of minority carriers in n and p regions, respectively [27]. It can be observed from Equation (2.14) that J_o is strongly determined by the intrinsic carrier density, and n_i can be represented as

$$n_i^2 = N_c N_v \, exp\left(-\frac{E_g}{k_B T}\right) = 4\left(\frac{2\pi k_B T}{h^2}\right)^3 m_e^{*3/2} \, m_h^{*3/2} \, exp\left(-\frac{E_g}{k_B T}\right) \tag{2.15}$$

where, N_c and N_v are effective density of states in conduction band and valence band, and m_e and m_h are effective mass of electron and hole, respectively [27]. An expression for J_o in terms of temperature and bandgap energy, can be obtained by combining Equation (2.14) and (2.15) as

$$J_o = CT^3 \, exp\left(-\frac{E_g}{k_B T}\right) \tag{2.16}$$

In Equation (2.16), C is a constant where doping and the material parameters of solar cells are combined. Further, the Equation (2.16) shows that the important solar cell parameters for model calculations are the temperature and bandgap. A high bandgap will give a low saturation current density by Equation (2.16) [27].

An increase in temperature will give an increase in the intrinsic carrier density (n_i), which again will give an increase in the dark saturation current density, J_o. V_o will be reduced as an effect from an increased dark saturation current. Increased temperature will at the same time reduce the bandgap and increase the photocurrent (J_{sc}), due to lower energy photons can now be absorbed. Hence, the net effect that occur is a reduction in efficiency, due to the reduction in V_{oc} which outweighs the increase in J_{sc} [23].

2.5 Interaction of Light with Matter

The basic physical picture of light has altered between a particle model and a wave-based model. Both models are equally valid and depend on the experiment performed. One experiment can be most natural explained by treating light as discrete particles (photons), while another experiment is most natural explained by treating light as a wave [28].

In the case of studying solar cells, the most natural model to use is the quantum field model, where light consists of photon particles which travel and interact with matter. The interaction depends upon details such as structure of the matter and wavelength of the light. The photovoltaic effect as described earlier in Section 2.4.1, is a significant aspect of the particle-like behaviour of light. The energy of a photon E_{ph} can be obtained by Equation (2.4), and is an important parameter when quantifying the order of magnitude of the phenomena [28].

The spectrum of light reaching the Earth's surface is both attenuated and changed in shape, due to light gets absorbed and scattered by various atmospheric constituents upon passing through the atmosphere (Section 2.3.1). Interaction between photons in incident light and a medium of bound absorbing electrons is known as absorption. Whereby, scattering is an interaction where photon is absorbed and immediately re-emitted,

normally in a different direction. The term elastic scattering is used when the incoming and the outgoing photon has the same energy. The most frequent photon-electron interaction in nature is elastic scattering.

2.5.1 Reflection and Different Surfaces

A bifacial solar cell can absorb light coming from both sides of the cell, in comparison to a monofacial solar cell where the rear side has a thick layer of metal paste, which do not allow light crossing through. The surroundings of a bifacial solar cell will affect the efficiency of the cell, depending on reflective characteristics. The cell can then take advantage of the albedo effect (Section 2.3.1.1) and the light transmitted through the cell, that has not been absorbed at the BSF. Hence, the reflected light back onto the rear side of the bifacial solar cell can increase the efficiency of the cell.

Reflectivity and reflectance can be defined as the fraction of incident electromagnetic power that is reflected at an interface[29]. Different surfaces possess different reflectivity characteristics, hence absorb different wavelengths of the light. Important points to be taken into consideration when choosing a material are good reflectivity characteristics, not too expensive, and also possesses god stability due to the different weather conditions.

2.5.1.1 Snow as a Reflectivity Material

The Nordic countries can have a lot of snow, especially during the winter season. Snow can then be used as a cheap reflectivity material during that season. Reflectance from snow is significant all across the visual spectrum, hence its white colour. The transmitted light through the bifacial solar cell, could easily be reflected back up into the rear side of the cell by the use of snow. The most significant effect on the solar cells, although, might be the contribution of radiation coming from the albedo when utilizing snow as a reflectivity material. For thin snow layers, albedo will be dependent on the snow depth, and typical values of albedo for a snow layer of a few centimetres deep is 70 to 90 %[30]. Figure 2.10 shows the albedo vs. snow depth for a shallow snow layer[31].

2.5.2 Snell's Law of Refraction and Fresnel's Equation

Snow and water/ice which might come upon a bifacial solar cell, can have a negative effect on the efficiency of the cell. Snow, for instance, has good reflectivity characteristics, and light can be reflected away from the cell even before it has reached it.

Incident radiation on a solar cell will be altered if the surface is "contaminated". Snell's law of refraction can be used to explain what will happen when light passes from one medium to another. When light travels through air and is incident upon a surface of a transparent material, a fraction of light will be transmitted into the material, while another fraction will be reflected.

Light changes speed as it passes from one medium to another, known as refraction, where the frequency of light does not change as it refracts. The ratio of the speed of light in vacuum to the speed of light in a medium is named the (absolute) real refractive index and is denoted by n[28]. The higher the index of refraction, the denser the medium. Refraction is dependent on the medium through which light passes.

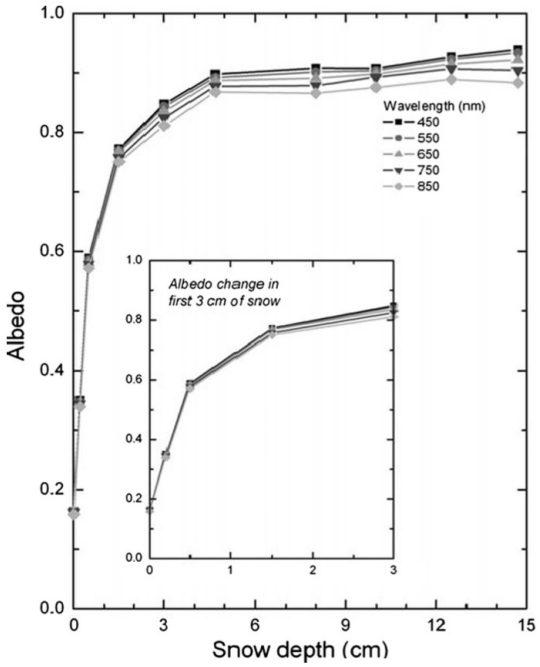

Figure 2.10: Albedo vs. snow depth for a shallow snow layer. The measurements were undertaken as snow fell, hence the snow studied is very fresh [31].

Snell's law describes the relationship between angle of incidence and refraction, when waves of light passes through a boundary of two dissimilar isotropic media, expressed as follows

$$\frac{n_2}{n_1} = \frac{v_1}{v_2} = \frac{\sin\theta_1}{\sin\theta_2} \tag{2.17}$$

where n_j is the refractive index and v_i is the speed of light in a specific medium. The angle of incidence, θ_i, is defined as the angle of incoming light beam with respect to the normal of the interface [23]. From Equation (2.17), it can be seen that the velocity of a ray in a medium also can be included as a ratio describing the refraction of light, due to the ratio of the phase velocities is equivalent to the angles of incidence and refraction. The angle of incidence is, however, the most important parameter which greatly affect the fraction of reflected rays. Figure 2.11 illustrates the geometry of the reflection from and transmission through an interface between two media with different indices of refraction n_1 and n_2 [28].

In the case when light is striking the interface at normal incidence, the reflectance (R) can be simplified by the Fresnel equation [23]

$$R = \left(\frac{n_1 - n_2}{n_1 + n_2}\right)^2 \tag{2.18}$$

2.5.3 The Beer-Lambert Law

Characteristics of the material have to be investigated, in order to understand how light is attenuated when entering a new medium. The Beer-Lambert law relates the attenuation of light to the properties of the

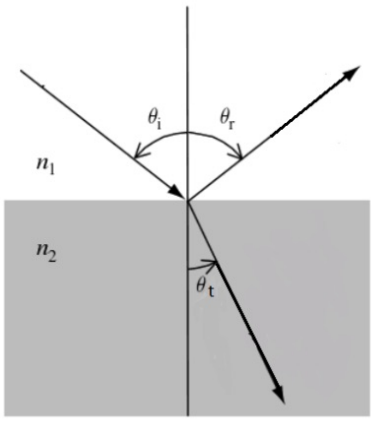

Figure 2.11: Geometry of the reflection from and transmission through an interface between two media with different indices of refraction n_1 and n_2 [28].

material through which the light is traveling, and is expressed as

$$A_{abs} = log_{10}\frac{P_o}{P} = \epsilon lc = \alpha l \tag{2.19}$$

where A_{abs} is the absorbance, P_o is the incident radiant power, P is the transmitted radiant power, ϵ is the molar absorptivity (sometimes called molar absorption coefficient) [$dm^3 mole^{-1} cm^{-1}$], l is the length of the light path [cm], and c is the concentration of the absorbing medium [mole dm^{-3}]. The molar absorptivity and the concentration of the absorbing medium, can be combined to form an absorption coefficient α [cm^{-1}] for a given medium of constant concentration. A sample has absorbed some of the light, if the power in a beam of electromagnetic radiation is different before and after having passed a sample of another matter [32].

The Beer-Lambert law has some conditions which have to be fulfilled in order to be valid. The beam of light should be monochromatic, that is light with only one wavelength. Additionally, the concentration parameter in the law should be the actual concentration of the absorbing medium, and the length of the light path should be known.

Deviations from the conditions mentioned above, will be present in real cases. Solar cells, for instance, which use the solar radiation as the energy source, is made up of a spectrum of UV, visible and infrared light with respective wavelengths. The absorption coefficient α also varies with the wavelength of the incident light [32].

2.6 How the Nordic Climate Affect the Bifacial Solar Cells

Where on Earth the solar cell is positioned, is of huge importance for how much solar radiation the cell gets upon it, thereby how much electricity the cell can produce. The radiation is weaker in higher latitudes, due to low solar elevation, compared with equatorial regions [24]. The climates in the different regions will also play an important role to how good the solar cell efficiency output will be, which again is affected by the solar radiation in that specific region.

2.6.1 Climatic Zones

The sun shines more obliquely, as latitudes increases, and provides less warming energy. Hence, average temperature cool with increasing latitude, producing well-defined climatic zones on the planet; tropic, temperate and polar zones. The Nordic climate consists of two zones; temperate and polar zone, respectively. Regions in the temperate zone experience moderate temperatures and large temperature variations. The summer tend to be hot and the winters cool. Whereby the regions in the polar zone experience cold temperatures and sparse vegetation [33].

The Nordic climate is characterized by relatively low temperatures and cold weather, in comparison to for instance countries like Spain, Italy and Greece. PV technology faces certain challenges in cold climates. Such as snow and ice that may form and accumulate on the panels, obstructing light from reaching the cells, and thus hampering electricity production. The electricity generation of the panels will be significantly reduced by full or partial obstruction, at a rate disproportional to the area being shaded [34]. Snow and ice may linger on the panels for extended periods of time after their formation, until it melts away or is otherwise removed. Figure 2.12 shows a map of the mean snow cover duration from 2000 to 2011 for Europe [35]. It can be seen from the map that the Nordic climate is to a large extent affected by snow cover.

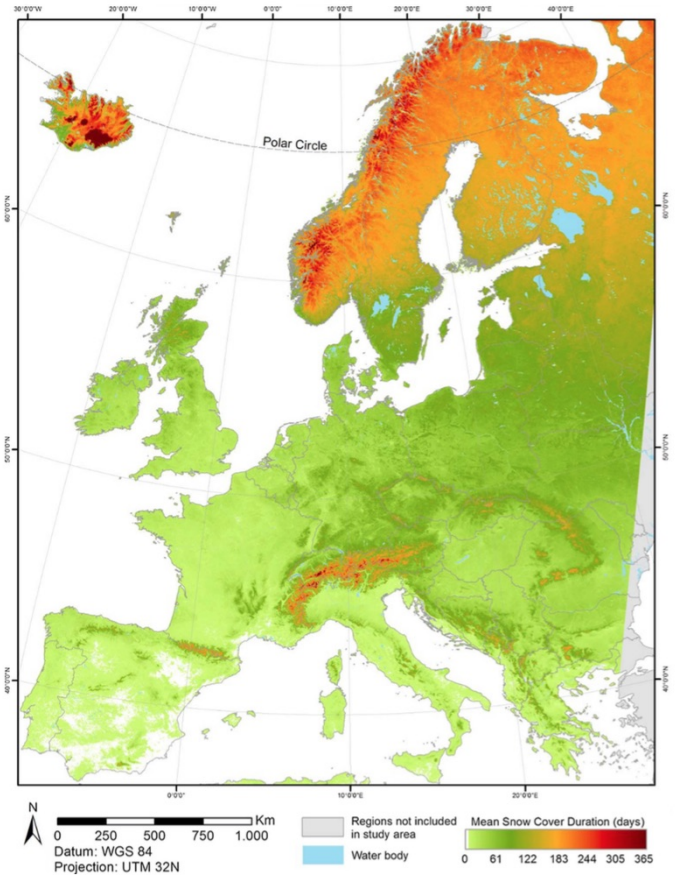

Figure 2.12: Mean snow cover duration from 2000 to 2011 for Europe [36].

2.6.2 Influence of Snow and Ice

Even though a bifacial solar cell can absorb solar radiation from both sides of the cell, a cover up of the front side due to snow (and ice) will reduce the electricity generation with a huge amount. Since the front side of a bifacial solar cell, without any cover-up, is the site where the most of the contribution to the high efficiency comes from. A distinction between snow and ice must be made, due to the fact that snow will reflect most of the radiation upon it, while ice is to a large extent transparent to the radiation [37].

Snow is not a homogeneous substance. The "active layer", the top few centimetres of the snow cover, has somewhat different optical properties than the snow deeper into the snowpack. This is due to the surface snow is not compressed by the weight of more snow above it, making it lighter and "fluffier". The optical properties of the snow pack will be influenced by its underlying surface, at snow depths lower than the thickness of the active layer. The active layer has a higher extinction coefficient than the deeper snow, resulting in a more rapid extinction of solar radiation passing through it [30].

When disregarding radiation absorption in snow, it is evident that a snow cover will inherently reduce the incident solar radiation to an underlying solar cell to a fraction by virtue of reflectance alone, regardless of the depth of the snow pack. The albedo will decrease as the snow melts, but as the snow's water content then will increase, radiation absorption will increase to make the snow even less transmissive [31]. As can be seen from Figure 2.10 earlier in the theory, impact of reflection (albedo) losses alone is great enough to severely hamper the electricity production, even for very thin snow layers [31]. It only takes a centimetre of snow to reduce the potential radiation transmission by two thirds, even without factoring in absorption.

Uniform shading due to clouds blocking solar radiation or the sun setting, reduces the output of the system of solar cells. While partial shading causes complex changes to the balance of electric currents against the conductive properties of the cells. Both uniform and partial shading can be caused by snow and ice under various circumstances. Hence, it is necessary in snow-prone areas to examine the behaviour and influence of snow and ice on photovoltaic panels, to accurately determine and improve the long-term performance of solar power [35].

Heavy snow loads may bend the frames of photovoltaic systems before any glass breakages occurs. A module may then survive a "fatal" snow load by itself, but the risk of micro-fractures might ruin the panel even without the glass taking any visual damage. Hence, it is advised to thoroughly inspect a module that is forced out of its fastenings rails, before putting it back to use [37].

It should be noted, however, high reflectivity of snow could be of advantage for photovoltaic production if the panels are not covered themselves, as mentioned in Section 2.5.1.1. Hence, some solar radiation will be reflected onto them from their surroundings, adding to that which hits the panels directly. It could be concluded by Williamson et al. (2016) [38] and Coppin et al. (1978) [39], that the incoming reflected light from the surroundings will be three to six times higher when they are covered in snow.

2.6.3 Temperature

Snow and ice only exist at temperatures below the freezing point of water, 0 °C, by definition. An implication of this is that a solar panel covered by snow or ice, will not be significantly warmer than 0 °C. As photovoltaic cells become less efficient at elevated temperatures, this cooling effect might somewhat compensate for the

effect loss caused by snow obstruction [40]. Performance of panels is given under assumption of the 25 °C STC temperature, hence in practice a PV module might even perform better than advertised in the given light conditions in winter. Although, it is no net benefit of keeping a snow cover on the panels in order to cool them.

2.6.4 Sun Intensity vs. Angle

The sun's intensity is of huge importance to how the climate is on the respective places on Earth. Where the angle of incidence, which is technically the angle formed by rays of sunlight hitting the Earth, plays an important role. The most intense rays striking the planet's surface are the ones from directly overhead – that is, at a 90 degree measured from the horizon. The sun forms an angle with the horizon less than 90 degrees at most times and locations, hence the sun usually sits lower in the sky. The surface area over which the sun's rays spread is greater the smaller the angle. This effect reduces the sun's intensity in any one place.

In general, the rays from the sun are the most intense at the equator and the least intense at the poles, as mentioned in Section 2.3.2. Areas north of the Arctic Circle receive, on an average yearly basis, only about 40 percent as much solar radiation as equatorial regions.

Area's seasons are determined by fluctuations in the intensity and duration of solar energy in a particular area. These fluctuations are again dictated by the way the Earth is tilted on its axis. The Earth slants at a 23.5 degree angle with respect to the plane of rotation around the sun, which means that at certain points during its orbit, the Northern Hemisphere faces the sun more than the Southern Hemisphere, and vice versa [41].

Based on what is mentioned above about the sun intensity, the Nordic climate do not have the most appropriate conditions for solar cells, due to the sun's intensity. Regardless, the Nordic climate might still have some advantageous conditions which might contribute in a positive way, when mounting solar cells in the Nordic countries.

3 Experimental

In this chapter, a description of the design of the experimental equipment and the methodology of the executed measurements are given. In addition, a description of the different environments where the experiment are performed is given. The accuracy of the measurements have been looked at, as well as some of the difficulties that were experienced during the experiment.

3.1 Plan of Action

An experimental procedure was planned and analyzed as a first phase of the study, along with how the set-up should be. It was decided which approach would be the most preferable during the experiment, along with which light source should be used and where to perform the experiment. It was used quite a bit of time on this phase, in order to give the experiment the best conditions achievable.

The second phase was to perform the actual experiment itself; to measure the output efficiency of the bifacial solar cell under various conditions. The experiment was first accomplished inside a constructed chamber with dark walls, and then outside with sunlight as the energy source. It was used different tilt angles on the cell and different reflection materials underneath, to see how changes like these affected the efficiency output of the bifacial solar cell. In addition, some conditions that resembles that of a Nordic climate were constructed and the efficiency output of the bifacial solar cell was measured.

3.2 Set-Up

The experiment was first performed in a constructed chamber, using an Equilight Solar Mass 480 W LED lamp as the light source, which has the spectrum as shown in Figure 3.1 [42]. The only radiation on the bifacial solar cell came from the light source, and hence also the increase in temperature on the cell. The set-up for the outside measurements will be described in Section 3.2.1.

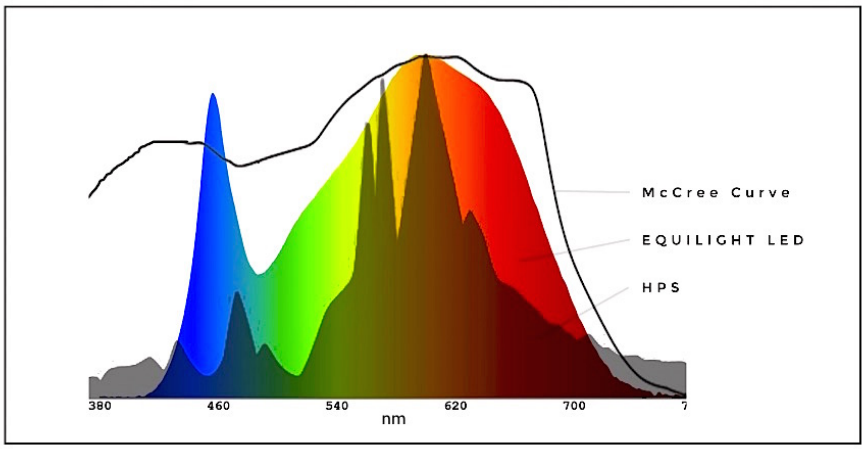

Figure 3.1: The spectrum of the light source; an Equilight Solar Mass 480 W LED lamp [42].

A bifacial solar cell and an ISET sensor - a calibrated unit - were placed in a stand and then into the constructed chamber. The measurements were conducted under controlled irradiance and temperature conditions. The ISET sensor was connected to a data logger (dataTaker, model: DT80M), which was programmed to measure radiation, temperature and voltage. The sensor converts solar radiation to a proportional current. The measured voltage was determined via a specific shut resistance, which was coupled thermally to the compact aluminum housing. The radiation, by which the solar cell was exposed to in the chamber, was determined by use of a conversion factor. The bifacial solar cell was connected to a potentiostat (ZAHNER, model: IM6e) with an amplifier (ZAHNER, model: PP201) and a voltage sweep was applied to measure the generated current. The set-up inside the chamber is shown in Figure 3.2.

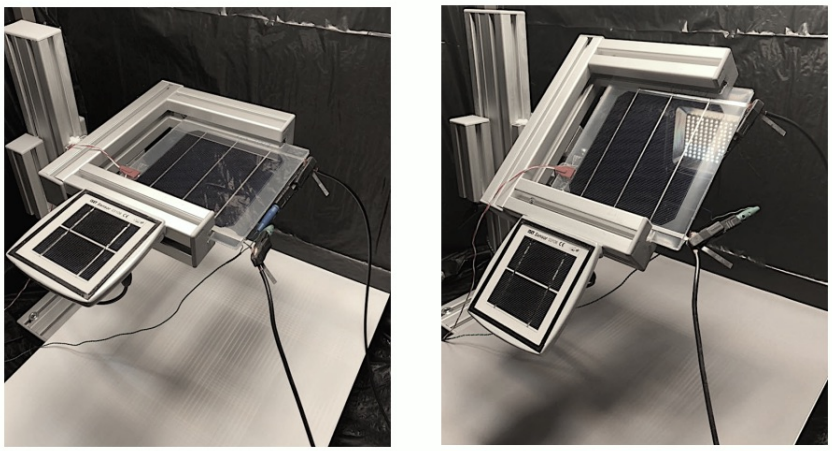

Figure 3.2: The images show the set-up inside the constructed chamber. To the left: 0° tilt angle on the bifacial solar cell (horizontal), and to the right: 45° tilt angle on the cell. The ISET sensor can be seen to the left of the bifacial solar cell on both the images. The red cord, which is attached to a data logger, gives the temperature on the bifacial solar cell.

3.2.1 Set-Up for the Outside Measurements

The stand with the bifacial solar cell and the ISET sensor was placed outside, where concrete and metal were the main reflection materials. It is common that the surroundings where solar cell modules are mounted, consist of several different materials. Hence, it was important to chose a location that was comparable with where solar cell modules usually are mounted, to get some realistic measurements of the efficiency output of the bifacial solar cell. Figure 3.3 shows the set-up outside, along with the surroundings.

Two pyranometer (sensors) (model: SP-500 Series) were additionally added to the set-up, along with the ISET sensor. This was done in order to be able to measure the irradiance that was reflected back on to the rear side of the bifacial solar cell, as well as the direct sunlight. The Pyranometer measuring the irradiance from the direct sunlight, can be seen on the right image of Figure 3.3.

Figure 3.3: The images show the set-up outside, along with how the surroundings looked like. The left image shows 45° tilt angle on the bifacial solar cell. Whereby the right image shows 0° tilt angle on the cell, along with two Pyranometer (one at the top and one beneath, which can not be seen).

3.3 The Bifacial Solar Cell Used

The bifacial solar cell used in the experiment is a Zebra cell, which is an integrated back contact (IBC) solar cell. The cell is made of a 156x156 mm^2 n-type Czochralski (Cz) silicon wafer, and the schematic cross section of the Zebra cell can be seen in Figure 3.4 [43]. In order to protect the solar cell from the environment, the cell is encapsulated with ethylene vinyl acetate (EVA) film and then covered with solar glass on both sides.

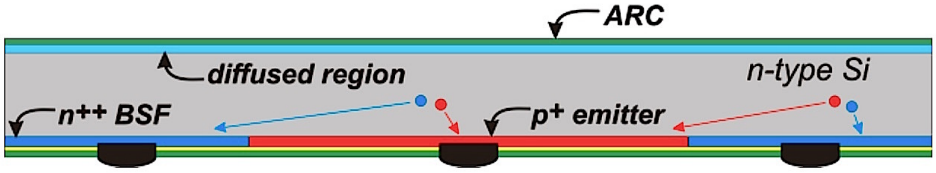

Figure 3.4: Schematic cross section of the Zebra cell showing diffused regions, passivation layers and metal fingers [43].

The EVA sheets play an important role in preventing humidity and dirt penetrating the solar cell. Also, with the help of the EVA, the cell is ”floating” between the glass and back sheet, which helps to soften shocks and vibrations and therefore protects the solar cell and its circuits [44].

Figure 3.5 shows a picture of the Zebra cell - the bifacial solar cell - which was used when performing the measurements in this study. Here, the busbars are clearly evident, along with the contacts by which the cord are attached, to give the output measurements.

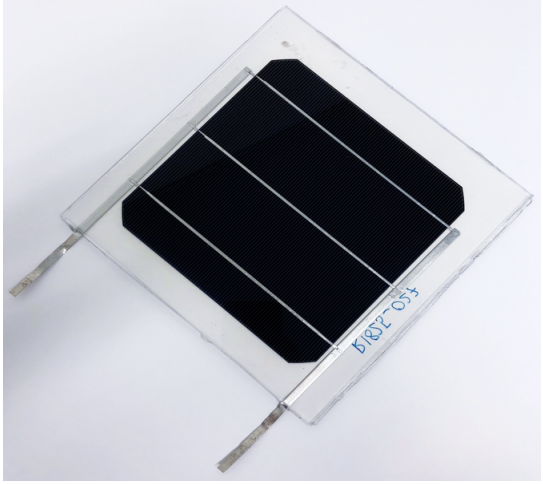

Figure 3.5: Picture of the bifacial solar cell (156x156 mm^2) used in this study.

3.4 Experimental Procedure

In this section it will be given a description on how the measurements were performed, for both inside and outside environments. Along with the prerequisites for the measurements.

3.4.1 Prerequisites for the Measurements

Before performing the measurements, several considerations were necessary. When using a solar cell, it is important to know what will have an impact on the measurements and then be able to correct for them. It was important to quantify the increase in temperature on the cell caused by the light source, since it will have an affect on the measured efficiency output. Figure 3.6 shows how the temperature increases with time, for both the bifacial solar cell and the ISET sensor, when exposed to the LED lamp. The ISET sensor shows a faster increase in temperature according to the bifacial solar cell, which can be due to the fact that the ISET sensor behaves as a monofacial solar cell and block the heat that strikes upon it. Whereby, the bifacial solar cell can, to a much larger degree, let the heat pass through it.

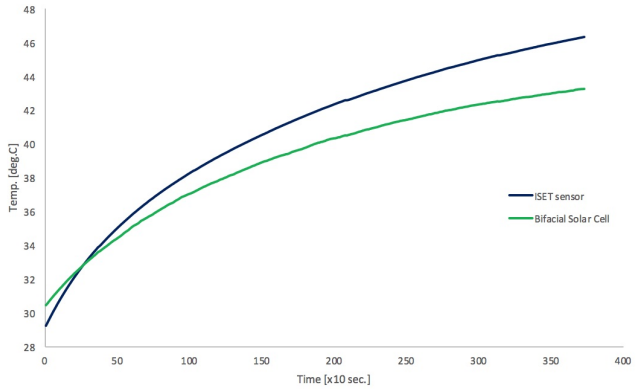

Figure 3.6: Difference in temperature between the bifacial solar cell and the ISET sensor, during time exposed to the LED lamp.

The distance from the bifacial solar cell to the light source was also quantified, since the irradiation on the cell changes with distance. Figure 3.7 shows how the irradiance on the solar cell changes with the distance to the light source (LED lamp). Small distance give high irradiance and vice versa.

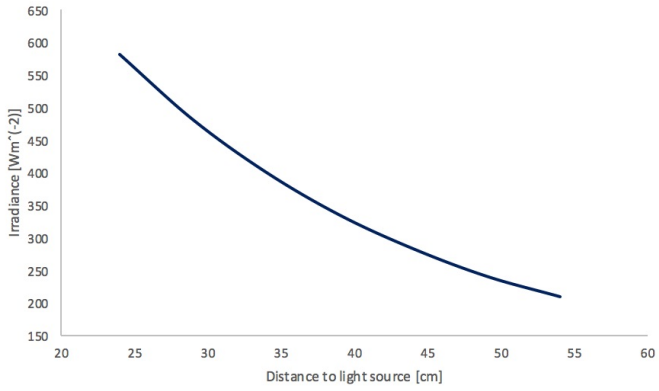

Figure 3.7: A plot showing the irradiance versus the distance to the light source, in this case the LED lamp.

Hence, for the inside measurements, a distance between the bifacial solar cell and the light source was chosen based on a compromise between irradiation and temperature on the cell.

3.4.2 Inside Measurements

The bifacial solar cell was placed 43.5 cm from the light source in the set-up, when mounted horizontally (0° tilt angle on the cell). The irradiance was then measured by the ISET sensor to be approximately 250 Wm^{-2}, which correspond to 25% of one-sun of illumination. This was done in order to achieve the compromise mentioned in Section 3.4.1, and to easy be able to compare the measurements obtained in the constructed chamber against measurements obtained under Standard Test Conditions (STC).

The measurements on the bifacial solar cell were performed by first measuring the efficiency output of the cell, and then cover up the rear side of the bifacial cell with a black cover and measure the output again. When the rear side of a bifacial solar cell is covered up, the cell can be seen as a monofacial solar cell. By using this method, it was possible to calculate how much the rear side of the cell contributed to the efficiency output of the bifacial solar cell. The difference between the two measurements corresponded then to the rear side's contribution to the efficiency output.

The bifacial solar cell was kept at different tilt angles: 0°, 22.5°, 45°, 67.5° and 90°, and papers with different reflection characteristics were used underneath the cell. This was done in order to see how different parameters could affect the efficiency output of the solar cell. Figure 3.8 shows the different colours on the papers, which were used to get different reflections back on to the rear side of the cell. The gray papers are distinguished with a number 1-3 and will be labelled: gray1, gray2 and gray3, throughout the report.

For each tilt angle it was taken ten measurements, where one parameter was changed from each measurement. First, the efficiency output of the bifacial solar cell was measured by changing the reflection material underneath the cell (in total five different paper colours), and then the rear side was covered up - as to get the bifacial cell to behave like a monofacial one - and the procedure with changing the reflection material

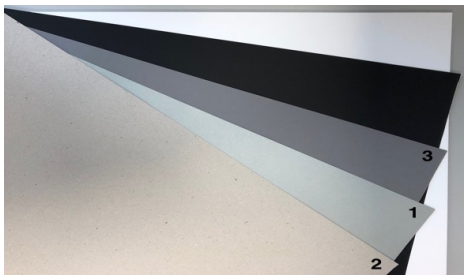

Figure 3.8: Papers (70x50 cm) with different colours were used to obtain different reflection characteristics. The different shades of gray are labeled with a number (1-3) to distinguish them apart.

was done again. This procedure was repeated for each of the five chosen tilt angles as mentioned earlier in this section. The measurements for each tilt angle were repeated couple of times, in order to see that the measurements taken were compliance with each other.

3.4.2.1 Snow Used as Reflection Material

Some measurements were performed with snow as reflection material and tilt angle of 0°, 45° and 90° on the bifacial solar cell. Only three tilt angles were chosen on the cell, in order to be able to take the measurements before the snow melted. Fresh snow was obtained by collecting it on two plates, which were then placed underneath the bifacial solar cell. The output efficiency of the cell was measured and compared to the output when using white paper as reflection material and same tilt angles as mentioned above. Figure 3.9 shows the set-up under these measurements, where snow was used as reflection material.

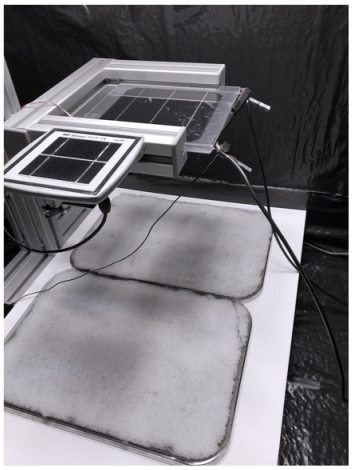

Figure 3.9: The set-up for 0° tilt angle on the bifacial solar cell and where snow was used as reflection material.

3.4.2.2 Rime Ice on the Bifacial Solar Cell

In order to see how rime ice and low temperature influence the efficiency output of the bifacial solar cell, measurements were performed with rime ice on the cell and with a cold cell. The measurements were then compared to see if there were any significant change between the two states of the cell. The cell was held at 0° tilt angle and white paper was used as the reflection material underneath the cell in both cases.

Rime ice on the bifacial solar cell was obtained by steaming the cell with hot water and then put it into the freezer over night. The cold cell was obtained by putting it into the freezer to obtain an as low temperature as possible.

3.4.2.3 Pyranometer: A Measure of the Direct and Indirect Irradiance

As mentioned in Section 3.2.1, two Pyranometer were additionally added to the set-up. These were used under the outside measurement, to see how much irradiance was reflected back on to the rear side of the bifacial solar cell. The sensors were also used to check how the different papers reflected light to the rear side of the cell. Figure 3.10 shows the irradiance the rear side of the bifacial solar cell could expect to get, when the tilt angle on the cell was 0° and the direct irradiance on the cell was between 243-255 Wm^{-2} (using the LED lamp), depending on the paper underneath the solar cell. The different direct irradiance could be due to the change of light in the chamber, which was caused by the different paper colours.

It can be seen from Figure 3.10 that the rear side of the cell experiences a decrease in irradiance going from white through gray1, gray2, gray3 and at the end black colour. This correlate well with theory that light colours reflect more and absorb less light, whereas dark colours reflect less and absorb more. White is the most reflective colour. Hence, when the colour white is being reflected, that means that all wavelengths are being reflected and none of them absorbed. Whereas black colour is the complete opposite. Black is the least reflective colour and it absorbs all light [45].

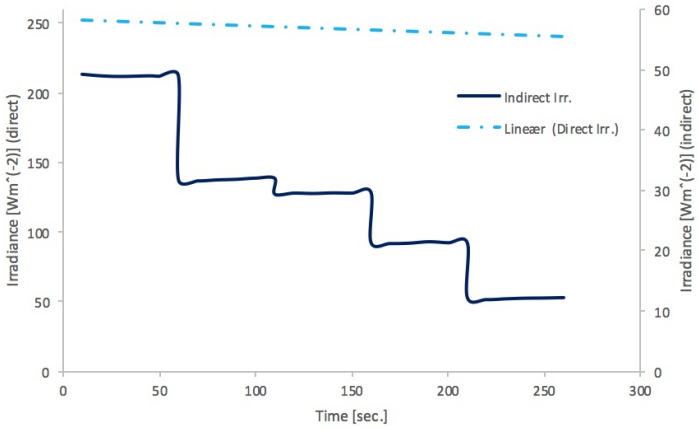

Figure 3.10: The irradiance the rear side of the bifacial solar cell can expect to get (dark blue line), when the tilt angle on the cell is 0°. The decrease in irradiance is due to the different reflection papers used, going from white, through gray1, gray2, gray3, and finally black. The direct irradiance (bright blue line) started on 255 Wm^{-2} for the white paper, then decreased to 243-244 Wm^{-2} for the remaining colour papers. LED lamp was used as the light source.

Appendix G contain the data to the graph shown in Figure 3.10, both the irradiance that would reach the rear side of the bifacial solar cell and the direct irradiance, for all the five paper colours used underneath the cell.

3.4.3 Outside Measurements

The outside measurements on the bifacial solar cell were performed in order to see how the efficiency output would be when using sunlight as the light source, according to the measurements done inside. The measurements were taken with the background as a fixed parameter and changing the tilt angle: 0°, 22.5°, 45°, 67.5° and 90° on the cell.

As with the inside measurements, the rear side of the bifacial solar cell was covered up in order to see how much the back of the cell contributed to the output efficiency. But in this instance, the measurements for the monofacial solar cell could not be used to calculate the rear side contribution of the bifacial solar cell. This was due to a large difference in irradiance from one measurement to another, which then gave the monofacial solar cell a higher output efficiency then the bifacial solar cell. This would not have been the case if the irradiance was approximately equal.

Due to unstable weather in the period when the measurements were taken, it was not obtained that much data. The IV-curves obtained were to a large degree affected by the unstable irradiation, which the bifacial solar cell was exposed to.

3.5 Accuracy of the Measurements

In order to see how accurate the measurements were, mean and standard deviation were calculated for three parallels done on each reflection material (the five paper colours), for 0°, 45° and 90° tilt angle on the bifacial solar cell. Standard deviation (σ) was calculated according to the equation

$$\sigma = \sqrt{\frac{\sum_{i=1}^{n}(x_i - \mu)^2}{n}} \tag{3.1}$$

where x_i is a value in the data set, μ is the mean of the data set, and n is the number of data points in the population. The more points, the more accurate the standard deviation will be, in this case only three points where achieved for each case.

Table 3.1 shows an example of the calculated mean and standard deviation for 45° tilt angle on the bifacial solar cell, and where white paper was used as a reflection material. Number 1-3 correspond to which parallel the data set comes from, whereby number 1 is the data set the IV-curves in the result are based on. The rest of the calculated values can be found in Appendix E, and the data to the two respective parallels 2 and 3 can be found in Appendix F.

Throughout the report the values for the short-circuit current (I_{sc}) will be presented with three decimals in order to not miss out on any trend that might occur. Although, the standard deviation (σ) calculated for the I_{sc} lies in the second and third decimal number. The same applies for the maximum power point (P_{max}), where the standard deviation was calculated to be in the second decimal number for 0° and 45° tilt angel on the cell, and in the third decimal number for 90° tilt angle.

Table 3.1: The calculated mean (μ) and standard deviation (σ) for the data set from 45° tilt angle on the bifacial solar cell and where white paper was used as a reflection material.

	White	I_{sc} [A]	V_{oc} [V]	P_{max} [W]	FF	η	Irradiance [Wm^{-2}]	Temp. Solar Cell [deg.C]	Temp. ISET [deg.C]
Data Set	1	1.687	0.561	0.705	0.745	0.334	86.880	39.120	35.760
	2	1.735	0.576	0.747	0.748	0.334	91.796	33.569	29.554
	3	1.741	0.576	0.752	0.751	0.337	91.792	33.782	29.951
	Mean Value (μ)	1.721	0.571	0.735	0.748	0.335	90.156	35.490	31.755
	Standard Deviation (σ)	0.021	0.006	0.018	0.002	0.001	2.006	2.224	2.457

The standard deviation for the irradiance for the three parallels were calculated to have values ranging between 0.1 and 2.9, but in order to give an accurate value for each measurement, the irradiance values will be given with one decimal number. The reason behind this decision, is that the number itself is quite accurate, but in comparing the parallels up against each other a small change occur. This can have been caused by the environment at the time the measurements were taken. Hence, it is the irradiance for one specific measurement that is important and the I_{sc}, V_{oc}, P_{max}, etc. that follow from that specific value, and which will be put up against another specific irradiance for another measurement. The same argument as above is the reason why also the values for the temperature are given with one decimal number. In this case, the calculated standard deviation had values also ranging between 0.1 and 2.9.

The standard deviation (σ) for the fill factor (FF) and the energy efficiency coefficient (η), when taken into consideration the three parallels, lied in the third and second decimal number, respectively. The values for FF and η will be given with three decimal numbers, to not miss out any trend that might have occurred. (The numbers for the standard deviation might be higher due to small deviations in the numbers used in the calculations.)

3.6 Experimental Challenges

Throughout the work by obtaining the data from the bifacial solar cell for both inside and outside measurements, there have been some experimental challenges that might have affected the efficiency output obtained on the cell.

For the inside measurements, keeping the cell temperature down has been important due to the fact that the efficiency output is affect negatively by an increase in temperature. The light source was shining directly on the cell for a certain amount of time and the chamber was closed, which lead to more heat inside the chamber as time went by. Hence, in order to be able to compare the measurement taken, it was important to keep track of the temperature.

When performing the measurements outside, the experimental challenge was the unstable weather during the period the measurements were taken. Which caused the irradiance to be unstable as well, which again had an affect on the efficiency output of the bifacial solar cell. This can be seen on the IV-curves in the results.

Due to the design of the set-up, measuring the tilt angle on the bifacial solar cell to be accurate was not easy, therefore it is assumed an uncertainty of the tilt angle to be $\pm 2°$. Another parameter that might have affected the efficiency output of the cell, was whether the stand to the set-up itself could have provided some

shadow. Which again could have lead to a small decrease in the efficiency output of the solar cell, but it is not known to what degree this might be the case.

4 Results

In this chapter, the results that were obtained will be given. The basic measurements performed inside the constructed chamber will be presented first. Then, the results where snow and rime ice were used will be presented. And at the end, results obtained from outside measurements are given.

The results will be given in forms of graphs and tables, along with illustrations to explain the conditions by which the measurements were taken, where that seem necessary.

4.1 Measurements Performed Inside the Constructed Chamber

4.1.1 IV-Curves and Important Values for the Solar Cell

IV-curves were obtained for both the bifacial solar cell itself, along with the monofacial version of it. In the case of the monofacial solar cell, the rear side of the bifacial solar cell was covered up with a black cover. For each plot, the reflection material underneath the cell is the fixed parameter, whereby the tilt angle is the changing parameter. The plots with the same reflection material and with bi- and monofacial characteristic of the solar cell are set next to each other, in order to compare the two. Figure 4.1 through 4.5 shows the IV-curves obtained.

Tables with values for the short-circuit current (I_{sc}), open-circuit voltage (V_{oc}), maximum power point (P_{max}), fill factor (FF) and energy conversion efficiency (η) are also given for both the bi- and monofacial solar cell for each reflection material, and can be seen in Table 4.1 through 4.5.

In Appendix B the IV-curves were plotted with the tilt angle as the fixed parameter and where the reflection material is the changing one. In addition, the appendix gives the values for the irradiance and the temperature for both the bi- and monofacial solar cell and the ISET sensor.

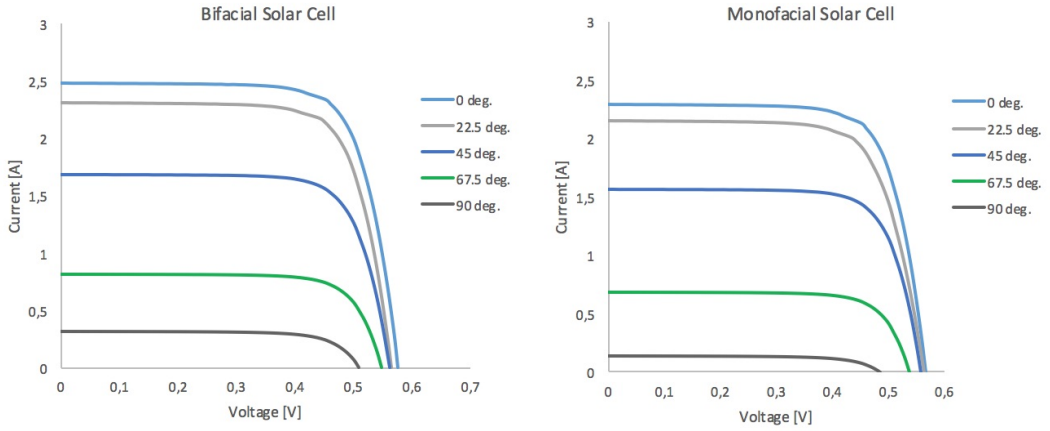

Figure 4.1: The IV-curves shown in the left and right image are for a bi- and monofacial solar cell, respectively. White paper was used as reflection material underneath the solar cell, and the different angles indicate at which tilt angle the measurement was performed.

Table 4.1: The table shows values for short-circuit current (I_{sc}), open-circuit voltage (V_{oc}), maximum power point (P_{max}), fill factor (FF) and energy conversion efficiency (η), for different tilt angles on the bi- and monofacial solar cell. White paper was used as reflection material.

		Tilt Angle				
	Bifacial Solar Cell	0°	22.5°	45°	67.5°	90°
White	I_{sc} [A]	2.487	2.305	1.687	0.814	0.317
	V_{oc} [V]	0.577	0.566	0.561	0.548	0.510
	P_{max} [W]	1.064	0.966	0.705	0.335	0.118
	Fill factor (FF)	0.742	0.740	0.745	0.750	0.727
	Energy conversion efficiency (η)	0.173	0.249	0.334	0.310	0.174
	Monofacial Solar Cell	0°	22.5°	45°	67.5°	90°
White	I_{sc} [A]	2.296	2.146	1.562	0.683	0.139
	V_{oc} [V]	0.568	0.563	0.557	0.539	0.485
	P_{max} [W]	0.967	0.870	0.648	0.275	0.049
	Fill factor (FF)	0.741	0.720	0.745	0.746	0.695
	Energy conversion efficiency (η)	0.157	0.225	0.306	0.269	0.074

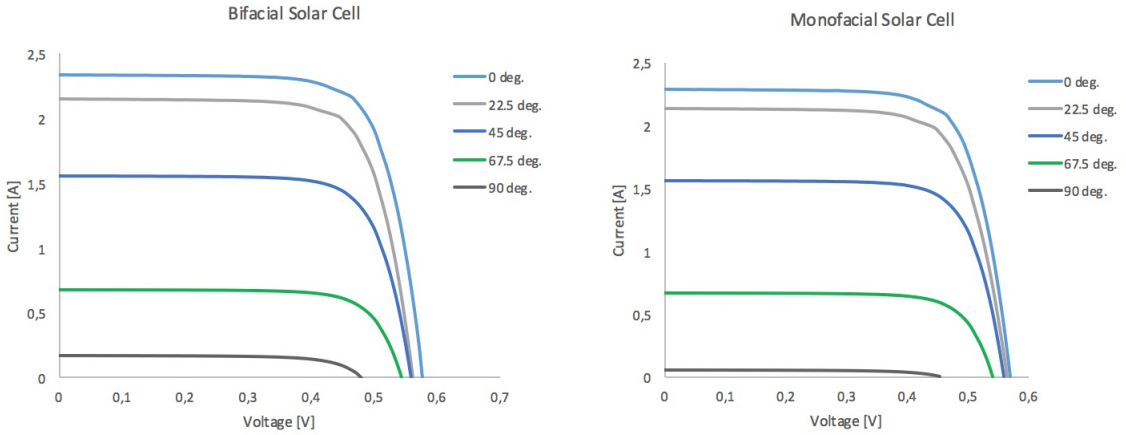

Figure 4.2: The IV-curves shown in the left and right image are for a bi- and monofacial solar cell, respectively. Black paper was used as reflection material underneath the solar cell, and the different angles indicate at which tilt angle the measurement was performed.

Table 4.2: The table shows values for short-circuit current (I_{sc}), open-circuit voltage (V_{oc}), maximum power point (P_{max}), fill factor (FF) and energy conversion efficiency (η), for different tilt angles on the bi- and monofacial solar cell. Black paper was used as reflection material.

		Tilt Angle				
	Bifacial Solar Cell	0°	22.5°	45°	67.5°	90°
Black	I_{sc} [A]	2.333	2.154	1.562	0.685	0.169
	V_{oc} [V]	0.577	0.563	0.560	0.544	0.480
	P_{max} [W]	1.003	0.900	0.652	0.279	0.057
	Fill factor (FF)	0.745	0.742	0.745	0.748	0.705
	Energy conversion efficiency (η)	0.163	0.233	0.311	0.326	0.453
	Monofacial Solar Cell	0°	22.5°	45°	67.5°	90°
Black	I_{sc} [A]	2.293	2.137	1.556	0.666	0.062
	V_{oc} [V]	0.571	0.565	0.559	0.540	0.453
	P_{max} [W]	0.970	0.882	0.649	0.268	0.018
	Fill factor (FF)	0.741	0.731	0.746	0.746	0.645
	Energy conversion efficiency (η)	0.157	0.229	0.308	0.332	0.168

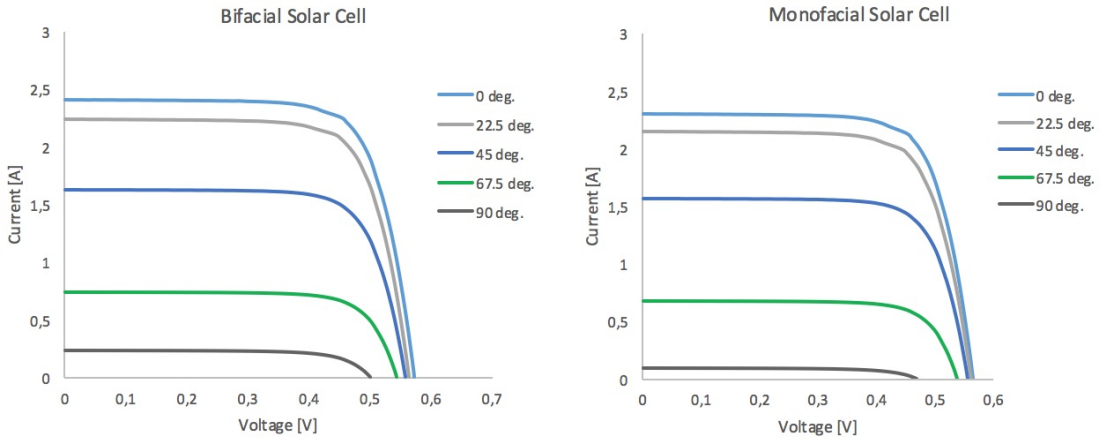

Figure 4.3: The IV-curves shown in the left and right image are for a bi- and monofacial solar cell, respectively. Gray1 paper was used as reflection material underneath the solar cell, and the different angles indicate at which tilt angle the measurement was performed.

Table 4.3: The table shows values for short-circuit current (I_{sc}), open-circuit voltage (V_{oc}), maximum power point (P_{max}), fill factor (FF) and energy conversion efficiency (η), for different tilt angles on the bi- and monofacial solar cell. Gray1 paper was used as reflection material.

		Tilt Angle				
	Bifacial Solar Cell	0°	22.5°	45°	67.5°	90°
Gray1	I_{sc} [A]	2.403	2.231	1.629	0.738	0.228
	V_{oc} [V]	0.573	0.565	0.559	0.544	0.500
	P_{max} [W]	1.019	0.934	0.678	0.300	0.082
	Fill factor (FF)	0.741	0.741	0.745	0.748	0.715
	Energy conversion efficiency (η)	0.167	0.240	0.320	0.331	0.234
	Monofacial Solar Cell	0°	22.5°	45°	67.5°	90°
Gray1	I_{sc} [A]	2.297	2.142	1.561	0.671	0.093
	V_{oc} [V]	0.566	0.562	0.555	0.537	0.468
	P_{max} [W]	0.963	0.881	0.645	0.268	0.029
	Fill factor (FF)	0.741	0.732	0.744	0.745	0.673
	Energy conversion efficiency (η)	0.157	0.224	0.303	0.293	0.088

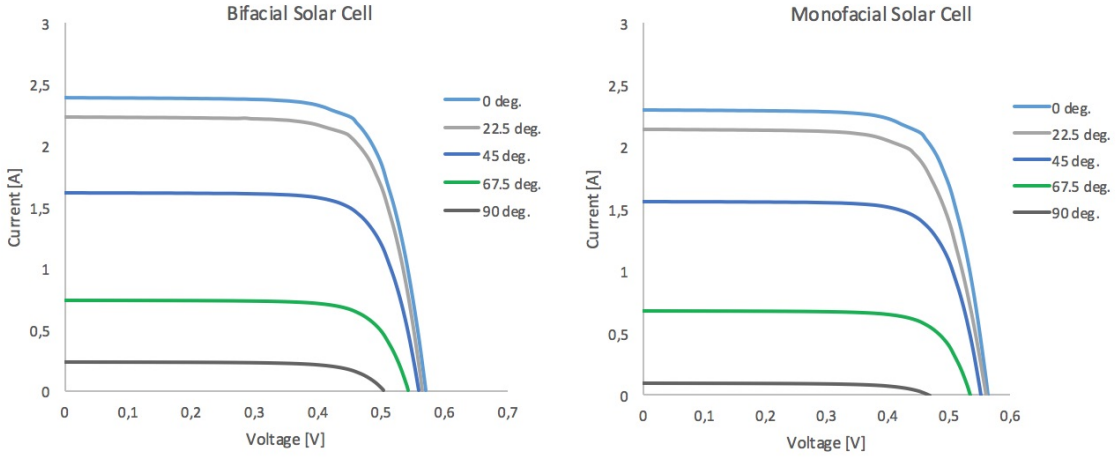

Figure 4.4: The IV-curves shown in the left and right image are for a bi- and monofacial solar cell, respectively. Gray2 paper was used as reflection material underneath the solar cell, and the different angles indicate at which tilt angle the measurement was performed.

Table 4.4: The table shows values for short-circuit current (I_{sc}), open-circuit voltage (V_{oc}), maximum power point (P_{max}), fill factor (FF) and energy conversion efficiency (η), for different tilt angles on the bi- and monofacial solar cell. Gray2 paper was used as reflection material.

		Tilt Angle				
	Bifacial Solar Cell	0°	22.5°	45°	67.5°	90°
Gray2	I_{sc} [A]	2.390	2.227	1.615	0.738	0.237
	V_{oc} [V]	0.571	0.564	0.558	0.543	0.503
	P_{max} [W]	1.010	0.932	0.672	0.300	0.085
	Fill factor (FF)	0.740	0.741	0.745	0.748	0.716
	Energy conversion efficiency (η)	0.166	0.237	0.308	0.333	0.223
	Monofacial Solar Cell	0°	22.5°	45°	67.5°	90°
Gray2	I_{sc} [A]	2.293	2.144	1.554	0.676	0.098
	V_{oc} [V]	0.564	0.560	0.554	0.536	0.470
	P_{max} [W]	0.956	0.863	0.640	0.270	0.031
	Fill factor (FF)	0.740	0.718	0.744	0.745	0.677
	Energy conversion efficiency (η)	0.156	0.221	0.291	0.287	0.087

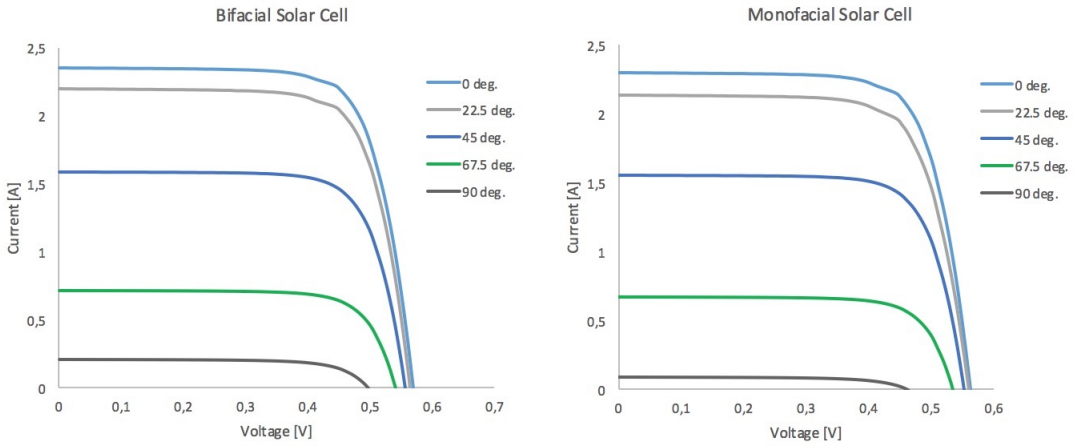

Figure 4.5: The IV-curves shown in the left and right image are for a bi- and monofacial solar cell, respectively. Gray3 paper was used as reflection material underneath the solar cell, and the different angles indicate at which tilt angle the measurement was performed.

Table 4.5: The table shows values for short-circuit current (I_{sc}), open-circuit voltage (V_{oc}), maximum power point (P_{max}), fill factor (FF) and energy conversion efficiency (η), for different tilt angles on the bi- and monofacial solar cell. Gray3 paper was used as reflection material.

		Tilt Angle				
	Bifacial Solar Cell	0°	22.5°	45°	67.5°	90°
Gray3	I_{sc} [A]	2.353	2.197	1.589	0.708	0.203
	V_{oc} [V]	0.570	0.564	0.558	0.541	0.498
	P_{max} [W]	0.992	0.918	0.660	0.286	0.072
	Fill factor (FF)	0.739	0.741	0.745	0.747	0.711
	Energy conversion efficiency (η)	0.163	0.235	0.307	0.323	0.283
	Monofacial Solar Cell	0°	22.5°	45°	67.5°	90°
Gray3	I_{sc} [A]	2.294	2.140	1.558	0.664	0.082
	V_{oc} [V]	0.563	0.559	0.553	0.535	0.462
	P_{max} [W]	0.953	0.873	0.641	0.265	0.025
	Fill factor (FF)	0.738	0.730	0.743	0.744	0.664
	Energy conversion efficiency (η)	0.155	0.224	0.300	0.302	0.099

It can be seen from the results above, that using white and black paper underneath the bifacial solar cell gives the highest and lowest differences between the short-circuit current (I_{sc}), respectively. This occur when comparing the bi- and monofacial solar cell measurements, for all the chosen tilt angles. Whereby the three papers on the grayscale lies in between this extreme, when comparing the values for the short-circuit current (I_{sc}) on the bi- and monofacial solar cell.

4.1.2 Snow vs. White Paper as Reflection Material

The IV-curves obtained comparing snow and white paper as reflection materials, can be seen in Figure 4.6. The aim behind the comparison, was to see if there were any significant differences in the output efficiency of the cell. By which the graphs in Figure 4.6 can confirm that is not the case. The snow used was wet, which could have had an affect on the amount of reflectivity that was achieved back on to the rear side of the cell.

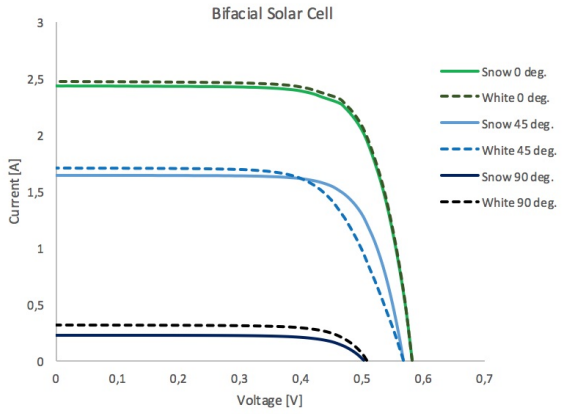

Figure 4.6: The plot shows IV-curves where snow and white paper are used as reflection materials, which correspond to the normal and dotted lines, respectively. The different angles indicate at which tilt angle the measurement was performed.

Table 4.6 gives the values for the short-circuit current (I_{sc}), open-circuit voltage (V_{oc}), maximum power point (P_{max}), fill factor (FF) and energy conversion efficiency (η) for the bifacial solar cell for different tilt angles, with snow and white paper used as reflection materials. In Appendix C the values for the irradiance and the temperature for both the bifacial solar cell and the ISET sensor are given.

Table 4.6: The table shows values for short-circuit current (I_{sc}), open-circuit voltage (V_{oc}), maximum power point (P_{max}), fill factor (FF) and energy conversion efficiency (η), for different tilt angles on the bifacial solar cell. Snow and white paper were used as reflection materials.

	Tilt Angle					
Bifacial Solar Cell	0° Snow	0° White	45° Snow	45° White	90° Snow	90° White
I_{sc} [A]	2.426	2.471	1.634	1.701	0.226	0.310
V_{oc} [V]	0.581	0.583	0.568	0.568	0.502	0.509
P_{max} [W]	1.052	1.076	0.695	0.654	0.083	0.115
Fill factor (FF)	0.747	0.747	0.749	0.677	0.737	0.731
Energy conversion efficiency (η)	0.171	0.176	0.320	0.299	0.240	0.166

4.1.3 Rime Ice on the Bifacial Solar Cell vs. Cold Cell

Figure 4.7 shows a comparison of two IV-curves, where one curve correspond to the bifacial solar cell with rime ice and the other to the same cell only cold. By using the same reflection material, in this case white paper underneath the solar cell, it was possible to compare the efficiency output of the two different states of the solar cell. It can be seen from Figure 4.7 that the differences are minimal.

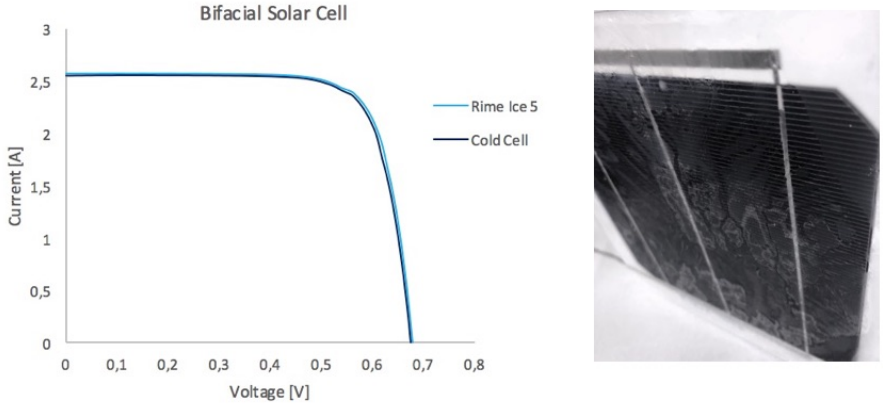

Figure 4.7: Left image: a comparison of IV-curves, where one curve correspond to the bifacial solar cell with rime ice and the other to the same cell only cold. White paper was used as reflection material underneath the bifacial solar cell. Right image: shows the rime ice on the bifacial solar cell.

In Table 4.7 the values for the short-circuit current (I_{sc}), open-circuit voltage (V_{oc}), maximum power point (P_{max}), fill factor (FF) and energy conversion efficiency (η) for the bifacial solar cell in the different states are given. In addition, the temperature on the cell is also shown in Table 4.7. In Appendix C the values for the irradiance and the temperature for both the bifacial solar cell and the ISET sensor are given.

Table 4.7: The table shows values for short-circuit current (I_{sc}), open-circuit voltage (V_{oc}), maximum power point (P_{max}), fill factor (FF) and energy conversion efficiency (η), for 0° tilt angle on the bifacial solar cell. The temperature on the cell is also shown. White paper was used as reflection material. The cell with rime ice is labelled 1-5, to indicate five different measurements.

	Bifacial Solar Cell	Rime Ice1	Rime Ice2	Rime Ice3	Rime Ice4	Rime Ice5	Cold Cell
White	I_{sc} [A]	2.564	2.587	2.563	2.590	2.565	2.555
	V_{oc} [V]	0.658	0.681	0.683	0.687	0.680	0.676
	P_{max} [W]	1.300	1.379	1.336	1.358	1.340	1.328
	Fill factor (FF)	0.770	0.783	0.763	0.763	0.768	0.769
	Energy conversion efficiency (η)	0.209	0.219	0.215	0.216	0.215	0.213
	Temperature on the cell [deg.C]	14.6	11.4	11.3	14.1	15.2	15.5

All the IV-curves that were taken in order to see how rime ice and low temperature influence the efficiency output of the bifacial solar cell, can be seen in Figure 4.8. In order to see the differences in short-circuit current (I_{sc}) and open-circuit voltage (V_{oc}) in the plot, this area on the y- and x-axis have been zoomed in on, respectively. It can be seen from the I_{sc} and V_{oc} values, that the differences are not too significant. It can be seen some irregularities on the IV-curves in Figure 4.8, which up until now is uncertain to what can have caused it.

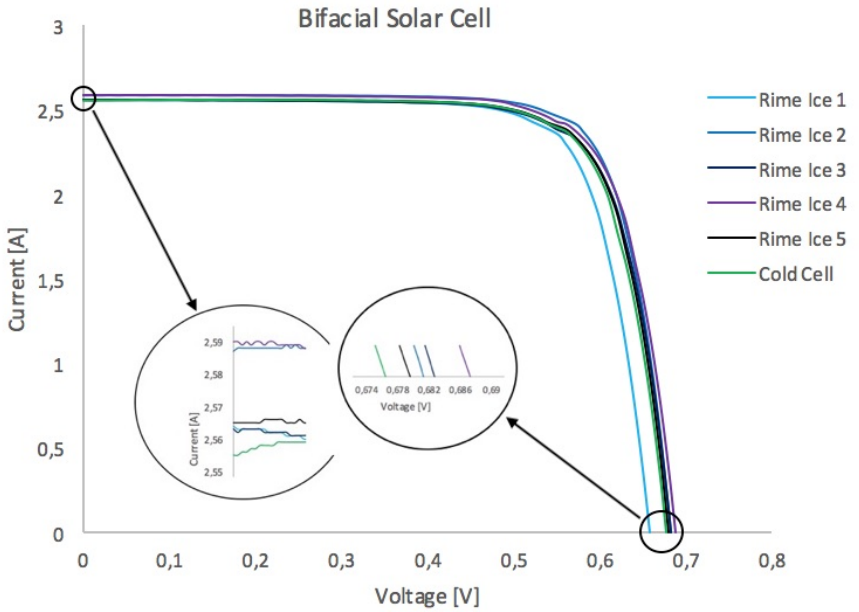

Figure 4.8: IV-curves, where five of the curves correspond to the bifacial solar cell with rime ice on and one curve of the same cell only cold, for comparison. The y- and x-axis, where the I_{sc} and V_{oc} values are present, have been zoomed in on in order to see the differences. White paper was used as reflection material underneath the bifacial solar cell and the cell had a tilt angle of 0°.

The rime ice that had accumulated on the bifacial solar cell was of a thin layer and did cover the whole cell. Though, it was a bit inhomogeneous at some spots on the cell, which could have affected the obtained results.

4.2 Measurements Performed Outside

The measurements performed outside could be seen as a case study, where the aim was to investigate how the bifacial solar cell's efficiency output got affected by the Nordic climate. In this case, the solar cell was greatly affected by the unstable weather that was present at the time being, when performing the measurements. The surroundings were of different materials, which will have an impact on how much light was reflected back on to the cell.

Figure 4.9 shows the IV-curves obtained, when doing the measurements as done inside the chamber - by changing the tilt angle. In the case of the monofacial solar cell, the rear side of the bifacial solar cell was covered up with a black cover. It can be seen that it is not possible to compare the measurements performed on the bifacial solar cell to the ones done on the monofacial cell, as can be done with the inside measurements. The reason is because when the measurements on the monofacial solar cell were taken, the irradiance was an amount higher than when taking the measurements on the bifacial solar cell. The weather changed abruptly.

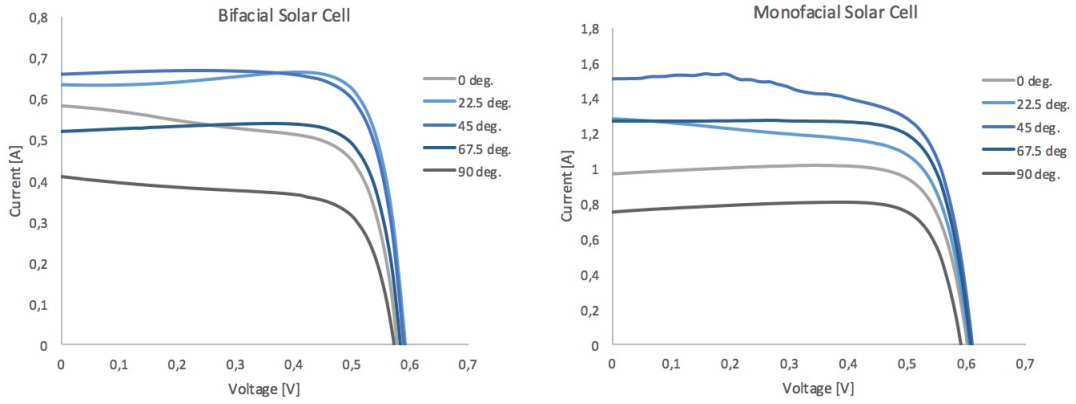

Figure 4.9: The IV-curves shown in the left and right image are for a bi- and monofacial solar cell, respectively. The different angles indicate at which tilt angle the measurement was performed. Note that the y-axis on the two plots are different.

The weather during the measurements was cloudy with some rain and sunshine in between, and the temperature was 10 °C. Figure 4.10 shows the rain that was present on the solar cell and how the sky looked like for the time being. In Table 4.8 the values for short-circuit current (I_{sc}), open-circuit voltage (V_{oc}), maximum power point (P_{max}), fill factor (FF) and energy conversion efficiency (η), for different tilt angles on the bi- and monofacial solar cell are given.

Figure 4.10: The image to the left and right shows the rain present on the bifacial solar cell and the sky during the measurements, respectively.

Table 4.8: The table shows values for short-circuit current (I_{sc}), open-circuit voltage (V_{oc}), maximum power point (P_{max}), fill factor (FF) and energy conversion efficiency (η), for different tilt angles on the bi- and monofacial solar cell. Outside environment (concrete).

		Tilt Angle				
	Bifacial Solar Cell	0°	22.5°	45°	67.5°	90°
Concrete	I_{sc} [A]	0.583	0.635	0.658	0.519	0.409
	V_{oc} [V]	0.580	0.591	0.592	0.585	0.573
	P_{max} [W]	0.229	0.312	0.301	0.246	0.161
	Fill factor (FF)	0.678	0.832	0.771	0.812	0.685
	Energy conversion efficiency (η)	0.157	0.182	0.175	0.187	0.180
	Monofacial Solar Cell	0°	22.5°	45°	67.5°	90°
Concrete	I_{sc} [A]	0.967	1.277	1.504	1.270	0.756
	V_{oc} [V]	0.602	0.605	0.609	0.607	0.592
	P_{max} [W]	0.471	0.537	0.639	0.596	0.379
	Fill factor (FF)	0.809	0.695	0.697	0.774	0.847
	Energy conversion efficiency (η)	0.157	0.156	0.150	0.171	0.166

4.2.1 Another Outside Measurement

Another measurement was performed as above, but only on the bifacial solar cell and not covering the rear side of the cell. In this case the weather was a bit worse then before, with more rain and some sunshine in between, and 10 °C. The IV-curves can be seen in Figure 4.11, and it can be seen that sunshine was present during the measurement when the tilt angle on the cell was 22.5°. Figure 4.12 shows the rain that was present on the solar cell and how the sky looked like for the time being.

In Table 4.9 the values for short-circuit current (I_{sc}), open-circuit voltage (V_{oc}), maximum power point (P_{max}), fill factor (FF) and energy conversion efficiency (η), for different tilt angles on the bifacial solar cell are given.

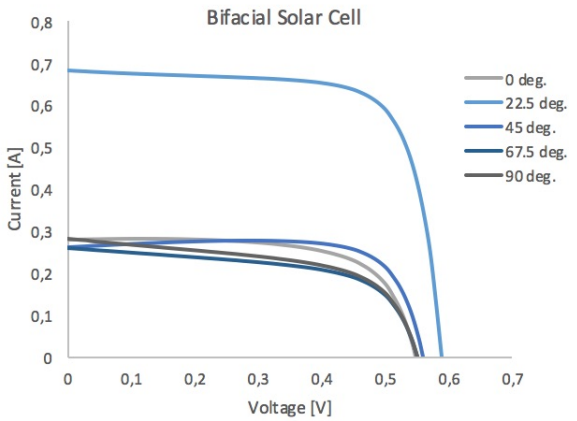

Figure 4.11: The IV-curves shown in the image are for a bifacial solar cell. The different angles indicate at which tilt angle the measurement was performed. At tilt angle 22.5° on the bifacial solar cell, the irradiance was quite high as opposed to the other measurements, due to more sunlight on the cell.

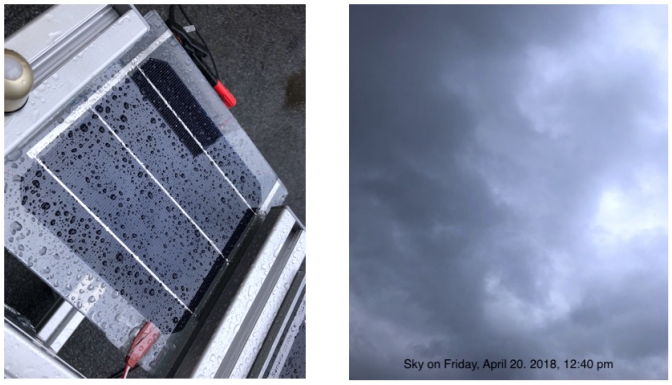

Figure 4.12: The image to the left and right shows the rain present on the bifacial solar cell and the sky during the measurements, respectively.

Table 4.9: The table shows values for short-circuit current (I_{sc}), open-circuit voltage (V_{oc}), maximum power point (P_{max}), fill factor (FF) and energy conversion efficiency (η), for different tilt angle on the bifacial solar cell. Outside environment (concrete).

		Tilt Angle				
	Bifacial Solar Cell	0°	22.5°	45°	67.5°	90°
Concrete	I_{sc} [A]	0.277	0.684	0.259	0.260	0.282
	V_{oc} [V]	0.546	0.589	0.558	0.549	0.550
	P_{max} [W]	0.102	0.297	0.114	0.085	0.089
	Fill factor (FF)	0.678	0.736	0.791	0.598	0.576
	Energy conversion efficiency (η)	0.135	0.167	0.159	0.143	0.146

4.2.2 Irradiance Experiment

The aim behind the IV-curves shown in Figure 4.13, was to see how different irradiance could affected the IV-curves, while keeping the tilt angle constant (0°). The weather during these measurements was cloudy with some rain and 11 °C. Rain was present on the bifacial solar cell, like that shown in Figure 4.12 in Section 4.2.1. In Table 4.10 the values for short-circuit current (I_{sc}), open-circuit voltage (V_{oc}), maximum power point (P_{max}), fill factor (FF) and energy conversion efficiency (η), for the bifacial solar cell are given. Along with the irradiance [Wm^{-2}] for each case.

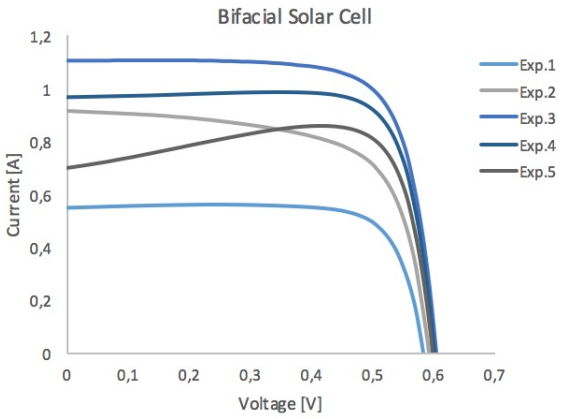

Figure 4.13: The IV-curves shown in the image are for a bifacial solar cell and where the measurements were performed at 0° tilt angle. The aim was to show how different irradiance could affect the IV-curves. Each curve is labelled exp. (experiment) with a number 1-5, indicating five different measurements.

It can be seen from the IV-curves in Figure 4.13 which one of the curves have had stable and unstable irradiance during the measurements, respectively. This can be seen especially for exp.5 (dark gray line), which has an IV-curve that deviate slightly from an ordinary IV-curve. The irradiance given in Table 4.10 are the values that were present in the middle of the measurements. Hence, the outside measurements, that have been affected by the unstable weather, have also been affected by a change in irradiance during the measurements.

Table 4.10: The table shows values for short-circuit current (I_{sc}), open-circuit voltage (V_{oc}), maximum power point (P_{max}), fill factor (FF) and energy conversion efficiency (η), for 0° tilt angle on the bifacial solar cell. In addition, the irradiance [Wm^{-2}] is also shown for each case. Outside environment (concrete).

		0 Degree Tilt Angle				
	Bifacial Solar Cell	Exp.1	Exp.2	Exp.3	Exp.4	Exp.5
Concrete	I_{sc} [A]	0.548	0.916	1.104	0.966	0.702
	V_{oc} [V]	0.584	0.593	0.604	0.602	0.598
	P_{max} [W]	0.249	0.360	0.498	0.460	0.407
	Fill factor (FF)	0.778	0.663	0.746	0.791	0.970
	Energy conversion efficiency (η)	0.166	0.145	0.166	0.171	0.177
	Irradiance [Wm^{-2}]	61.5	102.1	123.6	110.6	94.3

In Appendix D the values for the irradiance and the temperature for both the bi- and monofacial solar cell and the ISET sensor are given for all the outside measurements. A change in irradiance during a measurement can explain the strange IV-curves that appeared for the outside measurements. All the irradiance values that are given in the appendices, are the value that was observed halfway through a measurement.

5 Discussion

A discussion about the accuracy of the measurements and the results will be presented in this chapter. In addition, the results will be discussed according to others work in the same field of study and theory.

5.1 Accuracy of the Obtained Measurements

The standard deviation (σ) was calculated for three parallels, in order to see if the values obtained from these measurements correlated with each other. Based on the calculated values of the standard deviation for three tilt angles: 0°, 45° and 90°, for the short-circuit current (I_{sc}), open-circuit voltage (V_{oc}) and maximum power point (P_{max}), the mean standard deviations were 0.009, 0.003 and 0.009, respectively. This imply that the dispersion of the data set from each parallel did not vary much from its mean value and can be considered accurate, even though the numbers were small in itself. And most importantly the numbers achieved could be approximately reproduced based on the numbers achieved from the three parallels.

The mean standard deviation obtained on the irradiance for the three tilt angles was 1.027. Which indicate that the irradiance has been quite stable throughout the measurements, at least for tilt angle 0° and 45°. For these two tilt angles this mean standard deviation correspond to less than 1 % deviation for any of the irradiance values taken on these two parallels. Although, for 90° tilt angle on the bifacial solar cell, this mean standard deviation seem a bit too high, because in this case the irradiance lied between 5.1 Wm^{-2} and 28.8 Wm^{-2} depending on the paper colour underneath the cell. But the standard deviation for the irradiance on 90° tilt angle alone was lower, 0.487, respectively. Hence, the values for the two other tilt angles, 0° and 45°, were the ones that increased the mean value of the standard deviation on the irradiance.

The temperature on the bifacial solar cell has an important influence on the efficiency output of the cell, and the mean standard deviation was 1.315. This might be a high value and might even be seen as an error in comparing the obtained results. But under the circumstances, the values of the temperature were quite stable, when taken into consideration the environment where the experiment was performed and the fact that the light source heated the bifacial solar cell as time went by. The time used on the measurements for each parallel was not equal, hence the deviations in temperature.

The fill factor and energy conversion efficiency did also have small standard deviations, which indicate that the taken measurements from each parallel correlated well against each other. It has to be noted, that the standard deviations were only calculated based on the inside measurements, due to the fact that these measurements were performed under controlled conditions.

5.1.1 Influences on the Accuracy

Even though the measurements on the bifacial solar cell were performed in the same chamber with the same light source (a LED lamp), differences did occur. Small geometrical differences could have been the reason for these differences. Like, for instance, the stand with the bifacial solar cell and the ISET sensor was moved a couple of times. As a consequence, the stand might then have changed position according to the LED lamp. The distance between the solar cell and the LED lamp was always measured before the measurements were taken, but also here there was expected an uncertainty of ±1 mm. This will in turn influence the irradiance

and the temperature on the cell. In addition, the tilt angle on the bifacial solar cell was estimated to have an uncertainty of $\pm 2°$.

The temperature in the room where the chamber was located, was relatively cold throughout all the measurements, but still it could have been some marginally differences. The temperature was not measured in the room, but was assumed approximately the same all the time. The temperature on the electronics used, could also have contributed to the differences that occurred during the measurements.

When everything is taken into consideration, the calculated standard deviations indicate that the accuracy of the measurements obtained were not too bad. Small differences on the set-up have for certain some affect on the efficiency output of the bifacial solar cell. This could be seen, especially, on the irradiance and the temperature on the solar cell, which again affected the efficiency output.

5.2 The Results Obtained

In this section the results that were obtained will be discussed in detail, along with some new plots and tables based on the results in Chapter 4. A theoretical calculation on the effect of the tilt angle on the irradiance is performed. In addition, the irradiance that can be received on the bifacial solar cell during 24 hours has been calculated, for two different colours - white and black - on the reflection material.

5.2.1 Influence of Different Reflection Materials

The results showed that using white and black paper underneath the bifacial solar cell give the highest and lowest differences between the short-circuit current (I_{sc}), respectively. And it occurred when comparing the bi- and monofacial solar cell measurements for all the chosen tilt angles. White paper underneath the solar cell reflect the most light back to the rear side of the cell, thus gives the largest I_{sc}. Hence, when the rear side is covered up, the I_{sc} changed more than the same measurements with black paper underneath the cell. The same as above can be said with regard to comparing the maximum power point (P_{max}), due to P_{max} and I_{sc} are both dependent on the irradiance - the higher the irradiance, the higher is the value of both P_{max} and I_{sc}. Which implies that the more irradiance present around the cell, by e.g. using good reflection materials or the location by which the solar cell is located, the more important is the type of the solar cell. Hence, if it is a bi- or monofacial solar cell.

The three gray papers that were used underneath the bifacial solar cell as reflection material, showed similar values when comparing the differences between the short-circuit current (I_{sc}), between the bi- and monofacial solar cell measurements for all the chosen tilt angles. Though, using gray3 underneath the cell showed a bit smaller values in general, than using gray1 and gray2 paper. This indicate that the papers gray1 and gray2 have approximately the same reflection characteristic, while the gray3 paper has somewhat smaller reflection characteristics. This correlate well with the graph in Figure 3.10. The maximum power point (P_{max}) for these three gray papers, also show the same trend as for the short-circuit current (I_{sc}). Whereby the reason for this was explained in the previous paragraph.

Figure 5.1 shows the IV-curves obtained for the five chosen tilt angles: 0°, 22.5°, 45°, 67.5° and 90° on the bifacial solar cell, comparing white and black paper used as reflection material underneath the cell. It can be seen from the figure that using white versus black paper - the two extremes - there is a considerable

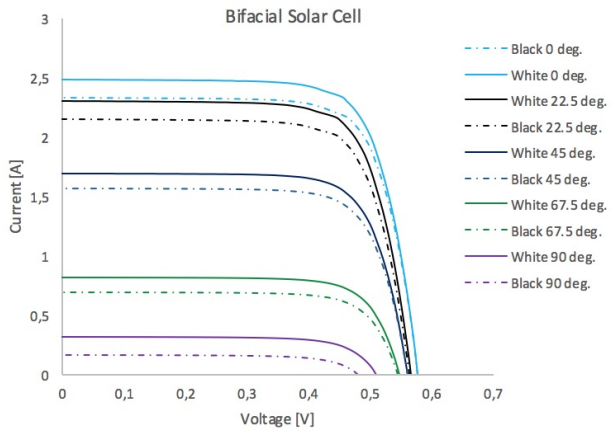

Figure 5.1: IV-curves for five different tilt angles: 0°, 22.5°, 45°, 67.5° and 90° on the bifacial solar cell. Comparing white and black paper used as reflection material underneath the cell. White and black reflection material correspond to the normal and dotted lines, respectively.

difference between the efficiency output of the bifacial solar cell, when comparing the IV-curves for the same tilt angle.

White is the most reflective colour based on the fact that white light contains all the wavelengths of the visible spectrum, and hence when the colour white is being reflected, all wavelengths are being reflected and none of them absorbed. Whereby, black is the least reflective colour, and it is the colour of a surface that absorbs all light[45]. This theory correlate well with the IV-curves shown in Figure 5.1.

5.2.2 Contribution From the Rear Side of the Bifacial Solar Cell

By using a bifacial solar cell, it is important to know how much the rear side of the cell contribute to the overall efficiency output of the solar cell. Because this will in turn indicate if the bifacial solar cell is preferable over a monofacial solar cell, hence if it is more cost effective.

Contribution from the rear side of the bifacial solar cell can be calculated according to the equation

$$100 - \frac{I_{sc(mono)} \cdot 100}{I_{sc(bi)}} \tag{5.1}$$

where $I_{sc(mono)}$ and $I_{sc(bi)}$ correspond to the short-circuit current for monofacial and bifacial solar cell, respectively. The bifacial solar cell can be seen as a monofacial solar cell, when the rear side of the cell it covered up with a black cover.

It is important to note how the irradiance varies from the bifacial measurement to the monofacial measurement, since this will have an affect on the measured output of the cell. It was not possible to measure both bi- and monofacial output at the same time. The equation below is used when calculating this difference in irradiance:

$$\left[\left(\frac{Irr._{(mono)}}{Irr._{(bi)}}\right) - 1\right] \cdot 100 \tag{5.2}$$

Here, the $Irr._{(mono)}$ and $Irr._{(bi)}$ correspond to the irradiance when the measurement was taken on the mono- and bifacial solar cell, respectively. Table 5.1 shows the contribution of the rear side of the bifacial solar cell at different tilt angles, when different reflection material (paper colours) was used underneath the cell, based on the short-circuit current (I_{sc}). Along with the differences in irradiance when measuring the bi- and monofacial solar cell output. The percentages calculated for the differences in the irradiance, have to be considered carefully though, since the irradiance value itself had a tendency to slightly change during a measurement, which might have been due to the environment - the constructed chamber was not completely closed. The data used for these calculations can be found in Section 4.1.1 and in Appendix B.

Table 5.1: The table shows the contribution of the rear side of the bifacial solar cell at different tilt angles, when different reflection material (paper colours) was used underneath the cell, based on the short-circuit current (I_{sc}). Along with the difference in irradiance when measuring the bi- and monofacial solar cell output.

Reflection Material	Tilt Angle	Contribution from the rear side of the bifacial solar cell [%]	Difference in irradiation from bi- to monofacial solar cell measurement [%]
White	0°	7.68	-0.23
	22.5°	6.90	0.02
	45°	7.41	0.12
	67.5°	16.15	-5.55
	90°	56.19	-5.90
Gray1	0°	4.41	0.82
	22.5°	3.99	0.89
	45°	4.17	0.28
	67.5°	9.19	1.00
	90°	59.18	-3.87
Gray2	0°	4.06	0.26
	22.5°	3.73	-0.39
	45°	3.78	0.88
	67.5°	8.42	4.83
	90°	58.41	-5.38
Gray3	0°	2.51	1.02
	22.5°	2.59	-0.01
	45°	1.95	-0.57
	67.5°	6.13	-1.15
	90°	59.58	0.10
Black	0°	1.71	0.31
	22.5°	0.79	-0.28
	45°	0.38	0.41
	67.5°	2.76	-5.41
	90°	63.28	-14.61

The irradiance play an important role for the efficiency output of a solar cell. The higher the irradiance, the higher the efficiency output from the solar cell. Hence, a linear photogeneration and recombination, increasing the intensity of the incident light will increase the photocurrent. In addition, Equation 2.9 indicates that V_{oc} should also increase, logarithmically, with irradiation. Therefore, cell efficiency is expected to increase with

light concentration. By use of a bifacial solar cell and good reflection material underneath (and around) the cell, the efficiency output could increase with a good amount, compared to a monofacial solar cell.

A somewhat diffuse trend that can be seen from Table 5.1 is that the larger the tilt angle, the more the rear side of the bifacial solar cell contribute to the efficiency output of the cell. In addition, the colour underneath the cell seem to also has an impact on the contribution of the rear side. The darker the colour, the larger the difference in the contribution from the rear side, going from a tilt angle of 0° to 90°. Figure 5.2 shows a plot of the values in Table 5.1.

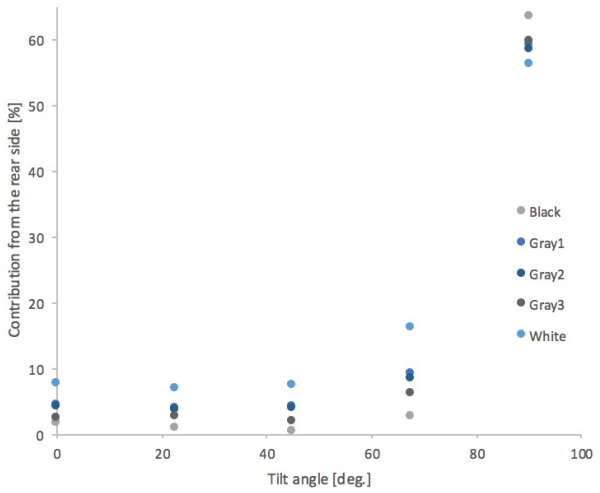

Figure 5.2: A plot of the values in Table 5.1, where the contribution from the rear side of the bifacial solar cell in percent is plotted against the tilt angle.

In the case above, the light source was fixed right above the bifacial solar cell when the cell had a tilt angle of 0°. From Table 5.1 it can be seen that the contribution from the rear side seemed to go down a bit in value before going higher then before. This might be due to the fact that the bifacial solar cell will cause some shadow on the reflection material as it gets a higher tilt angle. As the size of the shadow goes up, the contribution from the rear side goes down, until the size of the shadow has reached a maximum value. Then the contribution from the rear side goes up again, until it reaches a maximum value and the shadow has its minimum value at a tilt angle of 90° on the cell. The bifacial solar cell gets an equal amount of light onto both sides when having a tilt angle of 90°. Hence, more light will be present to the rear side alone, the larger the tilt angle is. Thereby, the rear side of the cell will contribute more the larger the tilt angle is.

An important point to notice for the case above, is that it will not necessary imply that the overall efficiency output will increase when the contribution from the rear side of the bifacial solar cell has increased. This is because as the cell get tilted more and more, less light get to hit the front side of the bifacial solar cell. Thereby, for most of the cases, the efficiency output tend to be lower, due to the fact that it is the front side of a bifacial solar cell that contribute the most to the efficiency output of the cell. By the means that the front side has a better conversion efficiency of the incident light to electricity, due to texturization of the surface.

Inaccurate/diffuse measurements may also be a reason to why the contribution from the rear side seem to go down in value before going higher. Hence, more measurements should have been taken in order to get better statistics, and maybe the observed "trend" may then have shown differently.

5.2.3 The Effect of the Tilt Angle on the Irradiance

Based on data from Appendix G, for white paper and a tilt angle of 0° on the bifacial solar cell, it can be seen that the direct and indirect radiance that reached the front and rear side of the cell was approximately 250 Wm^{-2} and 50 Wm^{-2}, respectively. Based on these values, it can be calculated how much radiance, theoretically, that was present on each side of the bifacial solar cell for the different tilt angles. The area of the cell is 156x156 mm^2. Table 5.2 shows the results and the equations used can be found in Appendix H.

Table 5.2: The table shows the effect of tilt angle on the irradiance. Where the calculations are based on the radiation numbers from Appendix G, when using white paper as reflection material and a tilt angle of 0° on the bifacial solar cell.

Tilt Angle [Deg.]	Direct Radiation, Front Side [W]	Indirect Radiation, Rear Side [W]	Total Radiation [W]	% From Rear Side	Projected area, % Radiation
0	6.1	1.2	7.3	16.7	100
22.5	5.6	1.1	6.7	16.7	92.4
45	4.3	0.9	5.2	16.7	70.7
67.5	2.3	0.5	2.8	16.7	38.3
90	$3.7x10^{-16}$	$7.5x10^{-17}$	$4.5x10^{-16}$	16.7	$6.1xx10^{-15}$

From Table 5.2 it can be seen that as the tilt angle increases, the direct and indirect radiation that hits the front and rear side of the bifacial solar cell decreases. As illustrated in Figure 5.3, it can be seen that fewer radiation beams hit the front side of the bifacial solar cell when the tilt angle increases. Whereas more of them will hit the reflection material underneath the cell and be reflected back up again to the rear side of the cell or away from the cell. Some of the radiation that reaches the front side of the bifacial solar cell, will go through the cell without being absorbed, and then be reflected due to the reflection material underneath the cell as well.

The radiation that hits the bifacial solar cell seem to be proportional to the cosine of the tilt angle:

$$radiation \sim A_c \cdot cos\,\varphi \tag{5.3}$$

where the surface area of the solar cell (A_c) is constant. Hence an increase in tilt angle, gives a decrease in radiation.

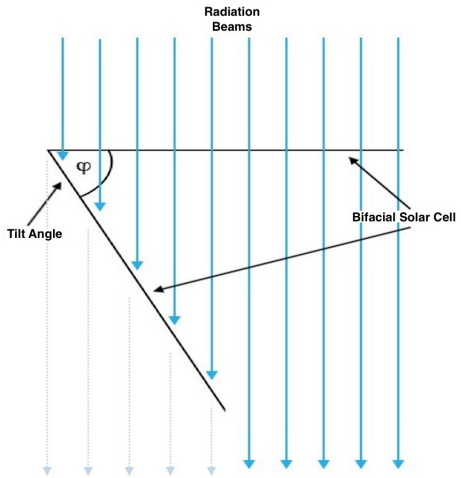

Figure 5.3: Illustration on how the radiation beams (blue arrows) hit the bifacial solar cell, when the tilt angle (φ) increases. Some of the radiation that reaches the front side of the bifacial solar cell, will go through the cell without being absorbed, and then be reflected due to the reflection material underneath the cell.

An interesting point to notice in Table 5.2 is that the percent radiation that hits the rear side according to the front side is constant and equal to 16.7 %. A question then arises, if the contribution from the rear side of the cell should have been constant as well, and independent of the tilt angle on the cell? This has been proven to not be the case and can be seen from Figure 5.2. An explanation to this might be that the radiation that hits the rear side of the cell do not have the same effect on the cell, as the direct radiation that hits the front side of the cell. By the means that the radiation hitting the rear side, contain light with a smaller range of wavelengths compared to the direct radiation, and hence the energy to some of the photons in the radiation are less than what is needed to convert the incident radiation to electricity. Different wavelengths of the light might have been absorbed on its way to the rear side of the cell. Hence, the explanation based on shadow according to the tilt angle in the previous Section 5.2.2 might still hold true. The ability of the rear side to convert the incident radiation to electricity, is somewhat decreased due to what is mentioned above according to the front side. In addition, the front side is textured, which enhances the conversion efficiency, whereby the rear side is not.

It is also important to remember, that the constant number of 16.7 % do not take into consideration any factors that might have an affect on the radiation, such as some of the radiance get reflected away to the surroundings, and other uncertainties. Hence, this number is hard to achieve in practice, due to the bifacial solar cell is not in a closed chamber with perfect conditions.

The projected area in Table 5.2 is based on the area when the bifacial solar cell has a tilt angle of 0° and the radiation received is at its maximum value. The area that gets illuminated by radiation decreases as the tilt angle increases, which leads to a decrease in efficiency output. The calculated values in Table 5.2 is based on the case where the light source is fixed above the solar cell. Hence, sunlight on the other hand, whereby the sun changes position throughout a day, will give somewhat different results.

5.2.4 Snow vs. White Paper as Reflection Material

The difference in output from using white paper to using snow as reflection material was calculated to be -1.85 %, -4.10 % and -37.05 % for tilt angle 0°, 45° and 90°, respectively. The snow that was used was fresh and wet, which most likely has had an affect on how much light the snow reflected back on to the rear side of the cell. Since the snow was collected onto two plates, the plates themselves might have absorbed some of the light as time went by and the snow melted. The plates were of a dark transparent colour and therefore the snow layer should have been a few centimetres more, so that the plates beneath could not shine through the layer of snow and absorb some of the light (the achieved snow layer was approximately a few centimetres thick). Because of the time at the year when the experiment was performed, this was not achievable. Hence, the absorption of light from the two plates could have been one of the reasons to the decrease in the output, when going from using white paper to snow as reflection material.

As the tilt angle got higher, the differences in output got larger. This might be explained due to the radiation reaching the bifacial solar cell, which then comes a larger extent from the reflected light and not directly from the light source itself. The light source, in this case, was fixed right above the bifacial solar cell, when the cell had a tilt angle of 0°. Because white colour reflects all light and absorbs nothing, and snow tend to be more grayish in colour due to e.g. pollution and hence reflect less light, the case where snow was used as the reflection material underneath the cell experienced a decrease in output.

It has to be mentioned that the colour of the snow, depends to a large extent to where it is. The snow in the cities tend to be more polluted, hence more grayish in colour, than the snow in the mountains for instance. Also, some of the radiance reaching the snow will be absorbed and start melting the snow itself, instead of being reflected away.

5.2.5 Rime Ice on the Bifacial Solar Cell vs. Cold Cell

In comparing the bifacial solar cell as cold versus with rime ice, the differences were not very significant. The temperature on the cell when rime ice was applied, lied between 11.2 °C and 15.2 °C for the five measurements taken. Whereby, the cold cell had a temperature of 15.6 °C. All the six measurements had an irradiance between 254.9 Wm^{-2} and 258.9 Wm^{-2}. Hence, the conditions throughout the measurements did not deviate much from each other, although some small differences were present.

In Figure 5.4 the IV-curves for three different states of the bifacial solar cell - rime ice, cold and normal cell[7] - have been compared. It can be seen from the IV-curves that both rime ice on the cell and cold cell give approximately the same efficiency outputs, whereby the normal cell has a lower efficiency output in comparison. Hence, the temperature has an important effect on the power output from the solar cell and the most significant is the temperature dependence of the voltage. The voltage decreases with increasing temperature, which is clearly evident in Figure 5.4. Hence, the cold climate that is present in the Nordic countries has a positive affect on the efficiency output from the solar cells.

From Figure 4.8 it can be seen only small differences in the voltage, when comparing the six measurement; five with rime ice on the bifacial solar cell and one with the same cell only cold. But in Figure 5.4 it can be seen a significant difference in voltage between the rime ice/cold cell and the normal cell, this is due to

[7] A normal cell is here related to a cell with normal temperature, by which the temperature has not been affected by other than light shining on to the cell.

the large difference in temperature, going from 15 °C to 38 °C. From theory it has been stated that the voltage decreases with increasing temperature, and the voltage decrease of a silicon cell is typically 2.3 mV per degree Celsius[24]. This did not quite hold true in this case, but again these measurements are not performed under Standard Test Conditions (STC).

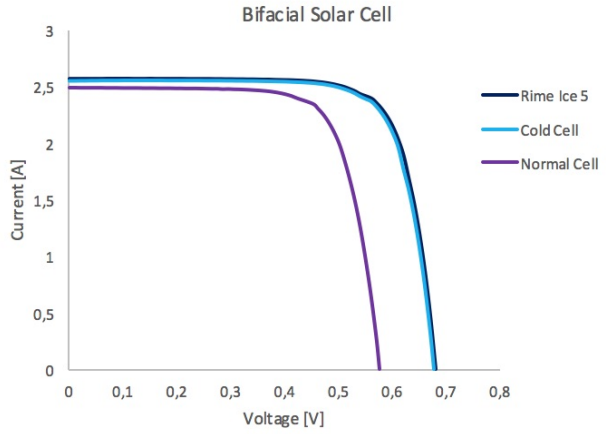

Figure 5.4: IV-curves for a comparison of the bifacial solar cell in three different states: rime ice, cold and normal. All the measurements were performed with 0° tilt angle on the bifacial solar cell and with white paper used as reflection material.

Table 5.3 gives the values for short-circuit current (I_{sc}), open-circuit voltage (V_{oc}), maximum power point (P_{max}), fill factor (FF), energy conversion efficiency (η), irradiance [Wm^{-2}] and the temperature on the bifacial solar cell [deg.C]. These values show the differences between the three states of the bifacial solar cell, and how the different values changes with lower temperature. The irradiance for the normal cell have a value that is 1.3 % lower than the values for the two cells that are cold, which is important to be aware of when considering these numbers.

Table 5.3: The table shows a comparison of the bifacial solar cell in three different states: rime ice, cold and normal, with values for short-circuit current (I_{sc}), open-circuit voltage (V_{oc}), maximum power point (P_{max}), fill factor (FF), energy conversion efficiency (η), irradiance [Wm^{-2}] and the temperature on the solar cell [deg.C]. The bifacial solar cell had a tilt angle of 0° and white paper was used as reflection material.

Tilt Angle: 0°	I_{sc} [A]	V_{oc} [V]	(P_{max})	FF	η	Irradiance [Wm^{-2}]	Temp. Solar Cell [deg.C]
Rime Ice5	2.565	0.680	1.340	0.768	0.215	256.5	15.2
Cold Cell	2.555	0.676	1.328	0.769	0.213	256.7	15.5
Normal Cell	2.487	0.577	1.064	0.742	0.173	253.2	37.6

5.2.6 The Results Obtained From the Measurements Performed Outside

The IV-curves that were obtained outside using sunlight, were to a large degree affected by the bad weather during the measurements, as shown in Section 4.2. The irradiance lied between 24 Wm^{-2} and 176 Wm^{-2}, which is a relatively large span, but again was due to the weather condition. Hence, the obtained efficiency outputs did vary a bit in value, as expected.

Another effect that can be seen from the IV-curves in Section 4.2 and is due to the unstable irradiance during the measurement, is the abnormal shape of some of the curves. When clouds are present on the sky, a suddenly shift in irradiance can appear and cause this abnormality to occur. It is not an unusual phenomena and will not inflict anything on the solar cell itself, but it is a point worth mentioning as to what degree the efficiency output can be comparable with measurement taken under stable conditions.

Rain did accumulate on the bifacial solar cell during the measurements as well, but this has been studied as to not have any affect on the measured efficiency output [46]. The temperature was also low (10-11 °C), which again cause low temperature on the cell itself, ranging between 13.0 °C to 15.8 °C and hence affect the efficiency output positively as mentioned earlier.

The direct and indirect irradiance that hit the bifacial solar cell were thoroughly measured with in total three sensors - the ISET sensor and the two Pyranometer. Table 5.4 shows the values obtained for the irradiance, for one of the measurements performed outside (see Appendix D for the rest of the irradiance values). The two values for the direct irradiance for each respective tilt angle, should in theory be in agreement. It can be seen from the table that they deviate slightly from each other, which can be due to the slightly difference in position of the two sensors on the set-up.

Table 5.4: The table gives the values for the direct irradiance [Wm^{-2}] measured on the ISET sensor, along with both the direct and indirect irradiance [Wm^{-2}] measured by the two Pyranometer. The measurements were performed at different tilt angles on the bifacial solar cell.

	Bifacial Solar Cell	Pyranometer			
	Tilt Angle	Direct Irr. (ISET) [Wm^{-2}]	Direct Irr. [Wm^{-2}]	Indirect Irr. [Wm^{-2}]	$\frac{\text{Indirect Irr. [Wm}^{-2}\text{]}}{\text{Direct Irr. [Wm}^{-2}\text{]}}$ [%] (Based on Pyranometer numbers)
Concrete	0°	31.2	36.5	10.8	29.6
	22.5°	73.1	78.1	16.2	20.8
	45°	29.4	37.3	9.1	24.3
	67.5°	24.5	33.4	11.3	33.9
	90°	25.1	36.7	13.3	36.2

In Table 5.4 it has been calculated how much irradiance that reached the rear side of the bifacial solar cell in comparison to the front side of the cell. Even though the irradiance to the rear side of the cell lies between 24.3 to 36.2 percent of that to the front side, does not mean that the rear side contribute that much to the efficiency output of the solar cell, as mentioned earlier. This can be explained due to the front side of the bifacial solar cell has been textured to reduce the surface reflectance. Hence, a pyramidal structure has been formed that can trap the light inside the cell by internal reflection, as mentioned in Section 2.1.4. The rear side of the bifacial solar cell has not been textured and hence will reflect away more of the light that strikes upon it than the front side does.

Uniform shading due to clouds blocking solar radiation or the sun setting, reduces the output of the system of solar cells [35]. Hence, a cloudless sky would have given a different efficiency output from the bifacial solar cell then what was the case. Not only would the front and rear side of the cell get more irradiance, but the irradiance itself would have been more stable throughout the measurement due to no blocking of the sunlight from clouds. The albedo effect would also be present to a larger extent and increase the output.

5.2.7 Irradiance on the Bifacial Solar Cell

Based on Figure 3.10 it can be calculated how much irradiance can be present on the bifacial solar cell during 24 hours, while using white paper as reflection material and a tilt angle of 0° on the cell. Based on the data from the figure (see Appendix G), it can be seen that the direct and indirect irradiance that reached the front and rear side of the cell was approximately 250 Wm^{-2} and 50 Wm^{-2}, respectively. Hence, 20 % of the direct irradiance was reflected from the surroundings.

The total irradiance that the bifacial solar cell would receive during a whole day would be

$$(250\,Wm^{-2} + 50\,Wm^{-2}) \cdot 24\,hours = 7200\,Whm^{-2} = 7.2\,kWhm^{-2} \tag{5.4}$$

Figure 3.10 also shows that using black paper as reflection material, will decrease the indirect irradiation to the rear side of the cell to only 5 %. Which will give a total irradiance during 24 hours of 6.1 kWhm^{-2}, using the same calculations as above. This implies a decrease in output by 15.3 %, if all the radiation is converted into electricity by both sides of the cell. Which implies further that both sides of the bifacial solar cell convert the incident radiation into electricity equally good. For most cases, this is not the case, whereas it is the front side of the cell that contribute the most to the conversion.

If this calculation above would have been performed with sunlight as the source for the radiation that hits the bifacial solar cell, the values obtained would then be strongly dependent on where the bifacial solar cell is mounted. Hence, the solar angle of incidence is important, which affect both how much direct irradiance is received by the bifacial solar cell and the albedo effect.

5.3 Discussion According to Others Work and Theory

In this section, it will be drawn some lines between the results obtained in this study and others work in the same field of study, and relevant theory will be used in the discussion.

5.3.1 The Design of a Bifacial Solar Cell and Reflection Materials

The design of a bifacial solar cell makes it possible to collect radiation from both sides of the cell. Hence, the cell can use the albedo effect (Section 2.3.1.1) as an advantage to increase it's efficiency output, by using a material of highly reflective characteristic surrounding the cell. And by use of a good reflection material, the light that has been transmitted trough the cell, which has not been absorbed at the BSF (back surface field), can be reflected back up again to the rear side of the bifacial solar cell. As mentioned earlier, the front side of a bifacial solar cell is the side that contribute the most to the efficiency output, both because of the amount of direct irradiance that reaches it and because of the textured surface. This gives a bifacial solar cell a large advantage over a monofacial solar cell.

The reflection material that was used in this study was paper in different colours, this was in order to investigate the effect of the reflectivity characteristic on the colours used. It was clearly evident that darker paper lead to less reflected light onto the rear side of the bifacial solar cell compared to lighter colours, and hence a smaller output.

Good reflection materials to be used, should have good reflectivity characteristics and be of light colour, due to the fact that darker colour absorb more light. It should be cheap, in order to be profitable and because there might be a large area that have to be covered up. In addition, it is of convenience that the material can withstand the weather conditions and last for a longer period of time.

5.3.2 The Nordic Climate

The Nordic climate is characterized by relatively low temperatures and cold weather as mentioned in Section 2.6, and which is due to the sun's low intensity in the Nordic countries compared to e.g. the intensity of the sun at the equator. These conditions are not the most ideal for solar cells, and PV technology tend to face certain challenges when mounted in cold climates. Such as snow and ice that may form and accumulate on the panels, obstructing light from reaching the cells, and thus hampering the electricity production.

Snow (and ice) might not only be of negatively impact on solar cells, as long as it does not cover the solar cell itself. A bifacial solar cell can take great advantage of the snow that lies in the surroundings, by the means of reflection of light back onto the rear side of the cell. This could again increase the efficiency output with a good amount. Using snow as a reflection material can be a cheap way to increase the efficiency output of the bifacial solar cell during the winter season, since this season in Nordic countries tend to give lower outputs then usual, compared to i.e. spring and summer season.

Temperature has an important effect on the power output from the solar cell, and the most significant is the temperature dependence of the voltage. The voltage decreases with increasing temperature (Section 2.4.4). Hence, there might be another benefit for solar cells to be mounted in the Nordic climate, alongside using snow as a reflection material, namely the relatively low temperature that tend to be present. The effect on the bifacial solar cell on temperature can be seen in Table 5.3. An increase in short-circuit current (I_{sc}), maximum power point (P_{max}), fill factor (FF) and energy conversion efficiency (η) can be observed, as well as the increase in open-circuit voltage (V_{oc}) with decreasing temperature. Hence, the values obtained correlate well with theory.

Accumulation of rime ice on the bifacial solar cell has shown to have a positive effect on the efficiency output, as with a cold cell. Both cases decrease the temperature on the cell, obviously, but the effect observed with rime ice on the cell was quite interesting. The rime ice on the cell did not hamper the output of the cell, but instead a slightly small increase was observed as can be seen from the comparison in Table 5.3. This was evident, even though the layer of rime ice on the bifacial solar cell was not completely homogeneous throughout the whole surface. Since partial shading on the cell causes complex changes to the balance of the electric current against the conductive properties of the cell, it might have been thought that an inhomogeneous layer of rime ice could have caused some of the same problems. This might be explained due to the fact that rime ice is to a large degree transparent and will let the irradiance get through the layer and onto the bifacial solar cell, and hence do not block the surface of the cell for any light.

Light changes speed as it passes from one medium to another, known as refraction, where the frequency of light does not change as it refracts. Also the direction of the light might have changed a bit according to Snell's law, Equation 2.17. But due to the fact that the refractive index for air is smaller than that for ice, 1.0 versus 1.3[47], respectively, the angle of incidence would be smaller when it hits the surface of the solar cell, then what it came in with (Equation 2.17). Hence, the change in medium going from air to ice would

not decrease the irradiance on the solar cell. In addition, rime ice might be on the solar cell a certain amount of time before melting away, hence the effect may last for some time, depending on the thickness of the rime ice layer.

5.3.3 Fill Factor (FF) and Energy Conversion Efficiency (η)

The fill factor (FF), which is essentially a measure of the quality of the solar cell, has typically values ranging from 0.5 to 0.82 [48]. Not only is the fill factor dependent on the parameters in Equation 2.10, such as the open-circuit current (I_{sc}) and open-circuit voltage (V_{oc}), but it also depend on the material by which the solar cell is based on, e.g. mono- or multicrystalline silicon. In this study a monocrystalline bifacial solar cell was used, as mentioned in Chapter 3. Monocrystalline silicon is a material of higher quality then multicrystalline silicon, hence gives better output from the solar cell.

A trend that can be seen from the basic measurements (Section 4.1.1) is that the fill factors have values between 0.705 and 0.750, which are quite good numbers. Whereby, the fill factors for the measurements using a cold cell and by use of rime ice on the cell, showed even higher values. In this case the average fill factor was calculated to be 0.769, which might be explained by the low temperature on the cell and hence a better output.

The irradiance that is present on the bifacial solar cell, influence the parameters by which the fill factor are dependent on. This was evident for the outside measurements, where the fill factors had quite different values, which most likely was due to the unstable weather that was present for the time being. The fill factors discussed in this section are for the bifacial solar cell only.

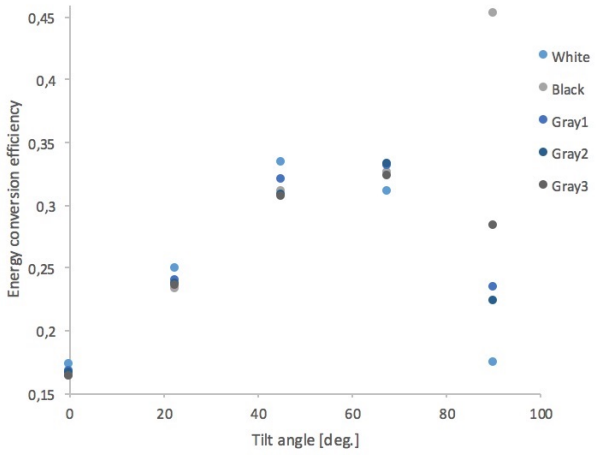

Figure 5.5: A plot of the values to the energy conversion efficiency (η), based on the results obtained in Section 4.1.1.

The energy conversion efficiency (η) is the percentage of incident light energy that actually ends up as electric power [11]. There can not be seen any clear trend for the energy conversion efficiency obtained in Section 4.1.1 and plotted in Figure 5.5, based on the five tilt angles that where used throughout the measurements. But there can be seen a linear trend through three of the tilt angles: 0°, 22.5° and 45°. Which indicate that the radiance that hits the front side of the cell play an essential part to how much energy from the incident

light that actually ends up as electricity, compared to the radiation that hits the rear side. Even though the energy conversion efficiency increases for these tilt angles, the efficiency output of the cell decreases as the tilt angle increases, since the cell get less radiance directly onto it, but more from reflection. This is because the light source, in this case, was fixed right above the bifacial solar cell.

5.3.4 Performance of Bifacial Solar Cells in the Nordic Climate

The performance to a bifacial solar cell depends strongly on latitude, diffuse fraction and albedo [8]. The results obtained inside (Section 4.1.1) using a fixed light source (LED lamp), gave very different outcome than the results obtained outside with the sunlight as the light source (Section 4.2). The weather present for the time being, made it impossible to replicate the same procedure when taking the outside measurements as done inside.

An important factor to take into consideration when performing an experiment outside, is that the sunlight will illuminate the bifacial solar cell in a different way than a fixed light source would do. Which can lead to an increase in the efficiency output of the cell, if the cell is properly mounted on its respective place. Guo et al. [8] has performed a global comparison between vertically mounted bifacial modules (VMBM) facing east-west and conventionally mounted monofacial modules (CMMM)[8], where it showed that VMBM facing east-west are preferable in the Nordic countries [8]. This is because only a small albedo value is required to result in a better performance of the VMBM in the Nordic area, and the real albedo value is relatively high - sun's rays spread is greater the smaller the angle of incidence, hence larger contribution from the albedo. When the albedo increases, diffuse radiation from the ground also increases, thus bifacial modules are more apt to receive more radiation for these places [8]. The monofacial modules can not take advantage of the albedo effect in the same way as the bifacial modules, due to only one side of the cell contribute to the efficiency output.

Vertically mounted bifacial modules have a generation profile that is significantly different to that of a conventionally mounted monofacial module. VMBM produces more energy in the early morning and late afternoon than CMMM, as can be seen in Figure 5.6 [8]. This indicate that the VMBM, in theory, can achieve higher efficiency output than the CMMM, when taken into consideration that the place where the solar cells are mounted is preferable to bifacial solar cells. Hence, that the latitude where the cells are positioned, diffuse fraction and albedo effect are accounted for.

[8] Conventionally mounted monofacial modules are tilted at latitude towards the equator.

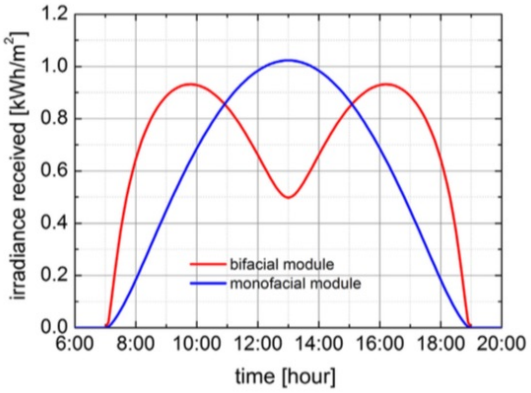

Figure 5.6: Simulated radiation received by a VMBM and a CMMM on a certain day in Singapore. The diffuse fraction is set to be 0.18, and albedo is set to be 0.35, which are practical values for clear-sky conditions in Singapore[8].

VMBM will not have any problem with snow covering the solar cells, as can be the case for the cells in the CMMM[8]. Bifacial solar cell can be installed e.g. as sound barriers along roadsides, as sun-shields and as building-integrated photovoltaics[11]. In addition, VMBM need less space than CMMM and hence a higher efficiency output can be achieved by use of fewer solar cells. This have a positive effect on the environment, and which will do good for the world we live in, in the long-term.

5.3.4.1 Midnight Sun and Polar Nights

Midnight sun is a natural phenomenon that appear on places north of the Arctic Circle (and south of the Antarctic Circle) during summer months. This phenomenon could be of great advantage for bifacial solar cells during that time of the year and hence increase the efficiency output of the cell. But having that said, places north of the Arctic Circle (and south of the Antarctic Circle) also experiences polar nights during the winter months. It would have been interesting to study the effect of the midnight sun and polar nights on the efficiency output of a bifacial solar cell during a year, to investigate if these two effects cancel each other out, due to the efficiency output from the cell. These two phenomenons are worth mentioning, since they are present north in the Nordic countries.

5.3.5 Characterization of a Bifacial Solar Cell

Bifacial solar cells present difficulties when measured due to their bilateral properties and hence external contributions from the measured systems itself[11]. The technique that was used in this study to investigate how much the rear side of the bifacial solar cell contributed to the efficiency output of the cell, was simply by covering the rear side with a black cover and perform the same measurement again. The difference between the two measurements then corresponded to the rear side's contribution to the efficiency output. It can be seen from the results in Section 4.1.1 that there are an overall increase in output going from a monofacial to a bifacial solar cell, as expected. The same can not be said about the results for the outside measurements, Section 4.2, though. Because the irradiance that was present during these measurements were very unstable, for both the bifacial and monofacial measurements. This gave a higher output for the monofacial solar cell,

since a higher irradiance was present than when the bifacial solar cell was measured. Hence, if the irradiance had been more stable, the results would have been different.

Reflection is the reason to why the efficiency output increases when going from a monofacial to a bifacial solar cell. Since the bifacial solar cells can collect photons from incident and albedo radiation reaching both the front and rear side of the solar cell, simultaneously. In addition, an increase in efficiency will occur if part of the light passing through the cell is reflected and re-entering the rear side of the cell.

6 Conclusion

A fast depletion of conventional energy sources and increasing energy demand are encouraging the development on PV (photovoltaic) technologies [49], and here the bifacial solar cells can be proven useful. Based on the fact that these solar cells can collect photons from incident and albedo radiation reaching both the front and rear side of the solar cell, simultaneously.

This study has looked at a bifacial solar cell in the Nordic climate, by which this climate is characterized by relatively low temperatures and cold weather. Bifacial solar cells in a climate like this, faces certain challenges, such as low irradiance due to the sun's low angle of incidence and the difference in irradiance due to the different seasons throughout a year (especially winter versus summer), and the weather conditions that are present. Snow and ice may form and accumulate on the panels, obstructing the light from reaching the cells, and thus hampering the electricity production. Which again can lead to the electricity generation of the bifacial solar cells get significantly reduced.

Despite these challenges it has been proven that bifacial solar cells can get good efficiency outputs also in a Nordic climate. Mainly due to the low temperatures that are present, which have shown to give a positive impact on the solar cells' efficiency outputs, which again correlate well with theory. In addition, rime ice on the bifacial solar cell has shown some interesting results. It has given good outputs and which is thought to be due to low temperature on the cell itself. Whereas it might be thought that rime ice could have hampered the conversion in the cell, since it covers the solar cell, but that was not the case.

In addition, it has been investigated how different tilt angels on the bifacial solar cell and reflection materials affect the efficiency output of the cell. It has been found that the larger the tilt angle, the more the rear side of the cell contribute to the cell's output. And that reflection materials with lighter colours are preferable, to get higher efficiency outputs from the solar cell. Snow can then be used to increase the output during the winter season, when behaving like a reflection material and not covering the cell itself, though. This can be related to the fact that the performance to a bifacial solar cell depends strongly on latitude, diffuse fraction and albedo. Hence, the way the bifacial solar cell is mounted, according to the sunlight on its respective position, play an important role to how the efficiency output will be.

To investigate how much the rear side of the bifacial solar cell contributed to the efficiency output of the cell, a technique was applied by simply cover the rear side of the cell with a black cover and perform the same measurement again. The difference between the two measurements corresponded then to the rear side's contribution to the efficiency output. An increase in efficiency was observed from the measurements on the bifacial solar cell according to the monofacial solar cell, which correlate well with theory. And is based on the ability the bifacial solar cell has to take advantage of the albedo effect, as well as the light that pass through the cell and is reflected and re-enter the rear side of the cell again.

Bifacial solar cells seem to give good efficiency outputs when mounted in the Nordic climate. How they are mounted play an important role, in order to obtain the best possible outcome from these cells, and Guo et al. [8] has studied that vertically mounted bifacial modules facing east-west is the best choice. This is based on the fact that the solar energy available to solar panel systems depends on different factors, such as latitude, weather and the angle of incoming sunlight, and each affect the amount of solar energy available at a location.

7 Further Work

The study of bifacial solar cells in Nordic climate is a relatively new study, hence it is only the imagination that sets the limits to what can be investigated further. A good approach might be to do more outside measurements, especially concerning parameters that characterizes the Nordic climate i.e. snow (and sleet), ice and cold temperatures. Rain is already proven to not have any affect on the measured efficiency output [46]. It might also be of interests to study the affect of the midnight sun and polar nights on the output efficiency from the bifacial solar cell during a year, since these phenomenons are present in the north of the Nordic countries.

In addition, the albedo effect on the bifacial solar cell could be investigated. Since this effect play an important role in the Nordic countries, due to the low angle of incidence of the sun, and hence the surface area over which the sun's rays spread is greater the smaller the angle. This effect reduces the sun's intensity in any one place.

Different reflection materials with good reflectivity characteristics could be of interest to study further, to increase the efficiency output of the bifacial solar cells mounted in the Nordic climate. The material should not be too expensive and also have god stability due to the different weather conditions.

Installation options for modules of bifacial solar cells could be of great advantage to also study, and an optimization can be carried out for the Nordic climate. Optimization can be influenced by restrictions imposed by the specific application and by the available installation site.

Bibliography

[1] A. Luque, A. Cuevas, and J.M. Ruiz. Double-sided n+-p-n+ solar-cell for bifacial concentration. *Sol Cells*, 2: 155–166, 1980.

[2] Mori H. *US. Patent No. 3,278,811*, October 1966.

[3] Linda Doman. EIA projects 28% increase in world energy use by 2040, 2017. URL `https://www.eia.gov/todayinenergy/detail.php?id=32912`. (cited 2018-03-10).

[4] European Commission. Paris Agreement, 2015. URL `https://ec.europa.eu/clima/policies/international/negotiations/paris_en#tab-0-0`. (cited 2018-02-22).

[5] European Renewable Energy Council. Renewable energy technology roadmap 20% by 2020, EREC press release, 2008. (cited 2018-02-22).

[6] A. Cuevas, A. Luque, J. Eguren, and J. del Alamo. 50 Per cent more output power from an albedo-collecting flat panel using bifacial solar cells. *Solar Energy*, 29(5):419 – 420, 1982. ISSN 0038-092X. doi: https://doi.org/10.1016/0038-092X(82)90078-0. URL `http://www.sciencedirect.com/science/article/pii/0038092X82900780`.

[7] Karsenty A. Drori A. Eisenberg N. Kreinin L., Bordin N. *Experimental analysis of the increases in energy generation of bifacial over mono-facial PV modules. In: Proceedings of the 26th European photovoltaic solar energy conference, Valencia, Spain;*, 2010.

[8] Siyu Guo, Timothy Michael Walsh, and Marius Peters. Vertically mounted bifacial photovoltaic modules: A global analysis. *Energy*, 61:447 – 454, 2013. ISSN 0360-5442. doi: https://doi.org/10.1016/j.energy.2013.08.040. URL `http://www.sciencedirect.com/science/article/pii/S0360544213007275`.

[9] R. Guerrero-Lemus, R. Vega, Taehyeon Kim, Amy Kimm, and L.E. Shephard. Bifacial solar photovoltaics – A technology review. *Renewable and Sustainable Energy Reviews*, 60:1533 – 1549, 2016. ISSN 1364-0321. doi: https://doi.org/10.1016/j.rser.2016.03.041. URL `http://www.sciencedirect.com/science/article/pii/S1364032116002768`.

[10] Jai Prakash Singh, Timothy Walsh, and Armin ABERLE. *A new method to characterize bifacial solar cells*, 08 2014.

[11] Claudia Duran. *Bifacial Solar Cells : High Efficiency Design, Characterization, Modules and Applications*. PhD thesis, Universität Konstanz, Konstanz, 2012.

[12] PV Education, (cited 2018-02-08). URL `http://www.pveducation.org/pvcdrom/pn-junctions/diffusion`.

[13] Ghandhi. *VLSI Fabrication Principles: Silicon and Gallium Arsenide*, 1994.

[14] Jayaprasad Arumughan. *Investigations on Solar Grade Silicon and Process Engineering of Advanced Silicon Solar Cells*. PhD thesis, Universität Konstanz, Konstanz, 2007.

[15] Solar Busbar and Fingers Explained, 2017. URL `http://www.novergysolar.com/solar-busbar-fingers-explained/`. (cited 2018-03-17).

[16] PV Education, (cited 2018-02-07). URL `http://www.pveducation.org/pvcdrom/design/metal-grid-pattern`.

[17] Solar cell busbar: 3BB, 5BB or 0BB?, 2016. URL `http://sinovoltaics.com/technology/solar-cell-busbar-3bb-5bb-or-0bb/`. (cited 2018-03-17).

[18] Gunnar Schubert, Frank Huster, and Peter Fath. *Current transport mechanism in printed Ag thick film contacts to an N-type emitter of a crystalline silicon solar cell*, 2004.

[19] Christophe Ballif, D. M. Huljic, G. Willeke, and A. Hessler-Wyser. Silver Thick-Film Contacts on Highly Doped n-Type Silicon Emitters: Structural and Electronic Properties of the Interface. -, 82:1878 – 1880, 04 2003.

[20] A. Hauser, G. Hahn, M. Spiegel, H. Feist, O. Breitenstein, J.P. Rakotoniaina, P. Fath, and Ernst Bucher. Comparison of different techniques for edge isolation. -, 01 2001.

[21] Bifacial PV: comparing apples with apples sometimes does not make sense, 2018. URL `https://www.pv-tech.org/technical-papers/bifacial-pv-comparing-apples-with-apples-sometimes-does-not-make-sense`. (cited 2018-05-30).

[22] Adrian Kitai. Principles of Solar Cells, LEDs and Diodes : The role of the PN junction, 2011.

[23] Jenny Nelson. The Physics of Solar Cells, 2003.

[24] Solar Electricity, 2000.

[25] Afshin Izadian, Arash Pourtaherian, and Sarasadat Motahari. Basic model and governing equation of solar cells used in power and control applications. -, pages 1483–1488, 09 2012.

[26] Purnomo Sidi Priambodo, Didik Sukoco, Wahyudi Purnomo, Harry Sudibyo, and Djoko Hartanto. Electric energy management and engineering in solar cell system. In Arturo Morales-Acevedo, editor, *Solar Cells - Research and Application Perspectives*, chapter 12. InTech, Rijeka, 2013. doi: 10.5772/52572. URL `http://dx.doi.org/10.5772/52572`.

[27] Priyanka Singh and N.M. Ravindra. Temperature dependence of solar cell performance—an analysis. *Solar Energy Materials and Solar Cells*, 101:36 – 45, 2012. ISSN 0927-0248. doi: https://doi.org/10.1016/j.solmat.2012.02.019. URL `http://www.sciencedirect.com/science/article/pii/S0927024812000931`.

[28] Miroslaw Jonasz. *Light Scattering by Particles in Water: Theoretical and Experimental Foundations : Theoretical and Experimental Foundations*. Elsevier Science, Amsterdam, June 2007. ISBN 9780080548678. URL `http://site.ebrary.com/id/10188239`.

[29] Miles V. Klein. Optics, 1986.

[30] Gray D.M O'Neill, A.D.J. *Solar radiation penetration through snow. In: Proceedings of UNESCO-WMO-IAHS Symposia on the role of snow and ice in hydrology, vol. 1. IAHS Press, Wallingford, UK*, 1973.

[31] Donald K. Perovich. Light reflection and transmission by a temperate snow cover. *Journal of Glaciology*, 53 (181):201–210, 2007. doi: 10.3189/172756507782202919.

[32] The Beer-Lambert Law, (cited 2018-02-14). URL `https://chem.libretexts.org/Core/Physical_and_Theoretical_Chemistry/Spectroscopy/Electronic_Spectroscopy/Electronic_Spectroscopy_Basics/The_Beer-Lambert_Law`.

[33] Chris Deziel. How Does Latitude Affect Climate?, 30 January 2018. URL `https://sciencing.com/latitude-affect-climate-4586935.html`. (cited 2018-02-26).

[34] B. Marion, J. Rodriguez, and J. Pruett. *Instrumentation for Evaluating PV System Performance Losses from Snow: Preprint*, 2009.

[35] Achim Woyte, Johan Nijs, and Ronnie Belmans. Partial shadowing of photovoltaic arrays with different system configurations: literature review and field test results. *Solar Energy*, 74(3):217 – 233, 2003. ISSN 0038-092X. doi: https://doi.org/10.1016/S0038-092X(03)00155-5. URL http://www.sciencedirect.com/science/article/pii/S0038092X03001555.

[36] Andreas J. Dietz, Christoph Wohner, and Claudia Kuenzer. European Snow Cover Characteristics between 2000 and 2011 Derived from Improved MODIS Daily Snow Cover Products. *Remote Sensing*, 4(8):2432–2454, 2012. ISSN 2072-4292. doi: 10.3390/rs4082432. URL http://www.mdpi.com/2072-4292/4/8/2432.

[37] Erlend Andenæs, Bjørn Petter Jelle, Kristin Ramlo, Tore Kolås, Josefine Selj, and Sean Erik Foss. The influence of snow and ice coverage on the energy generation from photovoltaic solar cells. *Solar Energy*, 159:318 – 328, 2018. ISSN 0038-092X. doi: https://doi.org/10.1016/j.solener.2017.10.078. URL http://www.sciencedirect.com/science/article/pii/S0038092X17309581.

[38] Scott N. Williamson, Luke Copland, and David S. Hik. The accuracy of satellite-derived albedo for northern alpine and glaciated land covers. *Polar Science*, 10(3):262 – 269, 2016. ISSN 1873-9652. doi: https://doi.org/10.1016/j.polar.2016.06.006. URL http://www.sciencedirect.com/science/article/pii/S1873965216300500. ISAR-4/ICARPIII, Science Symposium of ASSW2015.

[39] P.A. Coppin, B.W. Coppin, C.L. Penney, and P. Schwerdtfeger. Zonal characteristics of urban albedos. *Urban Ecology*, 3(4):365 – 369, 1978. ISSN 0304-4009. doi: https://doi.org/10.1016/0304-4009(78)90039-6. URL http://www.sciencedirect.com/science/article/pii/0304400978900396.

[40] G. Friesen A. Virtuani, D. Pavanello. *Overview of temperature coefficients of different thin film photovoltaic technologies. In: Proceedings of 25th European Photovoltaic Solar Energy Conference and Exhibition/5th World Conference on Photovoltaic Energy Conversion, Valencia, Spain, September 6–10*, 2010.

[41] Amy Harris. Sun Intensity vs. Angle., 24 April 2017. URL https://sciencing.com/sun-intensity-vs-angle-23529.html. (cited 2018-02-26).

[42] Equilight Solar Mass, (cited 2018-03-06). URL https://www.mikrogartneriet.no/products/equilight-solar-mass-pro.

[43] Andreas Halm, Valentin Mihailetchi, Giuseppe Galbiati, Lejo Koduvelikulathu, Razvan Roescu, Corrado Comparotto, Radovan Kopecek, Kristian Peter, and J Libal. The Zebra Cell Concept – Large Area n-type Interdigitated Back Contact Solar Cells and One-Cell Modules Fabricated Using Standard Industrial Processing Equipment. -, 09 2012.

[44] EVA (ethylene vinyl acetate) Film: composition and application, (cited 2018-03-07). URL http://sinovoltaics.com/learning-center/materials/ethylene-vinyl-acetate-eva-film-composition-and-application/.

[45] Chris Deziel. *Which Colors Reflect More Light?*, 23 April 2018. URL http://sciencing.com/colors-reflect-light-8398645.html.

[46] Christina Benjaminsen. *How well do solar cells really work in the Nordic climate?*, 16 March 2018. URL https://geminiresearchnews.com/2018/03/how-well-do-solar-cells-really-work-in-the-nordic-climate/.

[47] John Haugan and Eimund Aamot. *Gyldendals tabeller og formler i fysikk (Fysikk 1 og Fysikk 2)*. Gyldendal, 2nd. edition, 2011.

[48] *Part II – Photovoltaic Cell I-V Characterization Theory and LabVIEW Analysis Code*, 10 May 2012. URL http://www.ni.com/white-paper/7230/en/.

[49] G.K. Singh. Solar power generation by pv (photovoltaic) technology: A review. *Energy*, 53:1 – 13, 2013. ISSN 0360-5442. doi: https://doi.org/10.1016/j.energy.2013.02.057. URL http://www.sciencedirect.com/science/article/pii/S0360544213001758.

List of Figures

List of Tables

Appendices

A Calculation of the Open-Circuit Voltage (V_{oc})

In order to get the exact value of the open-circuit voltage (V_{oc}) from the obtained data set, the Pythagorean theorem was applied. The equation for the Pythagorean theorem is

$$a^2 + b^2 = c^2 \tag{A.1}$$

where a and b are the lengths of the two legs of the triangle, and c is the length of the hypotenuse, which can be seen from Figure A.1.

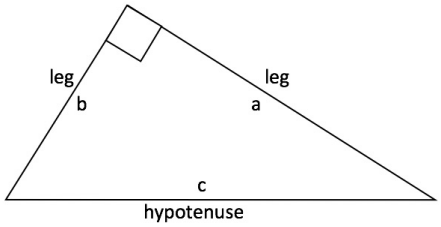

Figure A.1: A right triangle used for the Pythagorean theorem.

An imaginary triangle was constructed between the two nearest points where the current is equal to zero (I=0) on the IV-curve. Figure A.2 shows a schematic illustration of the constructed triangle and the different symbols used for the calculations on the V_{oc}.

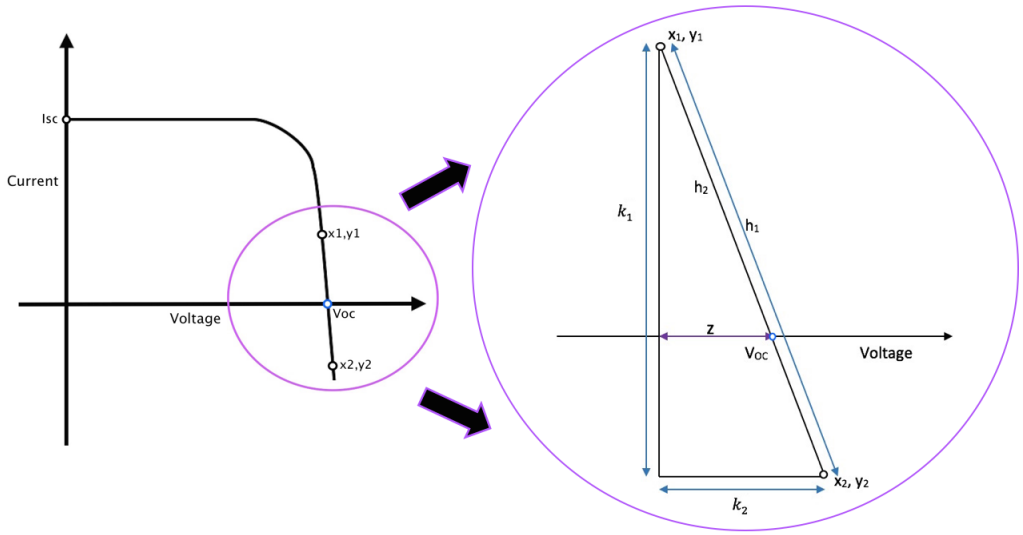

Figure A.2: Schematic illustration of the constructed triangle and the different symbols used for the calculations on the open-circuit voltage, V_{oc}.

The values of k_1 and k_2 in the constructed right triangle (Figure A.2) were first calculated, according to the equations:

$$\begin{aligned} k_1 &= y_1 + |y_2| \\ k_2 &= x_2 - x_1 \end{aligned} \tag{A.2}$$

Next, the hypotenuse, h_1, of the triangle was calculated:

$$h_1 = \left(k_1^2 + k_2^2\right)^{\frac{1}{2}} \tag{A.3}$$

Further, the percentage of the length y_1 of k_1 was calculated and used to find h_2. Then, the distance between x_1 and V_{oc}, z, was found by using the Pythagorean theorem again.

$$h_2 = h_1 \cdot \left(\frac{y_1}{k_1}\right) \tag{A.4}$$

$$z = \left(h_2^2 - y_1^2\right)^{\frac{1}{2}} \tag{A.5}$$

Finally, the open-circuit voltage, V_{oc}, was found by the equation

$$V_{oc} = x_1 + z \tag{A.6}$$

B IV-Curves, Irradiation and Temperature Values for the Basic Measurements - Performed Inside a Chamber

In this appendix the IV-curves for the performed basic measurements are shown, where the aim was to observe the changes that occur when changing between different parameters. The parameters that were changed were the tilt angle (0°, 22.5°, 45°, 67.5° and 90°) and the reflection material underneath the bifacial solar cell, which were used to obtain different reflection characteristics. The parameters were only changed one at a time.

The IV-curves were obtained both for the bifacial solar cell itself, along with the monofacial version of it. In the case of the monofacial solar cell, the rear side of the bifacial solar cell was covered up with a black cover. For each plot, the tilt angle is the fixed parameter and the reflection material underneath the cell is the changing parameter. The plots with the same tilt angle and with bi- and monofacial characteristic of the solar cell are set next to each other, in order to compare the two.

Some irregularities were observed on the plotted IV-curves, when the bifacial solar cell had a tilt angle of 0° and 22.5°. This could be due to some trouble with the electronics that were used or something else, which is not known up until this point. It seem to only occur on those two tilt angles: 0° and 22.5°.

The irradiance and the temperature values for both the bi- and monofacial solar cell and the ISET sensor are given in this appendix as well. This is important information, which to a large degree determines the efficiency output of the solar cell. The values are given in a table for each specific tilt angle.

B.1 0 Degree Tilt Angle on the Solar Cell

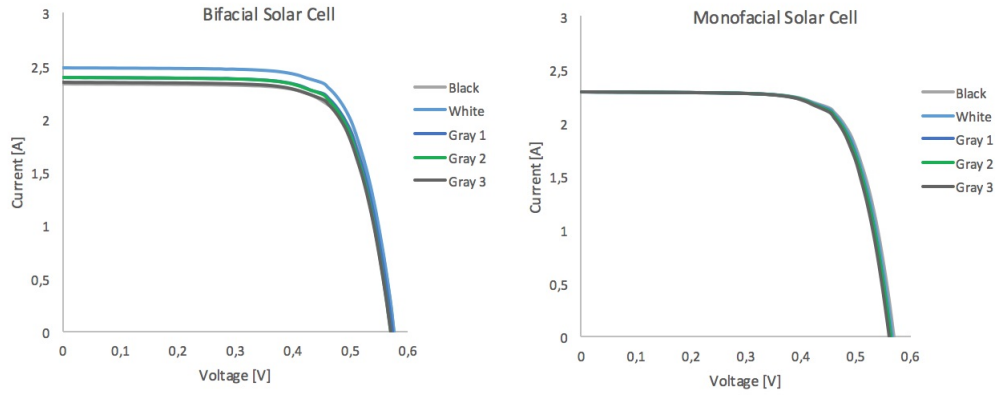

Figure B.1: The IV-curves shown on the left and right image are for a bi- and monofacial solar cell, respectively. The solar cell has a tilt angle of 0° (horizontal), and where the different colours refer to the paper underneath the cell to obtain different reflection characteristics.

Table B.1: The table gives the values for the irradiance [Wm^{-2}] and the temperature on both the solar cell and ISET sensor [deg.C], for measurements performed at 0° tilt angle on the solar cell.

	Bifacial Solar Cell	Irradiance [Wm^{-2}]	Temperature Solar Cell [deg.C]	Temperature ISET [deg.C]
0 Degree	White	253.2	37.6	37.8
	Black	253.3	36.4	36.4
	Gray1	250.5	38.8	39.4
	Gray2	250.7	39.2	40.1
	Gray3	249.7	39.5	40.7
	Monofacial Solar Cell	Irradiance [Wm^{-2}]	Temperature Solar Cell [deg.C]	Temperature ISET [deg.C]
0 Degree	White	252.6	40.5	41.7
	Black	254.1	39.1	41.1
	Gray1	252.5	41.5	42.2
	Gray2	251.3	42.1	42.6
	Gray3	252.3	42.6	43.0

B.2 22.5 Degree Tilt Angle on the Solar Cell

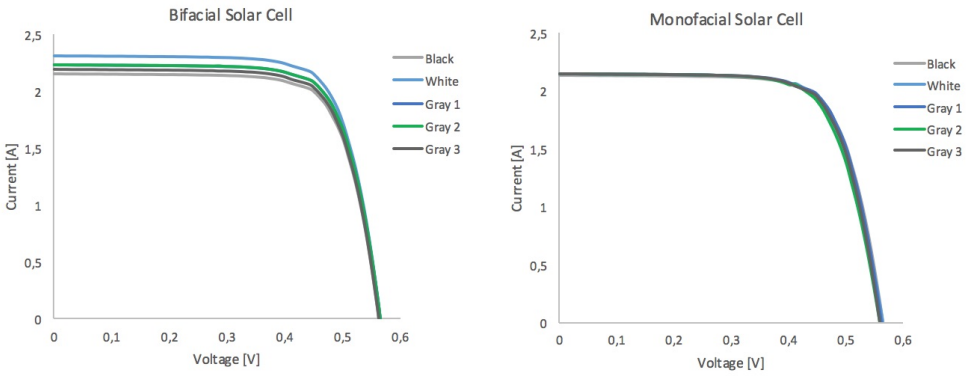

Figure B.2: The IV-curves shown on the left and right image are for a bi- and monofacial solar cell, respectively. The solar cell has a tilt angle of 22.5°, and where the different colours refer to the paper underneath the cell to obtain different reflection characteristics.

Table B.2: The table gives the values for the irradiance [Wm^{-2}] and the temperature on both the solar cell and ISET sensor [deg.C], for measurements performed at 22.5° tilt angle on the solar cell.

	Bifacial Solar Cell	Irradiance [Wm^{-2}]	Temperature Solar Cell [deg.C]	Temperature ISET [deg.C]
22.5 Degree	White	159.2	40.6	40.7
	Black	158.7	40.9	41.1
	Gray1	159.8	40.9	40.6
	Gray2	161.3	40.7	40.6
	Gray3	160.4	40.7	40.6
	Monofacial Solar Cell	Irradiance [Wm^{-2}]	Temperature Solar Cell [deg.C]	Temperature ISET [deg.C]
22.5 Degree	White	159.2	41.5	40.6
	Black	158.3	40.1	40.4
	Gray1	161.2	41.7	40.6
	Gray2	160.7	42.4	40.8
	Gray3	160.4	42.6	40.9

B.3 45 Degree Tilt Angle on the Solar Cell

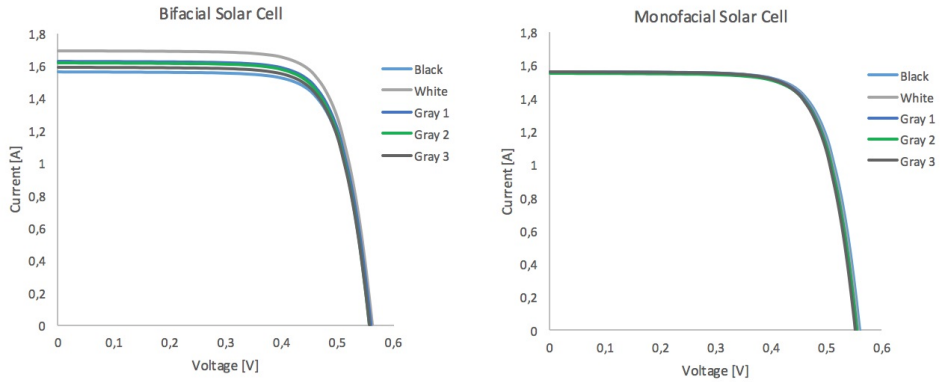

Figure B.3: The IV-curves shown on the left and right image are for a bi- and monofacial solar cell, respectively. The solar cell has a tilt angle of 45°, and where the different colours refer to the paper underneath the cell to obtain different reflection characteristics.

Table B.3: The table gives the values for the irradiance [Wm^{-2}] and the temperature on both the solar cell and ISET sensor [deg.C], for measurements performed at 45° tilt angle on the solar cell.

	Bifacial Solar Cell	Irradiance [Wm^{-2}]	Temperature Solar Cell [deg.C]	Temperature ISET [deg.C]
45 Degree	White	86.9	39.1	35.8
	Black	86.1	38.9	35.4
	Gray1	87.2	39.2	36.1
	Gray2	89.7	39.3	36.4
	Gray3	88.3	39.3	36.6
	Monofacial Solar Cell	Irradiance [Wm^{-2}]	Temperature Solar Cell [deg.C]	Temperature ISET [deg.C]
45 Degree	White	87.0	39.8	36.8
	Black	86.5	38.7	36.4
	Gray1	87.4	40.5	37.0
	Gray2	90.5	40.8	37.2
	Gray3	87.8	41.0	37.3

B.4 67.5 Degree Tilt Angle on the Solar Cell

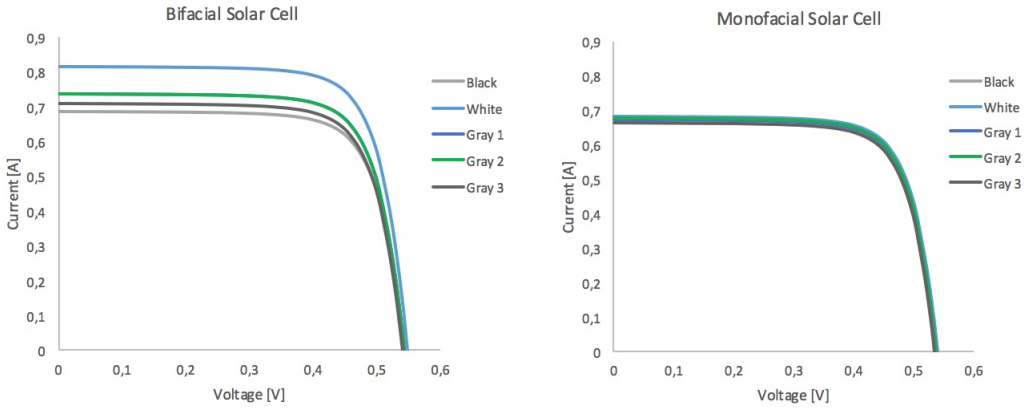

Figure B.4: The IV-curves shown on the left and right image are for a bi- and monofacial solar cell, respectively. The solar cell has a tilt angle of 67.5°, and where the different colours refer to the paper underneath the cell to obtain different reflection characteristics.

Table B.4: The table gives the values for the irradiance [Wm^{-2}] and the temperature on both the solar cell and ISET sensor [deg.C], for measurements performed at 67.5° tilt angle on the solar cell.

	Bifacial Solar Cell	Irradiance [Wm^{-2}]	Temperature Solar Cell [deg.C]	Temperature ISET [deg.C]
67.5 Degree	White	44.4	35.1	30.6
	Black	35.1	34.9	30.1
	Gray1	37.3	35.4	31.0
	Gray2	36.9	35.5	31.3
	Gray3	36.4	35.7	31.7
	Monofacial Solar Cell	Irradiance [Wm^{-2}]	Temperature Solar Cell [deg.C]	Temperature ISET [deg.C]
67.5 Degree	White	42.0	36.4	32.2
	Black	33.2	35.5	31.6
	Gray1	37.6	36.7	32.5
	Gray2	38.7	37.1	32.7
	Gray3	36.0	37.4	32.9

B.5 90 Degree Tilt Angle on the Solar Cell

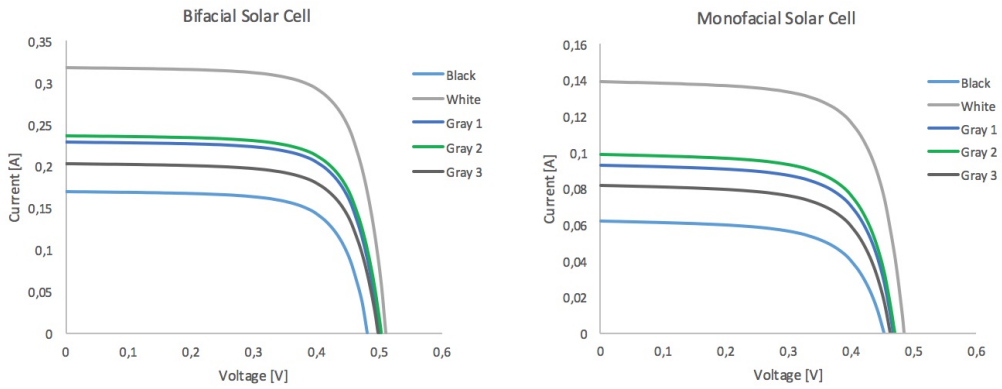

Figure B.5: The IV-curves shown on the left and right image are for a bi- and monofacial solar cell, respectively. The solar cell has a tilt angle of 90°, and where the different colours refer to the paper underneath the cell to obtain different reflection characteristics. Note that the y-axis do not have the same scale on both the images.

Table B.5: The table gives the values for the irradiance [Wm^{-2}] and the temperature on both the solar cell and ISET sensor [deg.C], for measurements performed at 90° tilt angle on the solar cell.

	Bifacial Solar Cell	Irradiance [Wm^{-2}]	Temperature Solar Cell [deg.C]	Temperature ISET [deg.C]
90 Degree	White	27.7	35.5	34.3
	Black	5.2	36.3	36.3
	Gray1	14.3	35.1	33.2
	Gray2	15.7	34.8	32.6
	Gray3	10.4	34.8	32.1
	Monofacial Solar Cell	Irradiance [Wm^{-2}]	Temperature Solar Cell [deg.C]	Temperature ISET [deg.C]
90 Degree	White	26.1	34.4	31.7
	Black	4.4	33.7	31.6
	Gray1	13.8	34.7	31.9
	Gray2	14.9	34.9	31.9
	Gray3	10.4	34.8	31.8

C Snow and Rime Ice Used in the Measurements

The irradiance and the temperature values for both the bifacial solar cell and the ISET sensor are given in this appendix. This is important information, which to a large degree determines the efficiency output of the solar cell.

C.1 Snow vs. White Paper as Reflection Material

Table C.1: The table gives the values for the irradiance [Wm^{-2}] and the temperature on both the solar cell and ISET sensor [deg.C], for measurements performed at 0°, 45° and 90° tilt angle on the bifacial solar cell. White paper and snow were used as reflection materials.

	Solar Cell Tilt Angle	Irradiance [Wm^{-2}]	Temperature Solar Cell [deg.C]	Temperature ISET [deg.C]
White	0°	250.9	35.2	34.6
	45°	89.9	35.8	34.8
	90°	28.5	34.7	33.2
	Solar Cell Tilt Angle	Irradiance [Wm^{-2}]	Temperature Solar Cell [deg.C]	Temperature ISET [deg.C]
Snow	0°	252.6	35.4	36.3
	45°	89.2	34.6	35.4
	90°	14.2	33.1	33.3

C.2 Rime Ice on the Bifacial Solar Cell vs. Cold Cell

Table C.2: The table gives the values for the irradiance [Wm^{-2}] and the temperature on both the solar cell and ISET sensor [deg.C], for measurements performed at 0° tilt angle on the bifacial solar cell. White paper was used as reflection material underneath the cell.

	State of Bifacial Solar Cell	Irradiance [Wm^{-2}]	Temperature Solar Cell [deg.C]	Temperature ISET [deg.C]
White	Rime Ice1	254.9	14.6	33.9
	Rime Ice2	258.8	11.4	30.4
	Rime Ice3	255.3	11.3	34.2
	Rime Ice4	258.1	14.1	32.3
	Rime Ice5	256.5	15.2	34.6
	Cold Cell	256.7	15.5	33.1

D Measurements Performed Outside

The irradiance and the temperature values for both the bi- and monofacial solar cell and the ISET sensor are given in this appendix, for the measurements performed outside. In addition, the irradiance [Wm^{-2}] measured by two Pyranometer is given, both the direct and indirect irradiance. Where in theory, the direct irradiance from the Pyranometer should be in agreement with the other irradiance value given from the ISET sensor. This can be seen to not quite be the case and can be due to the slightly difference in the positions of the two sensors on the set-up. The values given here are important, which to a large degree determines the efficiency output of the solar cell.

Table D.1: The table gives the values for the irradiance [Wm^{-2}] and the temperature on both the solar cell and ISET sensor [deg.C], for measurements performed at different tilt angles on the solar cell. In addition, the irradiance [Wm^{-2}] measured by two Pyranometer is given as well, both the direct and indirect irradiance. These values are for the first result in Section 4.2, where measurements were performed on both the bifacial solar cell and the monofacial version of it.

					Pyranometer	
	Tilt Angle on the Bifacial Solar Cell	Irradiance [Wm^{-2}]	Temperature Solar Cell [deg.C]	Temperature ISET [deg.C]	Direct Irr. [Wm^{-2}]	Indirect Irr. [Wm^{-2}]
Concrete	0°	60.1	14.2	13.4	57.2	10.3
	22.5°	70.5	13.9	13.0	70.0	11.3
	45°	70.5	13.5	12.6	71.6	12.6
	67.5°	54.3	13.4	12.3	60.0	15.5
	90°	36.7	13.1	11.9	45.6	17.8
	Tilt Angle on the Monofacial Solar Cell	Irradiance [Wm^{-2}]	Temperature Solar Cell [deg.C]	Temperature ISET [deg.C]	Direct Irr. [Wm^{-2}]	Indirect Irr. [Wm^{-2}]
Concrete	0°	123.6	14.3	12.3	117.8	19.3
	22.5°	141.1	14.8	12.8	140.9	21.4
	45°	175.3	15.3	13.4	181.5	24.5
	67.5°	143.1	15.7	14.0	160.2	28.7
	90°	94.0	15.8	13.9	109.5	29.9

D.1 Another Outside Measurement

Table D.2: The table gives the values for the irradiance [Wm^{-2}] and the temperature on both the solar cell and ISET sensor [deg.C], for measurements performed at different tilt angles on the bifacial solar cell. In addition, the irradiance [Wm^{-2}] measured by two Pyranometer is given as well, both the direct and indirect irradiance.

	Bifacial Solar Cell				Pyranometer	
	Tilt Angle	Irradiance [Wm^{-2}]	Temperature Solar Cell [deg.C]	Temperature ISET [deg.C]	Direct Irr. [Wm^{-2}]	Indirect Irr. [Wm^{-2}]
Concrete	0°	31.2	15.5	12.6	36.5	10.8
	22.5°	73.1	13.6	12.3	78.1	16.2
	45°	29.4	14.2	12.1	37.3	9.1
	67.5°	24.5	13.4	11.8	33.4	11.3
	90°	25.1	13.0	11.4	36.7	13.3

D.2 Irradiance Experiment

Table D.3: The table gives the values for the irradiance [Wm^{-2}] and the temperature on both the solar cell and ISET sensor [deg.C], for measurements performed at 0° tilt angle on the bifacial solar cell. In addition, the irradiance [Wm^{-2}] measured by two Pyranometer is given as well, both the direct and indirect irradiance.

					Pyranometer	
	Bifacial Solar Cell	Irradiance [Wm^{-2}]	Temperature Solar Cell [deg.C]	Temperature ISET [deg.C]	Direct Irr. [Wm^{-2}]	Indirect Irr. [Wm^{-2}]
Concrete	Exp.1	61.5	13.5	12.2	64.7	17.7
	Exp.2	102.1	13.5	12.1	99.1	19.1
	Exp.3	123.6	13.8	12.4	119.0	21.7
	Exp.4	110.6	13.9	12.8	106.2	20.0
	Exp.5	94.3	14.0	12.9	93.6	18.2

E Accuracy of the Measurements

In order to see how accurate the measurements were, mean and standard deviation were calculated for three parallels done on each reflection material (the five paper colours), for 0°, 45° and 90° tilt angle on the bifacial solar cell. Appendix F contains the data for parallel 2 and 3, and the data for parallel 1 comes from Section 4.1.1 and Appendix B.

As mentioned in Chapter 2, the temperature has an important effect on the power output from the cell, and the most significant is the temperature dependence of the voltage. The voltage decreases with increasing temperature, and the voltage decrease of a silicon cell is typically 2.3 mV per degree Celsius [24]. From the numbers of the open-circuit voltage (V_{oc}) and the temperature on the solar cell, this seem to hold true.

E.1 Calculations for 0 Degree Tilt Angle on the Bifacial Solar Cell

Table E.1: The calculated mean (μ) and standard deviation (σ) for the data set from 0° tilt angle on the bifacial solar cell and where white paper was used as reflection material.

	White	I_{sc} [A]	V_{oc} [V]	P_{max} [W]	FF	η	Irradiance [Wm^{-2}]	Temp. Solar Cell [deg.C]	Temp. ISET [deg.C]
Data Set	1	2.487	0.577	1.064	0.742	0.173	253.157	37.571	37.768
	2	2.466	0.564	1.025	0.737	0.168	250.595	43.406	44.708
	3	2.474	0.572	1.044	0.737	0.171	251.411	40.592	40.341
	Mean Value (μ)	2.476	0.571	1.044	0.739	0.171	251.721	40.523	40.939
	Standard Deviation (σ)	0.007	0.005	0.014	0.002	0.002	0.926	2.063	2.481

Table E.2: The calculated mean (μ) and standard deviation (σ) for the data set from 0° tilt angle on the bifacial solar cell and where black paper was used as reflection material.

	Black	I_{sc} [A]	V_{oc} [V]	P_{max} [W]	FF	η	Irradiance [Wm^{-2}]	Temp. Solar Cell [deg.C]	Temp. ISET [deg.C]
Data Set	1	2.333	0.577	1.003	0.745	0.163	253.295	36.396	36.389
	2	2.305	0.562	0.958	0.739	0.157	250.190	43.187	44.055
	3	2.312	0.575	0.988	0.743	0.161	250.794	39.280	37.766
	Mean Value (μ)	2.317	0.571	0.983	0.742	0.160	251.427	39.621	39.404
	Standard Deviation (σ)	0.010	0.006	0.016	0.002	0.002	1.164	2.410	2.890

Table E.3: The calculated mean (μ) and standard deviation (σ) for the data set from 0° tilt angle on the bifacial solar cell and where gray1 paper was used as reflection material.

	Gray1	I_{sc} [A]	V_{oc} [V]	P_{max} [W]	FF	η	Irradiance [Wm^{-2}]	Temp. Solar Cell [deg.C]	Temp. ISET [deg.C]
Data Set	1	2.403	0.573	1.019	0.741	0.167	250.450	38.830	39.386
	2	2.389	0.562	0.990	0.737	0.163	249.722	43.352	45.144
	3	2.397	0.569	1.005	0.737	0.164	251.249	41.119	41.468
	Mean Value (μ)	2.396	0.568	1.005	0.738	0.165	250.474	41.100	41.999
	Standard Deviation (σ)	0.005	0.004	0.010	0.002	0.001	0.540	1.599	2.062

Table E.4: The calculated mean (μ) and standard deviation (σ) for the data set from 0° tilt angle on the bifacial solar cell and where gray2 paper was used as reflection material.

	Gray2	I_{sc} [A]	V_{oc} [V]	P_{max} [W]	FF	η	Irradiance [Wm^{-2}]	Temp. Solar Cell [deg.C]	Temp. ISET [deg.C]
Data Set	1	2.390	0.571	1.010	0.740	0.166	250.696	39.235	40.108
	2	2.380	0.562	0.985	0.737	0.161	250.942	43.218	45.417
	3	2.391	0.567	1.000	0.738	0.164	250.859	41.496	42.412
	Mean Value (μ)	2.387	0.567	0.998	0.738	0.164	250.832	41.316	42.646
	Standard Deviation (σ)	0.004	0.003	0.009	0.001	0.002	0.088	1.413	1.883

Table E.5: The calculated mean (μ) and standard deviation (σ) for the data set from 0° tilt angle on the bifacial solar cell and where gray3 paper was used as reflection material.

	Gray3	I_{sc} [A]	V_{oc} [V]	P_{max} [W]	FF	η	Irradiance [Wm^{-2}]	Temp. Solar Cell [deg.C]	Temp. ISET [deg.C]
Data Set	1	2.353	0.570	0.992	0.739	0.163	249.711	39.458	40.681
	2	2.345	0.562	0.971	0.737	0.160	249.771	43.256	45.677
	3	2.356	0.566	0.982	0.737	0.161	250.661	41.872	43.223
	Mean Value (μ)	2.351	0.566	0.982	0.738	0.161	250.047	41.529	43.193
	Standard Deviation (σ)	0.004	0.003	0.007	0.001	0.001	0.376	1.359	1.766

E.2 Calculations for 45 Degree Tilt Angle on the Bifacial Solar Cell

Table E.6: The calculated mean (μ) and standard deviation (σ) for the data set from 45° tilt angle on the bifacial solar cell and where white paper was used as reflection material.

	White	I_{sc} [A]	V_{oc} [V]	P_{max} [W]	FF	η	Irradiance [Wm^{-2}]	Temp. Solar Cell [deg.C]	Temp. ISET [deg.C]
Data Set	1	1.687	0.561	0.705	0.745	0.334	86.880	39.120	35.760
	2	1.735	0.576	0.747	0.748	0.334	91.796	33.569	29.554
	3	1.741	0.576	0.752	0.751	0.337	91.792	33.782	29.951
	Mean Value (μ)	1.721	0.571	0.735	0.748	0.335	90.156	35.490	31.755
	Standard Deviation (σ)	0.021	0.006	0.018	0.002	0.001	2.006	2.224	2.457

Table E.7: The calculated mean (μ) and standard deviation (σ) for the data set from 45° tilt angle on the bifacial solar cell and where black paper was used as reflection material.

	Black	I_{sc} [A]	V_{oc} [V]	P_{max} [W]	FF	η	Irradiance [Wm^{-2}]	Temp. Solar Cell [deg.C]	Temp. ISET [deg.C]
Data Set	1	1.562	0.560	0.652	0.745	0.311	86.148	38.906	35.379
	2	1.615	0.576	0.678	0.750	0.304	94.228	32.635	28.624
	3	1.625	0.576	0.706	0.754	0.317	91.331	32.678	29.133
	Mean Value (μ)	1.601	0.571	0.679	0.750	0.311	90.569	34.739	31.046
	Standard Deviation (σ)	0.024	0.007	0.019	0.003	0.005	2.894	2.551	2.660

Table E.8: The calculated mean (μ) and standard deviation (σ) for the data set from 45° tilt angle on the bifacial solar cell and where gray1 paper was used as reflection material.

	Gray1	I_{sc} [A]	V_{oc} [V]	P_{max} [W]	FF	η	Irradiance [Wm^{-2}]	Temp. Solar Cell [deg.C]	Temp. ISET [deg.C]
Data Set	1	1.629	0.559	0.678	0.745	0.320	87.199	39.158	36.094
	2	1.669	0.572	0.713	0.746	0.313	93.601	34.199	30.323
	3	1.677	0.572	0.718	0.747	0.320	92.236	34.162	30.428
	Mean Value (μ)	1.658	0.568	0.703	0.746	0.318	91.012	35.840	32.282
	Standard Deviation (σ)	0.018	0.005	0.015	0.001	0.003	2.384	2.032	2.335

Table E.9: The calculated mean (μ) and standard deviation (σ) for the data set from 45° tilt angle on the bifacial solar cell and where gray2 paper was used as reflection material.

	Gray2	I_{sc} [A]	V_{oc} [V]	P_{max} [W]	FF	η	Irradiance [Wm^{-2}]	Temp. Solar Cell [deg.C]	Temp. ISET [deg.C]
Data Set	1	1.615	0.558	0.672	0.745	0.308	89.724	39.325	36.413
	2	1.663	0.571	0.707	0.745	0.314	92.544	34.961	31.076
	3	1.659	0.571	0.708	0.747	0.320	90.808	34.625	30.963
	Mean Value (μ)	1.646	0.567	0.696	0.746	0.314	91.026	36.303	32.817
	Standard Deviation (σ)	0.019	0.005	0.014	0.001	0.004	1.006	1.854	2.202

Table E.10: The calculated mean (μ) and standard deviation (σ) for the data set from 45° tilt angle on the bifacial solar cell and where gray3 paper was used as reflection material.

	Gray3	I_{sc} [A]	V_{oc} [V]	P_{max} [W]	FF	η	Irradiance [Wm^{-2}]	Temp. Solar Cell [deg.C]	Temp. ISET [deg.C]
Data Set	1	1.589	0.558	0.660	0.745	0.307	88.266	39.277	36.619
	2	1.631	0.568	0.690	0.745	0.306	92.690	35.302	31.598
	3	1.622	0.569	0.688	0.746	0.310	91.194	35.122	31.490
	Mean Value (μ)	1.614	0.565	0.679	0.745	0.308	90.717	36.567	33.236
	Standard Deviation (σ)	0.016	0.004	0.012	0.000	0.001	1.591	1.661	2.073

E.3 Calculations for 90 Degree Tilt Angle on the Bifacial Solar Cell

Table E.11: The calculated mean (μ) and standard deviation (σ) for the data set from 90° tilt angle on the bifacial solar cell and where white paper was used as reflection material.

	White	I_{sc} [A]	V_{oc} [V]	P_{max} [W]	FF	η	Irradiance [Wm^{-2}]	Temp. Solar Cell [deg.C]	Temp. ISET [deg.C]
Data Set	1	0.317	0.510	0.118	0.727	0.174	27.730	35.508	34.300
	2	0.312	0.511	0.117	0.730	0.167	28.728	35.670	32.310
	3	0.316	0.511	0.118	0.731	0.172	28.138	35.559	32.221
	Mean Value (μ)	0.315	0.511	0.118	0.729	0.171	28.199	35.579	32.944
	Standard Deviation (σ)	0.002	0.000	0.000	0.001	0.003	0.355	0.059	0.831

Table E.12: The calculated mean (μ) and standard deviation (σ) for the data set from 90° tilt angle on the bifacial solar cell and where black paper was used as reflection material.

	Black	I_{sc} [A]	V_{oc} [V]	P_{max} [W]	FF	η	Irradiance [Wm^{-2}]	Temp. Solar Cell [deg.C]	Temp. ISET [deg.C]
Data Set	1	0.169	0.480	0.057	0.705	0.453	5.180	36.289	36.331
	2	0.157	0.484	0.054	0.706	0.376	5.855	36.060	32.456
	3	0.162	0.485	0.056	0.708	0.433	5.272	35.851	32.399
	Mean Value (μ)	0.163	0.483	0.056	0.706	0.421	5.436	36.067	33.729
	Standard Deviation (σ)	0.004	0.002	0.001	0.001	0.028	0.259	0.155	1.594

Table E.13: The calculated mean (μ) and standard deviation (σ) for the data set from 90° tilt angle on the bifacial solar cell and where gray1 paper was used as reflection material.

	Gray1	I_{sc} [A]	V_{oc} [V]	P_{max} [W]	FF	η	Irradiance [Wm^{-2}]	Temp. Solar Cell [deg.C]	Temp. ISET [deg.C]
Data Set	1	0.228	0.500	0.082	0.715	0.234	14.309	35.087	33.224
	2	0.222	0.500	0.080	0.718	0.208	15.739	35.371	32.183
	3	0.226	0.501	0.081	0.719	0.222	15.078	35.272	32.108
	Mean Value (μ)	0.225	0.500	0.081	0.717	0.221	15.042	35.243	32.505
	Standard Deviation (σ)	0.002	0.000	0.001	0.001	0.009	0.506	0.102	0.441

Table E.14: The calculated mean (μ) and standard deviation (σ) for the data set from 90° tilt angle on the bifacial solar cell and where gray2 paper was used as reflection material.

	Gray2	I_{sc} [A]	V_{oc} [V]	P_{max} [W]	FF	η	Irradiance [Wm^{-2}]	Temp. Solar Cell [deg.C]	Temp. ISET [deg.C]
Data Set	1	0.237	0.503	0.085	0.716	0.223	15.696	34.801	32.628
	2	0.234	0.503	0.085	0.720	0.202	17.172	35.149	32.061
	3	0.237	0.503	0.086	0.721	0.207	17.054	34.979	31.977
	Mean Value (μ)	0.236	0.503	0.085	0.719	0.221	16.641	34.976	32.222
	Standard Deviation (σ)	0.001	0.000	0.000	0.002	0.008	0.580	0.123	0.250

Table E.15: The calculated mean (μ) and standard deviation (σ) for the data set from 90° tilt angle on the bifacial solar cell and where gray3 paper was used as reflection material.

	Gray3	I_{sc} [A]	V_{oc} [V]	P_{max} [W]	FF	η	Irradiance [Wm^{-2}]	Temp. Solar Cell [deg.C]	Temp. ISET [deg.C]
Data Set	1	0.203	0.498	0.072	0.711	0.283	10.421	34.786	32.143
	2	0.201	0.497	0.071	0.715	0.240	12.225	35.106	32.038
	3	0.204	0.498	0.073	0.715	0.243	12.307	34.998	31.923
	Mean Value (μ)	0.203	0.498	0.072	0.714	0.255	11.651	34.963	32.035
	Standard Deviation (σ)	0.001	0.000	0.001	0.002	0.017	0.754	0.115	0.078

F Data Used for Calculating the Accuracy of the Measurements

In this appendix, the data used for calculating the accuracy of the measurements can be found. The results given in Chapter 4 and Appendix B, have been labelled with number 1 in the accuracy calculations. Whereby, number 2 and 3 correspond to the two parallels, and the data can be found in this appendix.

The parallels 2 and 3 were performed at three tilt angles: 0°, 45° and 90°, whereby parallel 1 was performed at five tilt angles: 0°, 22.5°, 45°, 67.5° and 90°. Hence, it is the three tilt angles that are common for the tree parallels (0°, 45° and 90°) that have been used during the accuracy calculations (Appendix E).

F.1 0 Degree Tilt Angle on the Solar Cell

Table F.1: The table shows values for short-circuit current (I_{sc}), open-circuit voltage (V_{oc}), maximum power point (P_{max}), fill factor (FF), energy conversion efficiency (η), irradiance [Wm^{-2}] and the temperature on both the solar cell and ISET sensor [deg.C], for 0° tilt angle on the bi- and monofacial solar cell, parallel 2. The different colours refer to the colour on the paper used as a reflection material.

Parallel 2	Tilt Angle: 0°				
Bifacial Solar Cell	White	Black	Gray1	Gray2	Gray3
I_{sc} [A]	2.466	2.305	2.389	2.380	2.345
V_{oc} [V]	0.564	0.562	0.562	0.562	0.562
P_{max} [W]	1.025	0.958	0.990	0.985	0.971
Fill factor (FF)	0.737	0.739	0.737	0.737	0.737
Energy conversion efficiency (η)	0.168	0.157	0.163	0.161	0.160
Irradiance [Wm^{-2}]	250.6	250.2	249.7	250.9	249.8
Temperature Solar Cell [deg.C]	43.4	43.2	43.4	43.2	43.3
Temperature ISET [deg.C]	44.7	44.1	45.1	45.4	45.7
Monofacial Solar Cell	White	Black	Gray1	Gray2	Gray3
I_{sc} [A]	2.297	2.291	2.295	2.292	2.293
V_{oc} [V]	0.561	0.563	0.559	0.557	0.556
P_{max} [W]	0.950	0.954	0.945	0.940	0.939
Fill factor (FF)	0.738	0.740	0.737	0.736	0.736
Energy conversion efficiency (η)	0.157	0.158	0.157	0.155	0.155
Irradiance [Wm^{-2}]	248.2	248.8	248.0	249.3	249.1
Temperature Solar Cell [deg.C]	43.9	42.6	45.0	45.6	45.6
Temperature ISET [deg.C]	45.8	45.5	46.1	46.3	46.4

Table F.2: The table shows values for short-circuit current (I_{sc}), open-circuit voltage (V_{oc}), maximum power point (P_{max}), fill factor (FF), energy conversion efficiency (η), irradiance [Wm^{-2}] and the temperature on both the solar cell and ISET sensor [deg.C], for 0° tilt angle on the bi- and monofacial solar cell, parallel 3. The different colours refer to the colour on the paper used as a reflection material.

Parallel 3	Tilt Angle: 0°				
Bifacial Solar Cell	White	Black	Gray1	Gray2	Gray3
I_{sc} [A]	2.474	2.312	2.397	2.391	2.356
V_{oc} [V]	0.572	0.575	0.569	0.567	0.566
P_{max} [W]	1.044	0.988	1.005	1.000	0.982
Fill factor (FF)	0.737	0.743	0.737	0.738	0.737
Energy conversion efficiency (η)	0.171	0.161	0.164	0.164	0.161
Irradiance [Wm^{-2}]	251.4	250.8	251.2	250.9	250.7
Temperature Solar Cell [deg.C]	40.6	39.3	41.1	41.5	41.9
Temperature ISET [deg.C]	40.3	37.8	41.5	42.4	43.2
Monofacial Solar Cell	White	Black	Gray1	Gray2	Gray3
I_{sc} [A]	2.308	2.301	2.307	2.301	2.301
V_{oc} [V]	0.563	0.565	0.562	0.560	0.559
P_{max} [W]	0.960	0.963	0.955	0.950	0.948
Fill factor (FF)	0.739	0.740	0.737	0.737	0.737
Energy conversion efficiency (η)	0.158	0.159	0.157	0.155	0.155
Irradiance [Wm^{-2}]	250.4	248.8	250.3	251.4	250.5
Temperature Solar Cell [deg.C]	42.9	41.8	43.8	44.3	44.7
Temperature ISET [deg.C]	44.1	43.6	44.6	44.9	45.1

F.2 45 Degree Tilt Angle on the Solar Cell

Table F.3: The table shows values for short-circuit current (I_{sc}), open-circuit voltage (V_{oc}), maximum power point (P_{max}), fill factor (FF), energy conversion efficiency (η), irradiance [Wm^{-2}] and the temperature on both the solar cell and ISET sensor [deg.C], for 45° tilt angle on the bi- and monofacial solar cell, parallel 2. The different colours refer to the colour on the paper used as a reflection material.

Parallel 2	Tilt Angle: 45°				
Bifacial Solar Cell	White	Black	Gray1	Gray2	Gray3
I_{sc} [A]	1.735	1.615	1.669	1.663	1.631
V_{oc} [V]	0.576	0.576	0.572	0.571	0.568
P_{max} [W]	0.747	0.698	0.713	0.707	0.690
Fill factor (FF)	0.748	0.750	0.746	0.745	0.745
Energy conversion efficiency (η)	0.334	0.304	0.313	0.314	0.306
Irradiance [Wm^{-2}]	91.8	94.2	93.6	92.5	92.7
Temperature Solar Cell [deg.C]	33.6	32.6	34.2	35.0	35.3
Temperature ISET [deg.C]	29.6	28.6	30.3	31.1	31.6
Monofacial Solar Cell	White	Black	Gray1	Gray2	Gray3
I_{sc} [A]	1.587	1.580	1.582	1.572	1.583
V_{oc} [V]	0.565	0.567	0.563	0.561	0.560
P_{max} [W]	0.669	0.669	0.664	0.658	0.661
Fill factor (FF)	0.746	0.747	0.746	0.745	0.745
Energy conversion efficiency (η)	0.297	0.299	0.303	0.296	0.304
Irradiance [Wm^{-2}]	92.6	91.9	90.1	91.2	89.3
Temperature Solar Cell [deg.C]	36.4	35.5	37.3	37.8	38.4
Temperature ISET [deg.C]	32.6	32.1	33.2	33.6	34.0

Table F.4: The table shows values for short-circuit current (I_{sc}), open-circuit voltage (V_{oc}), maximum power point (P_{max}), fill factor (FF), energy conversion efficiency (η), irradiance [Wm^{-2}] and the temperature on both the solar cell and ISET sensor [deg.C], for 45° tilt angle on the bi- and monofacial solar cell, parallel 3. The different colours refer to the colour on the paper used as a reflection material.

Parallel 3	Tilt Angle: 45°				
Bifacial Solar Cell	White	Black	Gray1	Gray2	Gray3
I_{sc} [A]	1.741	1.625	1.677	1.659	1.622
V_{oc} [V]	0.576	0.576	0.572	0.571	0.569
P_{max} [W]	0.752	0.706	0.718	0.708	0.688
Fill factor (FF)	0.751	0.754	0.748	0.747	0.746
Energy conversion efficiency (η)	0.337	0.317	0.320	0.320	0.310
Irradiance [Wm^{-2}]	91.8	91.3	92.2	90.8	91.2
Temperature Solar Cell [deg.C]	33.8	32.7	34.2	34.6	35.1
Temperature ISET [deg.C]	30.0	29.1	30.4	31.0	31.5
Monofacial Solar Cell	White	Black	Gray1	Gray2	Gray3
I_{sc} [A]	1.580	1.574	1.573	1.574	1.569
V_{oc} [V]	0.565	0.567	0.563	0.562	0.561
P_{max} [W]	0.666	0.668	0.661	0.659	0.655
Fill factor (FF)	0.746	0.748	0.746	0.745	0.745
Energy conversion efficiency (η)	0.305	0.305	0.305	0.310	0.309
Irradiance [Wm^{-2}]	89.6	89.9	82.1	87.3	87.1
Temperature Solar Cell [deg.C]	36.3	35.4	37.0	37.7	38.0
Temperature ISET [deg.C]	32.4	31.9	32.9	33.4	33.7

F.3 90 Degree Tilt Angle on the Solar Cell

Table F.5: The table shows values for short-circuit current (I_{sc}), open-circuit voltage (V_{oc}), maximum power point (P_{max}), fill factor (FF), energy conversion efficiency (η), irradiance [Wm^{-2}] and the temperature on both the solar cell and ISET sensor [deg.C], for 90° tilt angle on the bi- and monofacial solar cell, parallel 2. The different colours refer to the colour on the paper used as a reflection material.

Parallel 2	Tilt Angle: 90°				
Bifacial Solar Cell	White	Black	Gray1	Gray2	Gray3
I_{sc} [A]	0.312	0.157	0.222	0.234	0.201
V_{oc} [V]	0.511	0.484	0.500	0.503	0.497
P_{max} [W]	0.117	0.054	0.080	0.085	0.071
Fill factor (FF)	0.730	0.706	0.718	0.720	0.715
Energy conversion efficiency (η)	0.167	0.376	0.208	0.202	0.240
Irradiance [Wm^{-2}]	28.7	5.9	15.7	17.2	12.2
Temperature Solar Cell [deg.C]	35.7	36.1	35.4	35.1	35.1
Temperature ISET [deg.C]	32.3	32.5	32.2	32.1	32.0
Monofacial Solar Cell	White	Black	Gray1	Gray2	Gray3
I_{sc} [A]	0.171	0.093	0.125	0.127	0.112
V_{oc} [V]	0.493	0.469	0.480	0.480	0.475
P_{max} [W]	0.060	0.030	0.042	0.042	0.037
Fill factor (FF)	0.709	0.680	0.696	0.696	0.690
Energy conversion efficiency (η)	0.086	0.190	0.109	0.099	0.119
Irradiance [Wm^{-2}]	28.4	6.4	15.8	17.6	12.7
Temperature Solar Cell [deg.C]	34.9	34.4	35.0	35.2	35.4
Temperature ISET [deg.C]	31.9	31.7	32.0	32.0	32.1

Table F.6: The table shows values for short-circuit current (I_{sc}), open-circuit voltage (V_{oc}), maximum power point (P_{max}), fill factor (FF), energy conversion efficiency (η), irradiance [Wm^{-2}] and the temperature on both the solar cell and ISET sensor [deg.C], for 90° tilt angle on the bi- and monofacial solar cell, parallel 3. The different colours refer to the colour on the paper used as a reflection material.

Parallel 3	Tilt Angle: 90°				
Bifacial Solar Cell	White	Black	Gray1	Gray2	Gray3
I_{sc} [A]	0.316	0.162	0.226	0.237	0.204
V_{oc} [V]	0.511	0.485	0.501	0.503	0.498
P_{max} [W]	0.118	0.056	0.081	0.086	0.073
Fill factor (FF)	0.731	0.708	0.719	0.721	0.715
Energy conversion efficiency (η)	0.172	0.433	0.222	0.207	0.243
Irradiance [Wm^{-2}]	28.1	5.3	15.1	17.1	12.3
Temperature Solar Cell [deg.C]	35.6	35.9	35.3	35.0	35.0
Temperature ISET [deg.C]	32.2	32.4	32.1	32.0	31.9
Monofacial Solar Cell	White	Black	Gray1	Gray2	Gray3
I_{sc} [A]	0.161	0.081	0.113	0.119	0.102
V_{oc} [V]	0.491	0.464	0.476	0.478	0.472
P_{max} [W]	0.056	0.025	0.037	0.040	0.033
Fill factor (FF)	0.708	0.673	0.692	0.694	0.686
Energy conversion efficiency (η)	0.082	0.180	0.104	0.096	0.114
Irradiance [Wm^{-2}]	28.0	5.8	14.8	16.9	11.9
Temperature Solar Cell [deg.C]	34.9	34.3	35.0	35.0	35.1
Temperature ISET [deg.C]	31.9	31.6	32.0	32.1	32.1

G Pyranometer: A Measure of the Direct and Indirect Irradiance

Table G.1 contain the data to the graph shown in Figure 3.10, which shows the irradiance that would reach the rear side of the bifacial solar cell and the direct irradiance, for five different paper colours used underneath the cell. The bifacial solar cell had a tilt angle of 0°.

Table G.1: The direct and indirect irradiance, measured on top and beneath the bifacial solar cell, respectively, for five different paper colours. The different colours on the paper had different reflectivity characteristics.

Reflection Material	Time [sec.]	Indirect Irradiance [Wm^{-2}]	Direct Irradiance [Wm^{-2}]
White Paper	10	49.2	255.1
	20	49.0	255.1
	30	48.9	255.2
	40	49.0	255.1
	50	48.9	255.2
	60	49.0	255.1
Gray1 Paper	60	31.8	244.7
	70	31.5	244.6
	80	31.7	244.6
	90	31.8	244.7
	100	32.0	244.6
	110	32.0	244.8
Gray2 Paper	110	29.3	243.7
	120	29.5	243.8
	130	29.4	243.8
	140	29.5	243.7
	150	29.5	243.8
	160	29.6	243.8
Gray3 Paper	160	21.3	243.2
	170	21.1	243.2
	180	21.2	243.3
	190	21.4	243.3
	200	21.3	243.3
	210	21.2	243.4
Black Paper	210	12.1	243.0
	220	11.8	243.0
	230	11.9	243.0
	240	12.0	243.0
	250	12.1	243.1
	260	12.1	243.1

H The Effect of the Tilt Angle on the Irradiance

The equations used in Table 5.2 can be found in this appendix. Based on data from Appendix G, for white paper and a tilt angle of 0° on the bifacial solar cell, it can be seen that the direct and indirect radiance that reached the front and rear side of the cell was approximately 250 Wm^{-2} and 50 Wm^{-2}, respectively. It has to be mentioned that these values changes according to where the solar cell is mounted, and here these values are used as an example. The surface area of the cell is A_c = 156x156 mm^2 = 0.024336 m^2.

The direct and indirect radiation reaching the front and rear side is, respectively:

$$dir.\ radiation\ (front\ side) = 250\ Wm^{-2} \cdot cos\,\varphi \cdot 0.024336\ m^2 \tag{H.1}$$

$$indir.\ radiation\ (rear\ side) = 50\ Wm^{-2} \cdot cos\,\varphi \cdot 0.024336\ m^2 \tag{H.2}$$

where φ is the tilt angle on the bifacial solar cell. The total radiation reaching both front and rear side of the bifacial solar cell, simultaneously, is

$$tot.\ radiation = dir.\ radiation\ (front\ side) + indir.\ radiation\ (rear\ side) \tag{H.3}$$

Percent radiation reaching the rear side is calculated by

$$\%\ radiation\ from\ rear\ side = \frac{indir.\ radiation\ (rear\ side)}{dir.\ radiation\ (front\ side)} \cdot 100\ \% \tag{H.4}$$

Projected area in terms of percent radiation is then

$$projected\ area, \%\ radiation = \frac{tot.\ radiation(x)}{tot.\ radiation(0°)} \cdot 100\ \% \tag{H.5}$$

where tot. radiation(0°) is total radiation when the tilt angle is 0° and tot. radiation(x) is total radiation for x = a tilt angle.